ABSTRACT

Title of Dissertation: PHOSPHOLIPID BEHAVIOR AND DYNAMICS IN CURVED BIOLOGICAL MEMBRANES

Haoyuan Jing, Doctor of Philosophy, 2020

Dissertation directed by: Professor Siddhartha Das, Department of Mechanical Engineering

Curvature in biological membranes defines the morphology of cells and organelles and serves key roles in maintaining a variety of cellular functions, enabling trafficking, recruiting and localizing shape-responsive proteins. For example, the bacterial protein SpoVM is a small amphipathic alpha-helical protein that localizes to the outer surface of a forespore, the only convex surface in the mother bacteria. Understanding several of these membrane curvature dependent events rely on a thorough understanding of the properties, energetics, and interactions of the constituent lipid molecules in presence of curvatures.

In this dissertation, we have used molecular dynamics (MD) simulations to explore how the curvature of the lipid bilayer (LBL), a simplified mimic of the cell membrane, affects the packing fraction and diffusivity of lipid molecules in the LBL, energetics of lipid flip flop in the LBL, and lipid desorption from the LBLs. We have

also investigated the interaction between LBLs and a small bacterial protein, SpoVM, which was previously shown to preferentially embed in positively curved membranes. Our work started with simulating convex surface, represented by the nanoparticle supported lipid bilayers (NPSLBLs) in MD. We first quantified the self-assembly, structure, and properties of a NPSLBL with a diameter of 20 nm and showed how the type of the nanoparticle (NP) affects the properties of the NPSLBLs. Second, we studied the energetics of lipid flip flop and desorption from LBLs for the cases of planar substrate supported lipid bilayer (PSSLBL) and NPSLBL. Finally, we investigated the energetics of SpoVM desorption from the PSSLBL and the NPSLBL providing clues to the fundamental driving forces dictating the curvature sensing of SpoVM.

In Chapter 1, we discuss the motivation, methods, biological relevance, and the overall structure of this thesis. In Chapter 2, the structure and properties of a pre-assembled NPSLBL were studied. In Chapter 3, we report the MD simulation results on the structure and properties, such as diffusivity, of the lipid molecules within the LBLs of the NPSLBLs formed through the self-assembly route. We compare our findings with that of unsupported lipid bilayer nanovesicles (NVs). Our results show that the structure of the NPSLBLs, although affected by the type of the NPs, is still similar with the free NV consisting of identical number and species of lipid. On the other hand, the properties such as the diffusivity of the lipid molecules within the LBL are significantly different between the cases of NPSLBL and the free vesicle. Results are provided for different combinations of the lipid molecules and the NP

materials. The findings described in Chapters 2 and 3 will be eventually useful in long-term for designing new generation of NPSLBLs as drug carrier. In Chapter 4, we focus on the lipid flip-flop and desorption from the LBLs for NPSLBLs and PSSLBLs. We investigated the energetics of a lipid molecule traversing through the lipid bilayer (from inner-to-outer and outer-to-inner leaflet) as a function of the position of the hydrophilic head group of the lipid within the LBL. We obtained the potential of mean force (PMF) by using umbrella sampling. Most importantly, we observed little effect of the curvature in the variation of the lipid flip-flop PMF, establishing that the energetics of lipid migration within the supported bilayer, which implies that energy changes associated with bilayer fluctuations, is independent of the shape of the supported bilayer. The conclusion is supported by the reported experimental results. Next, in Chapter 5, MD simulations are carried out to reveal the energetics of a single SpoVM protein undergoing desorption from LBLs of NPSLBLs and PSSLBLs. The free energy comprises of five different contributions: 1) the free energy change for deforming the protein in the bilayer with respect to the conformation of the protein in the membrane, 2) the free energy change for reorienting the protein in the bilayer about the first Euler angle with the conformation of the protein restrained, 3) the free energy change for reorienting the protein in the bilayer about the second Euler angle with the conformation and the first Euler angle restrained, 4) the free energy change for changing the position of the center of the protein from the membrane to the bulk water with conformation and both Euler angles restrained, and 5) the free energy change for deformation of the protein in the bulk water with respect to the conformation of the protein in the membrane. Through

these simulations, we confirmed that SpoVM prefers NPSLBLs rather than PSSLBLs, indicating by a lower free energy change. Additionally, we revealed that the SpoVM membrane sensing is based on the interplay between the packing of the hydrophilic head groups of the lipids and the packing of the acyl chains of the lipids. Our findings reported in Chapter 5 might be helpful in the development of diagnosis and treatment of diseases associated with protein mislocalization.

# PHOSPHOLIPID BEHAVIOR AND DYNAMICS IN CURVED BIOLOGICAL MEMBRANES

by

Haoyuan Jing

Dissertation submitted to the Faculty of the Graduate School of the
University of Maryland, College Park, in partial fulfillment
of the requirements for the degree of
Doctor of Philosophy
2020

Advisory Committee:
Associate Professor Siddhartha Das, Chair
Associate Professor Amir Riaz
Professor Doron Levy
Professor Peter W. Chung
Dr. Kumaran Ramamurthi
Associate Professor Silvina Matysiak, Dean's Representative

© Copyright by
Haoyuan Jing
2020

# Acknowledgements

This work was funded by the University-of-Maryland-National-Cancer-Institute Partnership for Integrative Cancer Research (H.J., K.S.R., and S.D.) and the Intramural Research Program of the National Institutes of Health, National Cancer Institute, Center for Cancer Research (K.S.R.). We also acknowledge the fact that the simulations reported in this study *utilized the computational resources of the NIH HPC Biowulf cluster.*

# Table of Contents

# List of Abbreviations

Lipid BiLayer (LBL)

Nanoparticle Supported Lipid BiLayer (NPSLBL)

Plane Substrate Supported Lipid BiLayer (PSSLBL)

NanoParticle (NP)

PhosphoCholine (PC)

headgroup inversed PhosphoCholine (CP)

Molecular Dynamics (MD)

Dissipative Particle Dynamics (DPD)

Monte Carlo (MC)

Root Mean Square Deviation (RMSD)

# Chapter 1: Background and Motivation

## *1.1. Protein Membrane Curvature Sensing*

The proper protein localization is a necessary condition for the protein conducting its function. Ploidy, cell shape, and cell migration may all be dysfunctional if the protein is mis-located[1]. Cells exploited geometric cues, self-assembly, and restricted sites of assembly to facilitate localization of anchor proteins which in turn, govern the localization of additional proteins.[2] Experiments show some amphipathic alpha helix protein can use membrane curvature as a beacon for its correct membrane binding site[3-5]. The specific example we study through this proposal is SpoVM. SpoVM is a 26 amino acid-long amphipathic alpha-helical protein that uses an affinity/cooperativity-driven mechanism to preferentially embed in convex membrane surface of a ~1-micron diameter internal daughter cell formed during sporulation in the model bacterium *Bacillus subtilis*.[6,7] Despite the mechanistic understanding of how the protein behaves with differently curved membranes, it remains unclear what physical features of appropriately curved membranes cause SpoVM to sense the subtle membrane curvature. Three possible mechanisms have been advanced to explain this phenomenon: (1) three are more surface defects on very highly curved membranes, which can provide a higher number of binding sites for certain shape-sensing proteins that shallowly insert into the membrane;[8-10] (2) in membranes that are curved at the micron scale, membrane curvature affects the packing of the acyl chains, which, in turn ,regulate the binding of proteins that are deeply buried in the lipid bilayer;[8] and (3) in the so-called "Velcro model",

membranes with higher curvature may facilitate the folding of certain proteins to drive preferential adsorption of that protein into the membrane[11]

*1.2. Nanoparticle Supported Lipid Bilayer*

The Nanoparticle Supported Lipid Bilayer (NPSLBL), or so called the Spherical Supported Vesicle (SSV), refers to a vesicle supported by a spherical nanoparticle (NP)[12]. The spherical NP is surrounded by a single spherical bilayer, either in direct connect with the NP if the NP is made of metal oxide[13] or separate from the surface of the NP by a thin layer of water if the NP is made of silica[12]. The NPSLBL has received tremendous recent interests for a large number of applications ranging from target-specific drug and gene delivery[14-18] to characterizing molecules that respond to the variations in curvatures.[8, 19] NPSLBL has better physical and chemical stability then lipid vesicles (liposomes) and offers opportunities to tune the charge type, charge density[20], and most importantly, better control of size, since the size of NPSLBL is basically the size of the NP.[12] These advantages of the NPSLBL make it become the model of the curved membrane system in the simulations employed in the present thesis.

*1.3 Dissertation Structure*

In Chapter 1, we discussed the background and motivation for this dissertation. The dissertation is inspired by the increasing usage of NPSLBL as drug delivery carrier and newly finding of the protein membrane curvature sensing. In Chapter 2 and 3, we carried out MD simulation to reveal the properties of pre-assembled and self-assembled NPSLBL. Our findings not only confirmed the experimental results such

as lipid diffusivity and the exist of thin a water layer between the NP and the LBL, but also revealed properties beyond the capacity of experiments, including lipid distribution and confined water diffusivity. In Chapter 4, the energetics of lipid flip flop in both NPSLBL and Planar Supported Lipid Bilayer (PSSLBL) are studies by MD simulation. We find out that curvature plays an insignificant role in the energetics of lipid flip flop, which is confirmed by experiments as well. In Chapter 5, The energetics of SpoVM binding to NPSLBL and PSSLBL are simulated by MD. We firstly confirmed that SpoVM prefers to NPSLBL than PSSLBL as the free energy changes associated with SpoVM binding to NPSLBL is lower than PSSLBL. Then we conclude that the SpoVM's preference to NPSLBL than PSSLBL is due the the higher hydrophobic density of the NPSLBL. Finally, in Chapter 6, we proposed how this topic can be advanced, including developing new polarizable force field to better simulate the SpoVM folding and experiments to confirm the conclusions of Chapter 5.

*Bibliography*


1. Hall, A. The Cytoskeleton and Cancer. Cancer and Metastasis Reviews 2009, 28 (1-2), 5–14.
2. Rudner DZ; Losick R. Protein Subcellular Localization in Bacteria. Cold Spring Harbor Perspectives in Biology 2010, 2 (4), 000307 DOI: 10.1101/cshperspect. a000307.
3. K. Machida and S.-I. Ohnishi, Effect of Bilayer Membrane Curvature on Activity of Phosphatidylcholine Exchange Protein. *Biochim. Biophys. Acta* **596**, 201–209 (1980).
4. H. Huang, J. M. Ball, J. T. Billheimer, and F. Schroeder, Interaction of the n-terminus of Sterol Carrier Protein 2 with Membranes: Role of Membrane Curvature. *Biochem. J.* **344**, 593–603 (1999).
5. J. Bigay, P. Gounon, S. Robineau, and B. Antonny, Lipid Packing Sensed by Arfgap1 Couples Copi Coat Disassembly to Membrane Bilayer Curvature. *Nature* **426**, 563–566 (2003).
6. K. S. Ramamurthi, S. Lecuyer, H. A. Stone, and R. Losick, Geometric Cue for Protein Localization in a Bacterium. *Science* **323**, 1354–1357 (2009).
7. R. L. Gill, J.-P. Castaing, J. Hsin, I. S. Tan, X. Wang, K. C. Huang, F. Tian, and K. S. Ramamurthi, Structural Basis for the Geometry-driven Localization of a Small Protein. *Proc. Natl. Acad. Sci.* **112**, E1908–E1915 (2015).
8. J. Bigay and B. Antonny, Curvature, Lipid Packing, and Electrostatics of Membrane Organelles: Defining Cellular Territories in Determining Specificity. *Developmental Cell* **23**, 886–895 (2012).

9. S.-T. Yang, J. Y. Lee, H.-J. Kim, Y.-J. Eu, S. Y. Shin, K.-S. Hahm, and J. I. Kim, Contribution of a Central Proline in Model Amphipathic α-helical Peptides to Self-Association, Interaction with Phospholipids, and Antimicrobial Mode of Action. *FEBS J.* **273**, 4040–4054 (2006).
10. N. S. Hatzakis, V. K. Bhatia, J. Larsen, K. L. Madsen, P.-Y. Bolinger, A. H. Kunding, J. Castillo, U. Gether, P. Hedegård, and D. Stamou, How Curved Membranes Recruit Amphipathic Helices and Protein Anchoring Motifs. *Nature Chem. Biol.* **5**, 835 (2009).
11. D. Higgins and J. Dworkin, Recent Progress in Bacillus Subtilis Sporulation. *FEMS Microbiol. Rev.* **36**, 131–148 (2012).
12. Bayer TM; Bloom M. Physical Properties of Single Phospholipid Bilayers Adsorbed to Micro Glass Beads. A New Vesicular Model System Studied by 2h-Nuclear Magnetic Resonance. *Biophys. J.* **1990**, *58* (2), 357–362.
13. Troutier, A.-L.; L. Catherine. An Overview of Lipid Membrane Supported by Colloidal Particles. *Adv. Colloid Interface Sci.* **2007**, *133*, 1–21.
14. Ashley, C. E.; Carnes, E. C.; Phillips, G. K.; Padilla, D.; Durfee, P. N.; Brown, P. A.; Hanna, T. N.; Liu, J.; Phillips, B.; Carter, M. B.; Carroll, N. J.; Jiang, X.; Dunphy, D. R.; Willman, C. L.; Petsev, D. N.; Evans, D. G.; Parikh, A. N.; Chackerian, B.; Wharton, W.; Peabody, D. S.; Brinker, C. J. The Targeted Delivery of Multicomponent Cargos to Cancer Cells by Nanoporous Particle-Supported Lipid Bilayers. *Nature Mater.* **2011**, *10*, 389-397.

15. Tarn, D.; Ashley, C. E.; Xue, M.; Carnes, E. C.; Zink, J. I.; Brinker, C. J. Mesoporous Silica Nanoparticle Nanocarriers: Biofunctionality and Biocompatibility. *Acc. Chem. Res.* **2013**, *46*, 792-801.
16. Liu, J.; Jiang, X.; Ashley, C.; Brinker, C. J. Electrostatically Mediated Liposome Fusion and Lipid Exchange with a Nanoparticle-Supported Bilayer for Control of Surface Charge, Drug Containment, and Delivery. *J. Am. Chem. Soc.* **2009**, *131*, 7567-7569.
17. Lin, Y.-S.; Haynes, C. L. Impacts of Mesoporous Silica Nanoparticle Size, Pore Ordering, and Pore Integrity on Hemolytic Activity. *J. Am. Chem. Soc.* **2010**, *132*, 4834-4842.
18. Liu, J.; Stace-Naughton, A.; Jiang, X.; Brinker, C. J. Porous Nanoparticle Supported Lipid Bilayers (Protocells) as Delivery Vehicles. *J. Am. Chem. Soc.* **2009**, *131*, 1354-1355.
19. Fu, R; Gill, R. L.; Kim, E. Y.; Briley, N. E.; Tyndall, E. R.; Xu, J.; Li, C.; Ramamurthi, K. S.; Flanagan, J. M.; Tian, F. Spherical Nanoparticle Supported Lipid Bilayers for the Structural Study of Membrane Geometry-Sensitive Molecules. *J. Am. Chem. Soc.* **2015**, *137*, 14031-14034.
20. Gopalakrishnan G; Rouiller I; Colman DR; Lennox RB. Supported Bilayers Formed from Different Phospholipids on Spherical Silica Substrates. *Langmuir* **2009**, *25*, 5455–5458.

# Chapter 2: Nanovesicles versus Nanoparticle-Supported Lipid Bilayers: Massive Differences in Bilayer Structures and in Diffusivities of Lipid Molecule and Nanoconfined Water*

***Abstract:*** *In this chapter, we conduct molecular dynamics (MD) simulations to compare the architecture and properties of preformed nanoparticle-supported lipid bilayers (NPSLBLs) with the free vesicles of similar dimensions. Three key differences emerge. First, we witness that for a free vesicle, a much larger number of lipid molecules occupy the outer layer as compared to the inner layer; on the other hand, for the NPSLBL the number of lipid molecules occupying the inner and outer layers is identical. Second, we witness that the diffusivities of the lipid molecules occupying both the inner and the outer layers of the free vesicles are identical, whereas for the NPSLBLs the diffusivity of the lipid molecules in the outer layer is more than twice the diffusivity of the lipid molecules in the inner layer. Finally, the NPSLBLs entrap nanoscopic thin water film between the inner lipid layer and the NP and the diffusivity of this water film is nearly 1 order of magnitude smaller than the diffusivity of the bulk water; on the other hand, the water inside the free vesicles has a diffusivity that is only slightly lower than that of the bulk water. Our findings,*

* The contents of this Chapter have been published as the following journal article: Jing, H.; Wang, Y.; Desai, P. R.; Ramamurthi, K. S.; Das, S. "Nanovesicles Versus Nanoparticle- Supported Lipid Bilayers: Massive differencesin Bilayer Structures and in Diffusivities of Lipid Molecules and Nanoconfined Water." *Langmuir* **2019**, *35*, 2702-2708.

*possibly the first probing the atomistic details of the NPSLBLs, are anticipated to shed light on the properties of this important nanomaterial with applications in a large number of disciplines ranging from drug and gene delivery to characterizing curvature sensitive molecules.*

## *2.1. Introduction*

Nanoparticle-supported lipid bilayer (NPSLBL) systems have emerged as remarkable nanomaterials widely employed for applications like targeted drug and gene delivery,[1-9] multi-modal diagnostics,[10] characterization of the curvature-sensitive molecules,[11] treatment of hydrophobic contaminants in soil,[12] and many more. The most prominent version of such NPSLBL system used for drug and gene delivery is the protocell,[1-8] which consists of LBL supported by a mesoporous NP. The presence of the LBL ensures a camouflaging nature of the NPSLBL that allows evading the immune response of the body, while the mesoporous silica particle affords advantages such as the ability to carry multiple cargos and cargos of various chemical compositions, larger circulation time, and an enhanced stability of the cargos being carried. While there has been some research in experimentally characterizing the properties and behaviors of such protocells and NPSLBLs,[13-15] very little investigation has been conducted to probe the detailed nanoscopic configurations and properties of these NPSLBLs by using Molecular Dynamics (MD) simulations. This is specially surprising given the significant amount of MD simulation studies of related systems such as NPs interacting with LBLs,[16-20] LBLs supported on planar substrates,[21-26] and free vesicles (which represents LBL-encapsulated liquid cavity).[27-33]

In this chapter, we employ MD simulations to study for the first time the properties of NPSLBLs with the LBL being composed of the POPC (phosphatidylcholine) lipid molecules. We compare our findings with the properties of a similar-sized free nanovesicle composed of the POPC lipid molecules and discover three startling differences. First, we witness that for the free vesicle the number of lipid molecules occupying the outer layer is larger than that occupying the inner layer, while for the NPSLBL the number of lipid molecules are identical in both the inner and the outer layers. Second, we identify identical diffusivities of the lipid molecules occupying the inner and outer layers in the free vesicle, while in the NPSLBL the diffusivity of the lipid molecules in the inner layer is less than half of the lipid molecules in the outer layer. We associate both these findings to the presence of the NP core in the NPSLBL that alters the pressure and the mobility environments of the inner layers of the NPSLBL. The third important observation concerns the confined water. For the free vesicle, the confined water is the water confined in the cavity formed by the LBL. On the other hand, for the NPSLBL, the confined water is a few-layer water molecules occupying the space between the inner layer of the lipid molecules and the NP core. We witness that while the confined water has a density identical to the bulk density in the free vesicle, for the NPSLBL the confined water has a distinctly reduced density as compared to the bulk water. Secondly and more importantly, the confined water in the NPSLBL shows a diffusivity value that is more than one order of magnitude smaller than that of the bulk water; on the other hand, for the free vesicle the confined water has a diffusivity that is $1/3^{rd}$ of that of the bulk water. We anticipate that all these fundamental and

*hitherto unknown* nanoscopic information concerning the structure and diffusivity of the LBLs as well as the property of the confined water will be essential for a better design of the NPSLBL system for applications in targeted drug delivery and molecular sensing.

## *2.2. Simulation Set Up*

A free vesicle of $r_0$ = 8nm (see Fig. 2.2a) was produced by packmol.[34] In the initial configuration, we started with 1639 POPC lipid molecules occupying both the inner leaflet/layer (shown in red in Fig. 2.2b) and the outer leaflet/layer (shown in green in Fig. 1b) of the vesicle. The POPC molecules were represented by the Coarse-Grained (CG) Martini model,[35] as shown in Fig. 2.1a. The vesicle was placed in a cubic box (28.8nm×28.8nm×28.8nm) filled with coarse-grained (CG) water beads.[35] One CG water bead represents four actual water molecules.[35] There were 12490 water beads (shown in pink in Fig. 2.2b) in the space outside the vesicle but inside the water box, while 42027 water beads (shown in blue in Fig. 1b) inside the vesicle. In addition, Anti-Freeze (AF) water beads were introduced (1/9$^{th}$ of the total number of normal water molecules) into the system to prevent ice formation.[36] The size of the initial configuration is inspired by the size of the smallest stable vesicles as revealed by the experiments.[4]

For the NPSLBL, the initial configuration was produced by replacing the water molecules present inside the vesicle in the free vesicle system (shown in blue in Fig. 2.2b) by a hydrophilic shell constructed with the Nda beads (shown in Fig. 2.1b).[37] We fixed the position of the Nda beads of the NP during the simulation. In

addition, as suggested by Charitat *et al.*,[38] we added two layers of CG water beads (shown in blue in Fig. 2.2c) along with 10% (number density) of AF water beads between the shell and the vesicle.

Simulations were conducted by using the NAMD software package[39] with Martini force field.[35] Periodic boundary conditions were applied in three directions in presence of the NPT thermostat. The simulations were carried out at a constant pressure of 1 bar and a constant temperature of 310 K. Finally, for the simulations we used a timestep of 40 fs; we first carried out a minimization involving 20000 steps, followed by an equilibration that lasted for 1000 ns.

## *2.3. Results*

### *2.3.1. Equilibration Process*

Here we first describe the equilibration procedure for the free vesicle starting from the initial configuration as described in section 2.2. First, a hole is formed on the surface of the vesicle during equilibration (see Fig. 2.3a). In a previous MD simulation study, similar spontaneous hole formation during the equilibration of free vesicles has been reported.[30] Formation of this hole meant that water from inside the vesicle flowed out towards the bulk. In addition, the path towards equilibration is characterized by several lipid molecules undergoing flip-flop events. “Flipping” refers to the movement of the lipids from the outer to the inner leaflet, while the “flopping” refers to the movement of the lipids from the inner to the outer leaflet.[40]

During this equilibration, the number of the “flopping” incidents are much more than the “flipping” incidents.

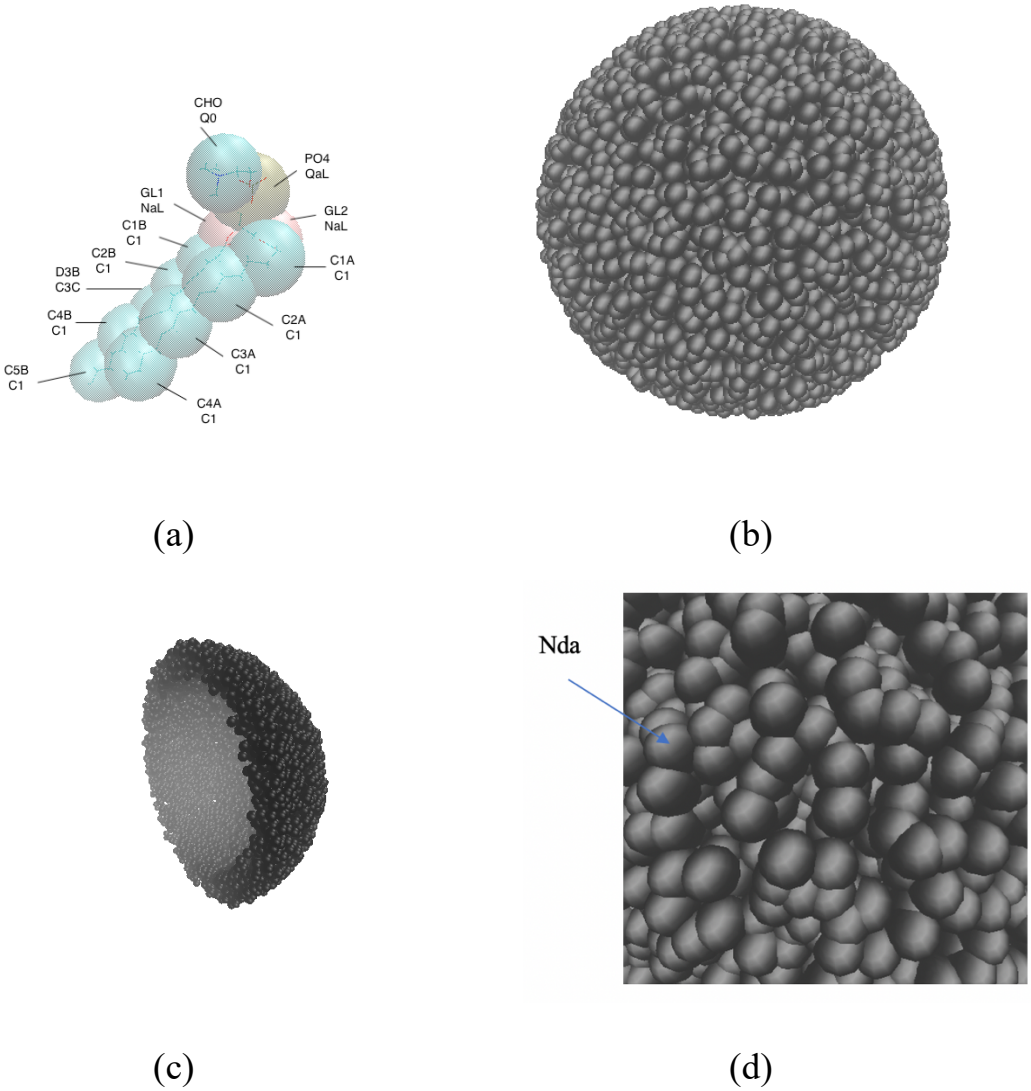


***Figure 2. 1: Model of POPC and NP***

*(a) Martini model of the POPC lipid molecule, where the lipid molecule is represented by 13 large spheres (beads). Each of the beads is so labelled that their names are identified on the upper row and their types are identified on the bottom row (for example, the name of the "golden" color bead is "$PO_4$" and its type is "QaL"). (b) Snapshot of the NP. (c) Snapshot of half of the NP. (d) Zoom in view of the NP surface.*

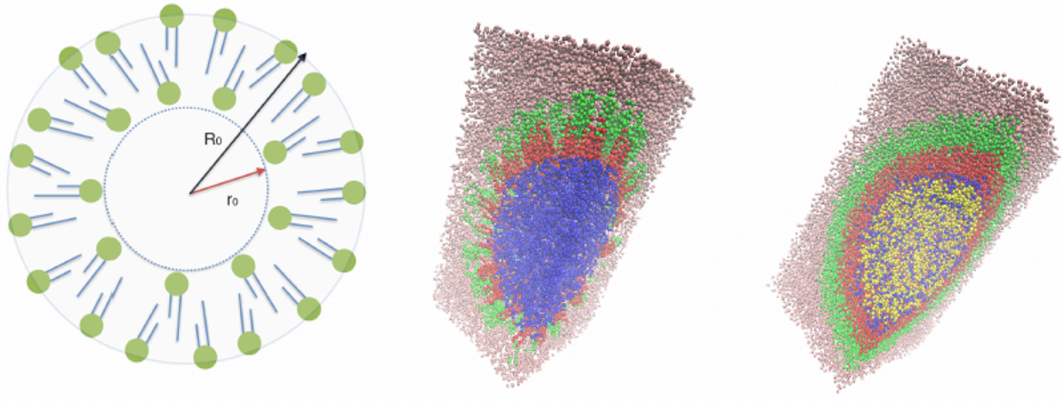


(a) (b) (c)

***Figure 2. 2: Structure of Free Vesicle and NPSLBL***

*(a) Schematic of the free vesicle vesicle and the NPSBL having an inner radius r and an outer radius R. For the free vesicle, the space within the bilayer is filled with water, while that for the NPSBL is filled by a hydrophilic particle and a thin (few) layer of water molecules. (b) The initial configuration of free vesicle (only 1/4$^{th}$ of the vesicle has been displayed); Blue: water surrounded by the bilayer; red: lipids of the inner leaflet/layer; green: lipids of outer leaflet/layer; pink: water box. (c) The initial configuration of NPSBL (only 1/4$^{th}$ of the NPSLBL has been displayed); red: lipids of inner leaflet/layer; green: lipids of outer leaflet; pink: water box; yellow: hydrophilic nanoparticle shell; blue: confined water.*

We identify that most of these "flopping" incidents occur around this hole (compare Figs. 2.3(a) and 2.3(b)) and these "flopping" and "flipping" events continue to occur even when the free vesicle has attained equilibrium (i.e., we are looking into a *dynamic equilibrium* with the continuously occurring flipping and flopping incidents, as has been well established experimentally[40]).

Unlike the free vesicles, during the equilibration process, the molecular architecture of the NPSLBL changes little as compared to the initial configuration with the

"flipping" and "flopping" incidents occurring much less frequently [compare Figs. 2.4 (a) and 2.4 (b)].

*2.3.2. Structure*

Here we compare the equilibrium structure of the free vesicle and the NPSBL. For the free vesicle, the outer radius is $R_0$=11.43 nm, while the inner radius is $r_0$=7.34 nm. The $R_0$ and $r_0$ values were defined as the average distance between the center of the vesicle and the respective $PO_4$ beads associated with the inner and the outer layers. More importantly, for the equilibrated free vesicle, we witness a large difference in the number of lipid molecules occupying the inner and the outer layers: 1302±2 lipid molecules occupy the inner layer, while a much large number (1976±2) of lipid molecules occupy the outer layer. Therefore, for the free vesicle, one can ascribe a surface area of 52Å$^2$ per lipid in the inner layer and a surface area of 83 Å$^2$ per lipid in the outer layer. These numbers are very close to previously reported values.[41]

For the NPSLBL, the outer radius is $R_0$=11.52 nm, while the inner radius is $r_0$=7.65 nm. Therefore, the size of the NPSLBL is very much similar to that of the free lipid vesicle. However, unlike the free vesicle, the number of the lipid molecules occupying the inner and outer layers is identical: there are 1639±2 lipids molecules occupying both the inner and the outer layers. This is the first important difference in the structure of the NPSLBL as compared to the free vesicle. For the NPSLBL, therefore, one can ascribe a surface area of 45 Å$^2$ per lipid in the inner layer and a surface area of 102 Å$^2$ per lipid in the outer layer. Mhashal and Roy[25] established that a LBL (composed of DPPC lipids) supported on a *planar substrate* demonstrated a

surface area of 76 $Å^2$ per lipid, which appears to be approximately the *mean* of the per lipid surface area values at the inner and outer layers for the NPSLBL.

Fig. 2.5 illustrates this variation in the number distribution of the lipid molecules (in the inner and outer layers) between the free vesicle and the NPSLBL. For the free vesicle, the significantly large Laplace pressure of the water confined inside the vesicle exerts a large outward force on the lipid molecules occupying the inner layer enforcing them to move out to the outer layer. This effect, which is evident from the significantly large number of the flipping events that occur during the equilibration process of the free vesicles, is responsible for ensuring this large difference in the number of lipid molecules between the outer and inner layers in the free vesicle. On the other hand, for the NPSLBL there is only a very thin layer of water entrapped between the inner layer of the lipid molecules and the hydrophilic NP core. This layer of water is unable to exert such a large pressure on the inner layer of lipid molecules. Accordingly, we witness a much less difference between the initial and the final configurations of the NPSLBL and the flipping events are also much less; eventually, this ensures that the number of lipid molecules in the inner and outer layers is almost identical for the NPSLBL.

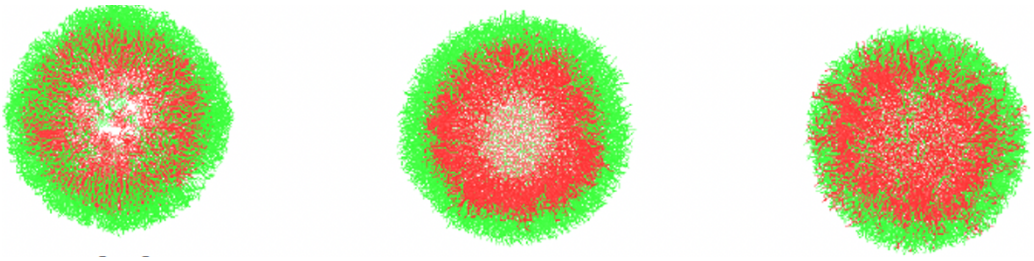

(a) (b) (c)

***Figure 2. 3: Evolution of free vesicle***

*(a) the initial configuration, (b) the hole formed on the vesicle surface, and (c) the equilibrated configuration. Green: lipids occupying the outer leaflet at the initial condition; Red: lipids occupying the inner leaflet at the initial condition. Water has been hidden for a clearer view.*

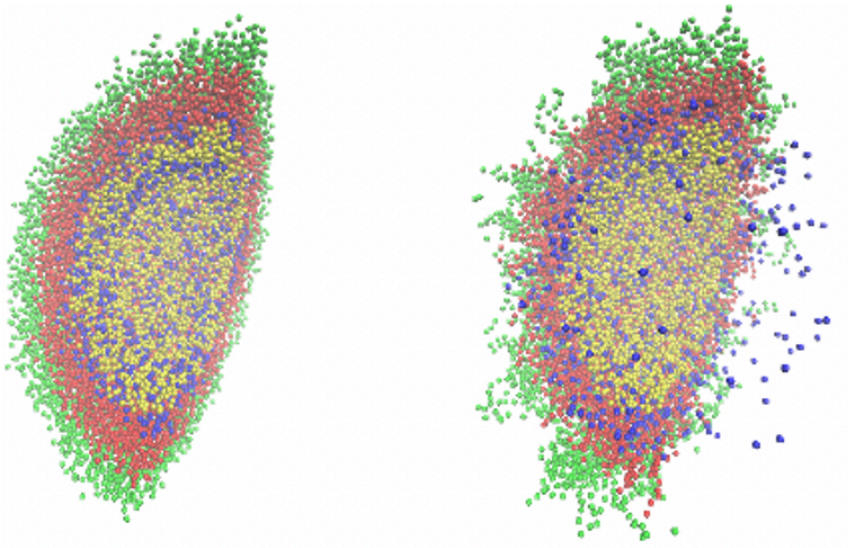

(a) (b)

***Figure 2. 4: Evolution of the NPSBL***

*(a) the initial configuration; (b) the equilibrated configuration of molecules shown in (a). In both (a) and (b), only 1/4$^{th}$ of the NPSLBL has been displayed and water has been hidden for cleaner view.*

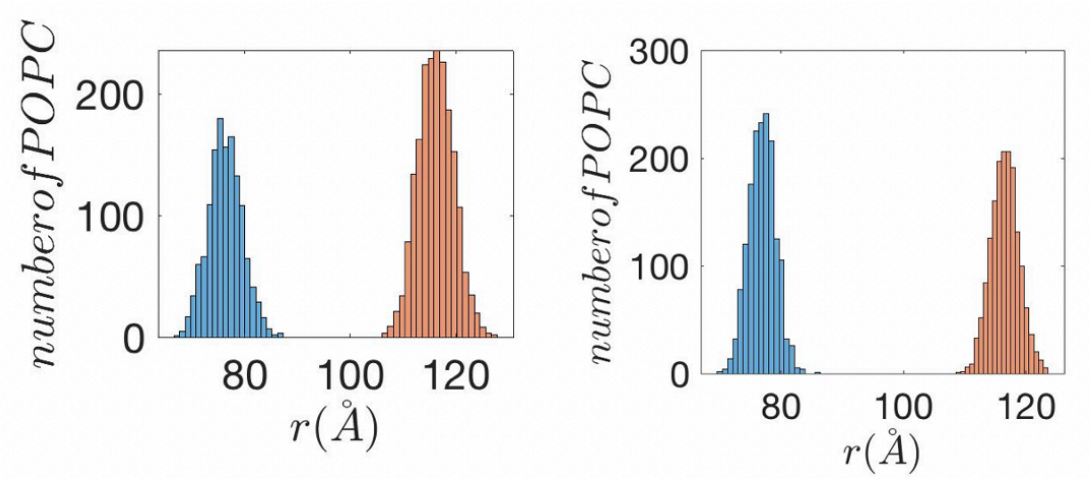


(a) (b)

***Figure 2. 5: POPC distribution***

*POPC number distribution along the radial direction for (a) a free vesicle and (b) a NPSLBL.*

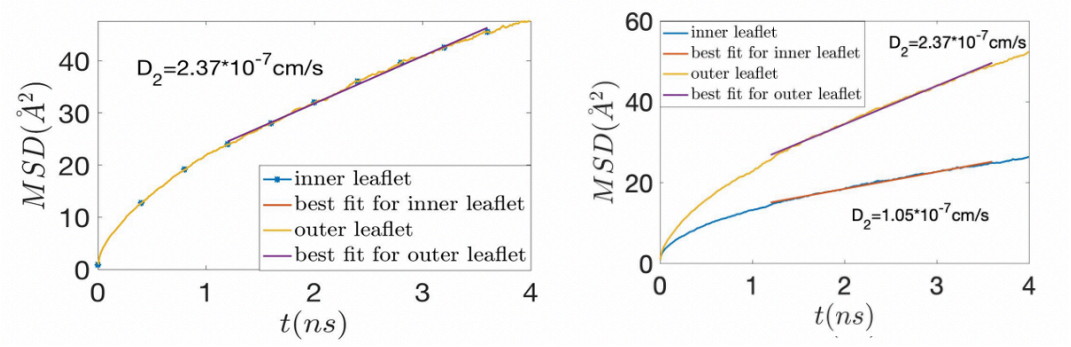


(a) (b)

***Figure 2. 6: MSD for POPC***

*MSD for the lipid molecules occupying the inner and outer layers in (a) a free vesicle and (b) a NPSLBL. In both (a) and (b), we demonstrate the manner in which we identify the slope in the linear region of the MSD-vs-time variation and accordingly quantify the diffusivity [see eq. (2.1)]. The diffusivity $D_2$ of the lipid molecules in the inner and outer layers of the free vesicle is identical.*

*2.3.3. Diffusivity of the Lipid Molecules*

Diffusivities of the lipid molecules occupying the inner and the outer layers in both the systems (free vesicles and the NPSLBLs) were calculated following the Einstein relation:

$$D_d = \lim_{t\to\infty} \frac{1}{2d} \frac{\langle MSD \rangle}{t}, \qquad (2.1)$$

where <MSD> is mean squared displacement, $t$ is the time and $d$ is the number of dimensions. For the lipid molecules occupying the inner and outer layers in both the free vesicle and the NPSLBL, $d=2$ and $D_2$ represents lateral diffusivity. The diffusivity $D_d$ is calculated as 1/(2d) of the slope of linear region of MSD-vs-*time* plot,[25,26] as illustrated in Fig. 2.6. The computed diffusivity values of the lipid molecules of different layers for the different systems are provided in Table 1. Like the number of lipid molecules occupying different layers, here too we witness a large difference between the two systems (free vesicle and the NPSLBL). For the free vesicle, the diffusivity values for the lipid molecules occupying both the inner and the outer layers are identical ($D_{2,\text{ inner}} = D_{2,\text{ outer}} = 2.27\times10^{-7}$ cm$^2$/s). On the other hand, for the NPSLBL, the diffusivity value for the lipid molecules occupying the outer layer ($D_{2,\text{outer}} = 2.37\times10^{-7}$ cm$^2$/s) is more than double than that of the lipid molecules occupying the inner layer ($D_{2,\text{inner}} = 1.05\times10^{-7}$ cm$^2$/s). The physical barrier imposed by the presence of the hydrophilic NP core restricts the movement of the lipid molecules located on the inner layer of the NPSLBL and thus enforces this significantly reduced diffusivity value of the lipid molecules occupying the inner layer of the NPSLBL. On the other hand, for the free vesicle, the lipid molecules occupying both the inner and the outer layers experience only water in their surroundings leading to $D_{2,\text{ inner}} = D_{2,}$

$_{outer}$. This is the second important difference in the properties of the NPSLBL as compared to the free vesicle as unraveled by our MD simulations.

*2.3.4. Properties of the Confined Water:*

Both the free vesicle and the NPSLBL confine water but to completely different extents. The free vesicle, for example, confines the water within the hollow space created by the LBL. On the other hand, the NPSLBL confines the water in a very thin layer between the inner lipid layer and the NP core. This is evident from the radial variation of the density of the water molecules for both the free vesicle and the NPSLBL (see Fig. 2.7).

A better assessment of the degree of the confinement can be obtained by probing the variation in the diffusivity of the confined and the bulk water. For the diffusivity calculation, we employ eq. (1) again; however, here the number of dimensions for the water molecules is $d$=3 and hence $D_d$=$D_3$ represents self-diffusivity. Similar to Fig. 2.6, the diffusivity values are obtained by obtaining the slope in the linear region of the MSD-vs-time curve, as shown in Fig. 2.8. The diffusivity of the bulk water is $2.58\times10^{-5}$ cm$^2$/s for the free vesicle and $2.52\times10^{-5}$ cm$^2$/s for the NPSLBL (the numbers are also provided in Table 2.1). So, our numbers are very close to the experimentally reported bulk water diffusivity of $2.0\times10^{-5}$ cm$^2$/s at 300 K.[35]

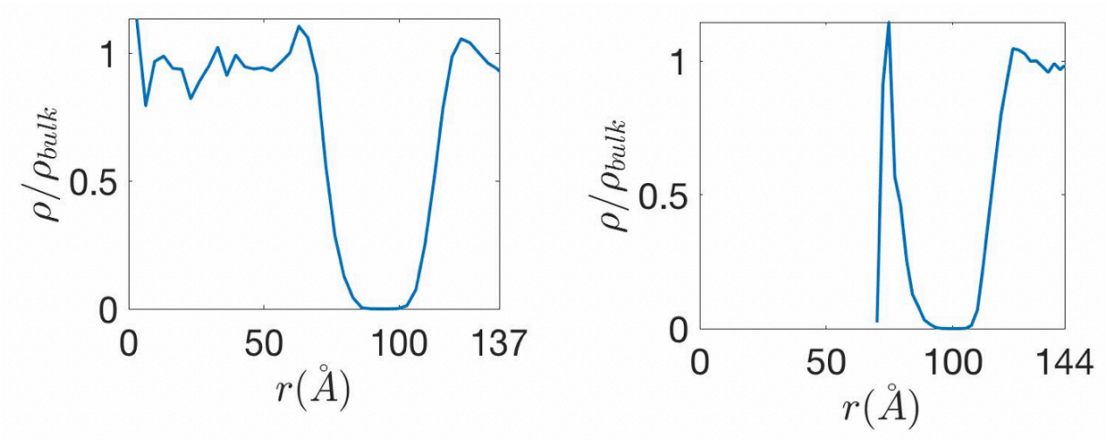


(a) (b)

***Figure 2. 7: Water Molecules Distribution***

*Variation of the water density along the radius for (a) a free vesicle and (b) a NPSLBL.*

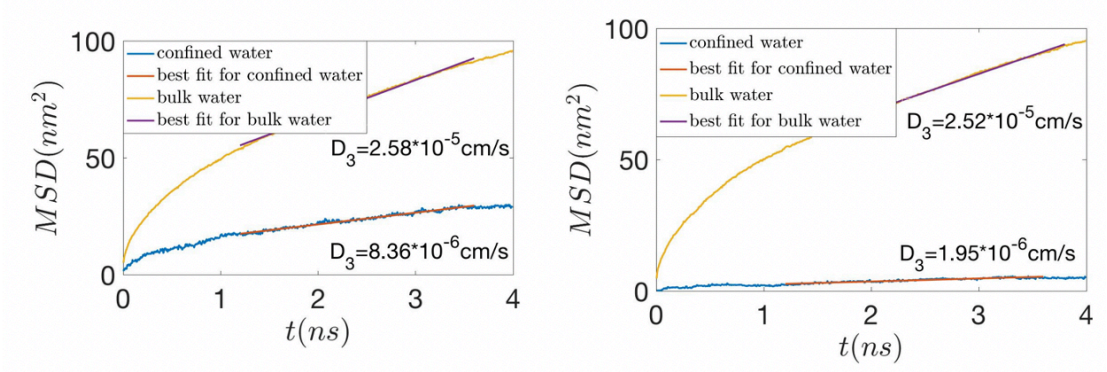


(a) (b)

***Figure 2. 8: MSD for water***

*MSD for the water molecules (in the bulk and confined state) in (a) a free vesicle and (b) a NPSLBL. In both (a) and (b), we demonstrate the manner in which we identify the slope in the linear region of the MSD-vs-time variation and accordingly quantify the diffusivities of the bulk and confined water in both the systems [see eq. (2.1)].*

On the other hand, there is a large difference in the diffusivity values between the confined water molecules in the free vesicle and the NPSLBL. The diffusivity of the confined water for the free vesicle is $8.36\times10^{-6}$ $cm^2/s$ (see Fig. 2.8 and Table 2.1), which is $1/3^{rd}$ of the bulk water. The result agrees well with that reported in previous studies.[26] On the other hand, for the confined thin water layer between the inner lipid layer and the NP for the NPSLBL, we witness a diffusivity value ($1.95\times10^{-6}$ $cm^2/s$) that is more than one order of magnitude smaller than that of the bulk value (see Fig. 2.8 and Table 2.1). The diffusivity of the water molecules in the water layer entrapped between the inner lipid layer and the solid support for the *LBL supported by a planar substrate* is found to be $1/3^{rd}$ of the bulk water.[26] Therefore, this large lowering (suggesting a possible ordering of the water molecules) in the diffusivity of the confined water is unique to the spherically-supported or the NP-supported LBL. This vast difference in the diffusivity values between the confined water in NPSLBL and the free vesicle is the third important finding of this paper.

***Table 2. 1: Summary of the Conditions at Different States and Equilibrium Properties of the Free Vesicle and the NPSLBL***

| **Conditions/ Properties** | **Free Vesicle** | **NPSLBL** |
|---|---|---|
| Initial configuration | • 1639 POPC in the inner layer<br>• 1639 POPC in the outer layer<br>• $r_0$ = 80 Å (inner radius)<br>• $R_0$ = 118 Å (outer radius) | • 1639 POPC in the inner layer<br>• 1639 POPC in the outer layer<br>• $r_0$ = 80 Å (inner radius)<br>• $R_0$ = 118 Å (outer radius) |
| Equilibrated configuration | • 1302 POPC in the inner layer<br>• 1976 POPC in the outer layer<br>• $r_0$ = 73.4 Å (inner radius)<br>• $R_0$ = 114.3 Å (outer radius) | • 1641 POPC in the inner layer<br>• 1637 POPC in the outer layer<br>• $r_0$ = 76.5 Å (inner radius)<br>• $R_0$ = 115.2 Å (outer radius) |
| Later Diffusion Coefficient | • $D_{2,\text{inner}} = 2.27\times10^{-7}$ cm$^2$/s<br>• $D_{2,\text{outer}} = 2.27\times10^{-7}$ | • $D_{2,\text{inner}} = 1.05\times10^{-7}$ cm$^2$/s<br>• $D_{2,\text{outer}} = 2.37\times10^{-7}$ cm$^2$/s |

| | | |
|---|---|---|
| ($D_2$) of the Lipids | $cm^2/s$ | |
| Self Diffusion Coefficient ($D_3$) of Water | • $D_{3,bulk} = 2.58\times10^{-5}$ $cm^2/s$<br>• $D_{3,confined} = 8.36\times10^{-6}$ $cm^2/s$<br>(confined water for the free vesicle is the water confined in the cavity formed by the LBL) | • $D_{3,bulk} = 2.52\times10^{-5}$ $cm^2/s$<br>• $D_{3,confined} = 1.95\times10^{-6}$ $cm^2/s$<br>(confined water for the NPSLBL is the water confined between the NP and the inner layer of the NPSLBL) |

## *2.4. Conclusions*

MD simulations have been employed to provide for the first time to study a very important emerging nanomaterial, namely NPSLBL. In the process, we provide simulation-based evidence of the large differences in the between the NPSLBL and a similar-sized free vesicle. These differences manifest as (a) identical number of lipid molecules in the inner and outer leaflet for the NPSLBL, while a distinctly larger number of lipid molecules in the outer layer as compared to that in the inner layer for the free vesicle, (b) identical diffusivities of the lipid molecules in the inner and outer layers for the free vesicle, while the diffusivity of the lipid molecule in the outer layer

is more than double of that in the inner layer for the NPSLBL, and (c) the nanoconfined water molecules for the NPSLBL has diffusivity that is more than one order of magnitude smaller than bulk water diffusivity, while for the free vesicle this diffusivity difference between the bulk and nanoconfined water is much less.

## *Bibliography*


1. Ashley, C. E., Carnes, E. C.; Phillips, G. K.; Padilla, D., Durfee, P. N., Brown, P. A., Hanna, T. N., Liu, J.; Phillips, B., Carter, M. B., Carroll, N. J., Jiang, X., Dunphy, D. R., Willman, C. L., Petsev, D. N., Evans, D. G., Parikh, A. N., Chackerian, B., Wharton, W., Peabody, D. S., and Brinker, C. J., The Targeted Delivery of Multicomponent Cargos to Cancer Cells by Nanoporous Particle-Supported Lipid Bilayers. *Nat. Mater.* **2011**, 10, 389-397.
2. Tarn, D., Ashley, C. E., Xue, M., Carnes, E. C., Zink, J. I., and Brinker, C. J., Mesoporous Silica Nanoparticle Nanocarriers: Biofunctionality and Biocompatibility. *Acc. Chem. Res.* **2013**, 46, 792-801.
3. Liu, J., Jiang, X., Ashley, C., and Brinker, C. J., Electrostatically Mediated Liposome Fusion and Lipid Exchange with a Nanoparticle-Supported Bilayer for Control of Surface Charge, Drug Containment, and Delivery. *J. Am. Chem. Soc.* **2009**, 131, 7567-7569.
4. Lin, Y.-S., and Haynes, C. L., Impacts of Mesoporous Silica Nanoparticle Size, Pore Ordering, and Pore Integrity on Hemolytic Activity. *J. Am. Chem. Soc.* **2010**, 132, 4834- 4842.
5. Liu, J., Stace-Naughton, A., Jiang, X., and Brinker, C. J., Porous Nanoparticle Supported Lipid Bilayers (Protocells) as Delivery Vehicles. *J. Am. Chem. Soc.* **2009**, 131, 1354- 1355.
6. Al-Jamal, W. T., and Kostarelos, K., Liposome–nanoparticle Hybrids for Multimodal Diagnostic and Therapeutic Applications. *Nanomedicine* **2007**, 2, 85-98.

7. Fu, R., Gill, R. L., Kim, E. Y., Briley, N. E., Tyndall, E. R., Xu, J., Li, C., Ramamurthi, K. S., Flanagan, J. M., and Tian, F., Spherical Nanoparticle Supported Lipid Bilayers for the Structural Study of Membrane GeometrySensitive Molecules. *J. Am. Chem. Soc.* **2015**, 137, 14031-14034.
8. Gill Jr., R. L., Castaing, J-P., Hsin, J., Tan, I. S., Wang, X., Huang, K. C., Tian, F., and Ramamurthi, K. S., Structural Basis for the Geometry-driven Localization of a Small Protein. *Proc. Natl. Acad. Sci. USA* **2015**, *112*, E1908-E1915.
9. Kim, E. W., Tyndall, E. R., Huang, K. C., and Tian, F., Dash-and-Recruit Mechanism Drives Membrane Curvature Recognition by the Small Bacterial Protein SpoVM. *Cell Syst.* **2017**, *5*, 518-526.
10. Wang, H., Kim, B., and Wunder, S. L., Nanoparticle-Supported Lipid Bilayers as an in Situ Remediation Strategy for Hydrophobic Organic Contaminants in Soils. *Environment. Sci. Tech.* **2015**, 49, 529-536.
11. Wu, I-L., Narayan, K., Castaing, J-P., Tian, F., Subramaniam, S., and Ramamurthi, K. S., A Versatile Nano Display Platform from Bacterial Spore Coat Proteins. *Nature Comm.* **2015**, *6*, 6777.
12. Karauzum, H., Updegrove, T. B., Kong, M., Wu, I. L., Datta, S. K., and Ramamurthi, K. S. Vaccine Display on Artificial Bacterial Spores Enhances Protective Efficacy Against Staphylococcus Aureus Infection. *FEMS Microbiol. Lett.* **2018**, *365*, doi: https://doi.org/10.1093/femsle/fny190.

13. Ahmed, S., Nikolov, Z., and Wunder, S. L., Effect of Curvature on Nanoparticle Supported Lipid Bilayers Investigated by Raman Spectroscopy. *J. Phys. Chem. B* **2011**, 115, 13181-13190.

14. Wright, A. J., Richens, J. L., Bramble, J. P., Cathcart, N., Kitaev, V., O'Shea, P., and Hudson, A. J., Surface-Enhanced Raman Scattering Measurement from a Lipid Bilayer Encapsulating a Single Decahedral Nanoparticle Mediated by an Optical Trap. *Nanoscale* **2016**, 8, 16395-16404.

15. Guo, Y., Terazzi, E., Seemann, R., Fleury, J. B., and Baulin, V. A., Direct Proof of Spontaneous Translocation of Lipid-Covered Hydrophobic Nanoparticles Through a Phospholipid Bilayer. *Sci. Adv.* **2016**, 2, e1600261.

16. Van Lehn, R. C., and Alexander-Katz, A., Pathway for Insertion of Amphiphilic Nanoparticles into Defect-Free Lipid Bilayers from Atomistic Molecular Dynamics Simulations. *Soft Matt.* **2015**, 11, 3165-3175.

17. Gupta, R., and Rai, B., Effect of Size and Surface Charge of Gold Nanoparticles on Their Skin Permeability: A Molecular Dynamics Study. *Sci. Rep.* **2017**, 7, 45292.

18. Lei, J.-C.; Zhang, X.; Zhou, Z. Recent Advances in Mxene: Preparation, Properties, and Applications. *Frontiers of Physics : Selected Publications from Chinese Universities***2015**, *10* (3), 276–286 DOI: 10.1007/s11467-015-0493-x.

19. Lin, J-Q., Zheng, Y-G., Zhang, H-W., and Chen, Z., A Simulation Study on Nanoscale Holes Generated by Gold Nanoparticles on Negative Lipid Bilayers. *Langmuir* **2011**, 27, 8323-8332.

20. Fiedler, S. L., and Violi, A., Simulation of Nanoparticle Permeation Through a Lipid Membrane. *Biophys. J.* **2010**, 99, 144-152.
21. Lin, X., Wang, C., Wang, M., Fang, K., and Gu, N., Computer Simulation of the Effects of Nanoparticles' Adsorption on the Properties of Supported Lipid Bilayer. *J. Phys. Chem. C*, **2012**, 116, 17960-17968.
22. Schneemilch, M., and Quirke, N., Free Energy of Adsorption of Supported Lipid Bilayers from Molecular Dynamics Simulation. *Chem. Phys. Lett.* **2016**, 664, 199-204.
23. Richter, R. P., Berat, R., and Brisson, A. R., Formation of Solid-Supported Lipid Bilayers: An Integrated View. *Langmuir* **2006**, 22, 3497-3505.
24. Mannelli, I., Sagués, F., Pruneri, V., and Reigada, R., Lipid Vesicle Interaction with Hydrophobic Surfaces: A Coarse-Grained Molecular Dynamics Study. *Langmuir* **2016**, 32, 12632-12640.
25. Mhashal, A. R., and Roy, S., Self-Assembly of Phospholipids on Flat Supports. *Phys. Chem. Chem. Phys.* **2015**, 17, 31152-31160.
26. Xing, C., and Faller, R., Interactions of Lipid Bilayers with Supports: A Coarse-Grained Molecular Simulation Study. *J. Phys. Chem. B* **2008**, 112*,* 7086-7094.
27. Markvoort, A. J., van Santen, R. A., and Hilbers, P. A. J., Vesicle Shapes from Molecular Dynamics Simulations. *J. Phys. Chem. B* **2006**, 110*,* 22780-22785.

28. de Vries, A. H., Mark, A. E., and Marrink, S. J., Molecular Dynamics Simulation of the Spontaneous Formation of a Small DPPC Vesicle in Water in Atomistic Detail. *J. Am. Chem. Soc.* **2004**, 126, 4488-4489.
29. Marrink, S. J., and Mark, A. E., Molecular Dynamics Simulation of the Formation, Structure, and Dynamics of Small Phospholipid Vesicles. *J. Am. Chem. Soc.* **2003**, 125, 15233-15242.
30. Braun, A. R., and Sachs, J. N., Determining Structural and Mechanical Properties from Molecular Dynamics Simulations of Lipid Vesicles. *J. Chem. Theor. Comput.* **2014**, 10, 4160-4168.
31. Chng, C-P., *Soft Matt.* **2013**, 9, 7394.
32. Nakamura, T., and Shinoda, W., Method of Evaluating Curvature-Dependent Elastic Parameters for Small Unilamellar Vesicles Using Molecular Dynamics Trajectory. *J. Chem. Phys.* **2013**, 138, 124903.
33. Sun, X-L., Pei, S., Wang, J-F., Wang, P., Liu, Z-B., and Zhang, J., Coarse Grained Molecular Dynamics Simulation Study on Spherical and Tube like Vesicles Formed by Amphiphilic Copolymers. *J. Pol. Sci. B* **2017**, 55, 1220-1226.
34. Martínez, L., Andrade, R., Birgin, E. G., and Martínez, J. M., PACKMOL: A Package for Building Initial Configurations for Molecular Dynamics Simulations. *J. Comput. Chem.* **2009**, 30, 2157-2164.
35. Marrink, S. J., de Vries, A. H., and Mark, A. E., Coarse Grained Model for Semiquantitative Lipid Simulations. *J. Phys. Chem. B* **2004**, 108, 750-760.

36. Marrink, S. J., Risselada, H. J., Yefimov, S., Tieleman, D. P., and de Vries, A. H., The MARTINI Force Field: Coarse Grained Model for Biomolecular Simulations *J. Phys. Chem. B* **2007**, 111, 7812-7824.

37. Lin, X., Wang, C., Wang, M., Fang, K., and Gu, N., Computer Simulation of the Effects of Nanoparticles' Adsorption on the Properties of Supported Lipid Bilayer. J. Phys. Chem. C, **2012**, 116, 17960–17968.

38. Charitat, T., Bellet-Amalric, E., Fragneto, G., and Graner, F., Adsorbed and Free Lipid Bilayers at the Solid-Liquid Interface. *Eur. Phys. J. B* **1999**, 8, 583-593.

39. Phillips, J. C., Braun, R., Wang, W., Gumbart, J., Tajkhorshid, E., Villa, E., Chipot, C., Skeel, R. D., Kale, L., and Schulten, K., Scalable Molecular Dynamics with NAMD. *J. Comput. Chem.* **2005**, 26, 1781-1802.

40. Allhusen, J. S., and Conboy, J. C., The Ins and Outs of Lipid Flip-Flop. *Acc. Chem. Res.* **2017**, 50, 58-65.

41. Jambeck, J. P. M., Eriksson, E. S. E., Laaksonen, A., Lyubartsev, A. P., and Eriksson, L. A., Molecular Dynamics Studies of Liposomes as Carriers for Photosensitizing Drugs: Development, Validation, and Simulations with a Coarse-Grained Model. *J. Chem. Theory Comput.* **2014**, 10, 5-13.

# Chapter 3: Formation and Properties of Self-Assembled Nanoparticle Supported Lipid Bilayer Probed Through Molecular Dynamics Simulations*

***Abstract:*** *In this chapter, we have carried out coarse-grained molecular dynamics (MD) simulations to study the self-assembly procedure of a system of randomly placed lipid molecules, water beads, and a nanoparticle (NP). The self-assembly results in the formation of the nanoparticle-supported lipid bilayer (NPSLBL), with the self-assembly mechanism being driven by events such as the formation of small lipid clusters, merging of the lipid clusters in the vicinity of the NP to form NP-embedded vesicle with a pore, and collapsing of that pore to eventually form the equilibrated NPSLBL system overcoming a large free energy barrier. Subsequently, we quantify the properties and the configurations of this NPSLBL system. We reveal that unlike our proposition of equal number of lipid molecules occupying the inner and outer leaflets in a recent report studying the properties of preassembled lipid bilayer, the equilibrated self-assembled NPSLBL system demonstrates a much larger number of lipid molecules occupying the outer leaflet as compared to the inner leaflet. Secondly, the thickness of the water layer entrapped between the NP and the inner leaflet shows similar values as that predicted by experiments and our previous study. Finally, we reveal that, similar to our previous study, the diffusivity of the lipid molecules in the outer leaflet is larger than that in the inner leaflet but, due to higher*

*The contents of this Chapter have been published as the following journal article: Jing, H.; Wang, Y.; Desai, P. R.; Ramamurthi, K. S.; Das, S. "Formation and Properties of Self-Assembled Nanoparticle-Supported Lipid Bilayer Probed Through Molecular Dynamics Simulations." *Langmuir* **2020**, *36*, 5524-5533.

*temperature employed during our simulations, are even larger than that predicted by our previous study.*

## *3.1. Introduction*

The self-assembly of lipid molecules to form planar bilayers, or vesicles, or other heterogeneous structures (with entities such as proteins, DNA, carbon nanotubes, etc.) has been extensively probed using Molecular Dynamics (MD) and Monte Carlo (MC) simulations.[1-25] These studies have revealed critical information on issues such as (1) the conditions that decide if the self-assembly process will lead to the formation of a planar bilayer, or a closed vesicle, or a micelle;[3,9] (2) the structural and the packing orders in the lipid molecules during the process of self-assembly;[3,5,12] (3) the effect of temperature on the phase change and the structural order;[3] (4) the equilibrium protein position and configuration within a bilayer;[14] (5) the effect of polyethylene glycol (PEG) on the self-assembled structure;[17] (6) the structure of the carbon-nanotube-impregnated self-assembled bilayers;[18,20] (7) the formation and the structure of DNA-lipid complexes;[19] (8) the micelle formation by the lipid molecules around characteristic membrane proteins;[15] (9) the properties and structures of mixed bilayers;[21,25] (10) the lateral tension, elasticity, and mobility of the self-assembled membranes;[1,3] (11) the trans-membrane electrostatic potential for charged lipids;[10] (12) the conditions that lead to the rupture of the bilayer and enable the formation of worm-like micelle;[24] (13) the formation of lipid corona on a nanoparticle;[26] etc.

In this chapter, we employ MD simulations to study the self-assembly in a system of a nanoparticle and randomly placed POPC (palmitoyl-2-oleoyl-sn-glycero-

3-phosphocholine) lipid molecules. The system eventually evolves to form a self-assembled nanoparticle-supported lipid bilayer (NPSLBL). The NPSLBL is a nanomaterial that has received tremendous recent interests for a large number of applications ranging from target-specific drug and gene delivery[27-31] to characterizing molecules that respond to the variations in curvatures.[32-34] Over the years,, extensive experiments have been carried out to study the formation, properties, and applications of the NPSLBLs by using different kinds of lipids and different kinds of NPs. Pioneering works used the combination of $SiO_2$ NPs and zwitterionic phospholipids.[35] Wittenberg *et al.* used sub-micron (~700 nm) $SiO_2$ NPs to fabricate such NPSLBLs using a mixture of different lipids (including egg phosphatidylcholine, ganglioside GM1, and other): these NPSLBLs were employed to form arrays, which in turn were used to obtain the equilibrium constant for cholera toxin binding to ganglioside GM1.[36] Magnetic iron oxide NP based NPSLBLs has received increasing attentions as they can be used for bimolecular recognition with a magnetic separation.[37,38] In addition, the lipids contact with the iron oxide NP directly in such iron oxide NP based NPSLBLs, unlike in silica NP based NPSLBLs, where there is a thin layer of water between the lipid bilayer and the NP.[38] Recent developments include (a) fabricating NPSLBLs by combing negatively charged silica with anionic lipids by modifying the silica surface by using Avidin[39] and (b) fabricating NPSLBLs by utilizing the interactions between the $TiO_2$ NPs and zwitterionic inverse phosphocholine (CP) instead of normal phosphocholine (PC), and for this case, the $TiO_2$ NPs and the lipid phosphate are chemically bonded, and hence the resultant NPSLBLs are more stable than the silica NP based NPSLBLs, where silica NP and

the lipids are bonded by van der Waals force.[40] In another study, Chung *et al.* demonstrated the formation of NPSLBLs via the interactions of highly charged (zeta potential of +60 mV) amine-functionalized 60-nm NPs with the negatively charged 50% DOPA/50% DOPC vesicles in presence of osmotic shock.[41] Liu and co-workers, in a very interesting study, classified NPs into three distinct categories depending on whether it forms NPSLBLs or simply leads to a configuration where a NP is externally adsorbed on the surface of the vesicle.[42] For example, they identified as type 1 oxide NP as NPs of $Fe_3O_4$, $TiO_2$, $ZrO_2$, $Y_2O_3$, $In_2O_3$, and $Mn_2O_3$ that formed NPSLBLs by interacting with DOCP (inverse phosphocholine version of DOPC) vesicles but led to NP-adsorbed-vesicle configuration with DOPC vesicles. They also identified as type 2 oxide NP as NPs of $SiO_2$ that formed NPSLBLs with DOPC vesicle but led to NP-adsorbed-vesicle configuration with DOCP vesicles. Finally, they identified as type 3 oxide NPs as cationic ZnO and NiO NPs that damaged the vesicles by creating pores. In another study, Liu and co-workers showed that gold NPs undergo such surface adsorption (on the outer surface) of DOPC liposomes and the thickness of the interface between the NP and the DOPC liposome depends on the nature of the halide ions ($Cl^-$, $Br^-$, and $I^-$) with which the gold NPs are capped.[43] In this same study,[43] the authors pointed out the manner in which the adsorption of the NPs on the vesicle surface led to a local phase transition of the vesicle. In another study, Liu and co-workers considered $SiO_2$ NP (it was negatively charged for all ranges of studied pH) and $TiO_2$ NP [it was positively (negatively) charged for small (large) pH] interacting with neutral liposomes (DOPC and DOCP) and negatively charged liposomes (DOPS and DOCP).[44] $SiO_2$ NPs formed NPSLBL with the neutral

liposomes, while the $TiO_2$ NPs formed the NPSLBLs with the negatively charged liposomes at all pH (indicating that at larger pH, where the $TiO_2$ NPs are negatively charged, forces other than the electrostatic interactions dictate the formation of the NPSLBL) and with neutral liposomes at a very small pH. In this study,[44] the authors associated the formation of the NPSLBLs with the adsorption and the subsequent fusion of the NPs with the liposomes, which in turn implied the "leaking" of the liposomes releasing its original cargo (calcein for this study). Such leakage of liposomes thereby releasing their cargo due to the formation of NPSLBLs was also studied in another paper by the same group.[45] Liu and co-workers also demonstrated the effect of particle hydrophobicity on the structure of the lipid layers: they showed that a hydrophilic NP (e.g., $SiO_2$) forms a NPSLBL with the hydrophilic head of the lipid molecules of the inner layer (leaflet) facing the NP, while a hydrophobic NP (PLGA NP) forms only a *supported monolayer* (i.e., we get nanoparticle-supported lipid monolayer) with the hydrophobic tail of the lipid molecule facing the NP.[46] Finally, Liu has provided a detailed picture of the problem of NPs interacting with liposomes and vesicles, thereby forming NPSLBLs as well as other non-supported bilayer configurations in a recent review article.[47]

In a recent study,[48] we had employed MD simulations to probe the configuration and properties of a *pre-assembled* NPSLBL. Previous MD simulation studies had probed the conditions that lead to the clustering of multiple lipid-encapsulated NPs trapped inside lipid bilayers.[49] In another study, Chong *et al.* employed DPD (Dissipative Particle Dynamics) simulations to show that the insertion of self-assembled-monolayer (or SAM) functionalized NPs to lipid vesicles can be

promoted by defects in the SAM structure: of course, such insertion did not lead to the formation of the NPSLBLs.[50] On the other hand, Stelter and Keyes used hybrid MD/MC approach to study the number of lipids in the inner and the outer leaflets of a NPSLBL as a function of nanoparticle size.[51] However both our previous paper (Ref. 48) and this paper (Ref. 51) considered a *preformed* NPSLBL rather than considering the NPSLBL to be formed by a self-assembly process. Furthermore, Ref. 51 used a three-bead coarse-grained model for describing the lipids: such a representation might not be a rigorous enough description of the lipids [for example, in both the present and previous study (Ref. 48), we considered a 13-bead Martini coarse-grained model (discussed later) for describing the lipids]. Olenick *et al.* also considered the interactions between a NP and lipid molecules by employing experiments and MD simulations; however, their study did not consider a *closed* NPSLBL system (by such a "closed" system, we refer to a structure where a lipid bilayer completely encapsulates the NP) and considered a system that had fragments of lipid bilayers supported on a NP.[26] In this light, the present study is the one of the early attempts to quantify the properties and distribution of the lipid molecules in the leaflets of a *closed* NPSLBL obtained from self-assembly.

In the present study, we significantly improve the inferences of our previous report[48] by (a) quantifying the process of the self-assembly that leads to the formation of the NPSLBL, (b) quantifying the configuration and the properties of the self-assembled NPSLBL and not the *pre-formed* NPSLBL, and (c) quantifying the influence of the type of NP on the configuration and the properties of the self-assembled NPSLBL. The simulation results point to interesting mechanisms of the

self-assembly procedure: first, the randomly placed lipid molecules form small clusters, followed by the merging of these clusters in the vicinity of the NP to form NP-embedded vesicle. Such cluster merging or the nanostructure-embedded (when the nanostructure is a nanotube and not a NP) vesicle formation has been reported in previous studies on lipid bilayer self-assembly.[3,18] Once the equilibrated self-assembled NPSLBL structure has been achieved, the properties and the configurations of the NPSLBL are quantified by pinpointing (a) the number distribution of the lipid molecules in the inner and the outer leaflet, (b) the number distribution of the water molecules entrapped between the NP and the inner leaflet, and (c) the diffusivity of the lipid molecules occupying the inner and outer leaflets and the bulk diffusivity of the entrapped water molecules. For the self-assembled NPSLBL system, the number of lipid molecules occupying the outer leaflet is found to be significantly larger than the number of lipid molecules occupying the inner leaflet. This is in stark contrast to what has been proposed for the *preformed* NPSLBL system (where we previously assumed identical number of lipid molecules occupying the inner and outer leaflets).[48] The number of the entrapped water molecules and the thickness of this entrapped water layer is close to what has been predicted experimentally and by our previous study on *preassembled* NPSLBL system.[48] Thirdly, our simulations establish that the diffusivities of the lipid molecules occupying both the inner and the outer leaflets are larger than those obtained in our previous study on pre-assembled NPSLBL system,[48] although in both the present and the previous study,[48] we witness that the diffusivity of the lipid molecules occupying the outer leaflet is significantly greater than that occupying the inner leaflet. Fourthly,

we quantify the bulk diffusivity of the entrapped water and find it to be slightly larger than that obtained in our previous study on *preformed* NPSLBL system.[48] Finally, we establish the influence of the nature of the NP of the NPSLBL on dictating the overall properties of the NPSLBL. Overall, we propose that this study provides a more realistic computational estimate of the properties of the NPSLBL by studying the self-assembled NPSLBL equilibrated from an initially random system, instead of considering a *preformed* NPSLBL system.[48]

## *3.2. Simulation Set Up*

The simulations were conducted with the POPC lipid molecules, a NP, and water molecules. The POPC molecule, which was represented by the Martini model,[52] is shown in Fig. 3.1(a). The NP consisted of Nda beads,[52] which were randomly distributed in a spherical shell space of outer radius 7 nm and inner radius 5.5 nm, as shown in figure 3.1(b) and 3.1(c). The density of the Nda beads was 44 per $nm^3$ so as to ensure that the water cannot penetrate the NP. We choose the Nda beads since this bead is hydrophilic and can serves as hydrogen donator and acceptor in the Martini model. In addition, this bead is not used in the POPC molecule. The positions of the Nda beads of the NP are kept fixed during the simulation. This system consisting of the POPC lipids and a NP composed of Nda beads is referred to as *system A*.

The simulations are started from the initial structure shown in Figure 3.2(a). The initial configuration consists of the randomly distributed 3268 POPC molecules and water molecules around a NP (comprising of the Nda beads) in a cubic box of 22nm×22nm×22nm. This initial structure was obtained by using packmol.[53] The

water box consisted of 129163 Martini water beads and 14351 anti-freeze water beads.[52] The purpose of adding such anti-freeze water beads has been discussed in our previous paper.[48] Simulations were conducted by using the NAMD software package[54] with the Martini force field.[52] Periodic boundary conditions were employed by applying the NPT thermostat. The pressure was set to 1 bar and simulations were conducted with a 40fs time step. A total of four trajectories were run. The data were acquired every 50000 steps. 50 frames per trajectory were averaged over to obtain the results.

We also consider another combination of lipid molecule and NP system: the lipid molecules are still POPC, while the NP is composed of P5 beads, which are more hydrophilic than the Nda beads.[52] The positions of the P5 beads of the NP are kept fixed during the simulation. This system consisting of the POPC lipids and a NP composed of P5 beads is referred to as *system B*. The same simulation setting, and processes employed for system A were employed for system B as well.

The interactions between Nda and water as well as P5 with water are both modelled using the Lennard-Jones (LJ) potential ($U_{LJ}$) and the corresponding parameters are shown in table 3.1.[52]

$$U_{LJ} = \varepsilon \left(\frac{\sigma}{r}\right)^{12} - 2\varepsilon \left(\frac{\sigma}{r}\right)^{6}, \qquad (3.1)$$

where $r$ is the distance between the two atoms.

***Table 3. 1: Parameters for the Water-P5 and Water-Nda Lennard-Jones (LJ) interactions.***

| | Water-P5 | Water-Nda |
|---|---|---|
| $\varepsilon$ | -1.33843000 | -0.95602300 |
| $\sigma$ | 5.27557163 | 5.27557163 |

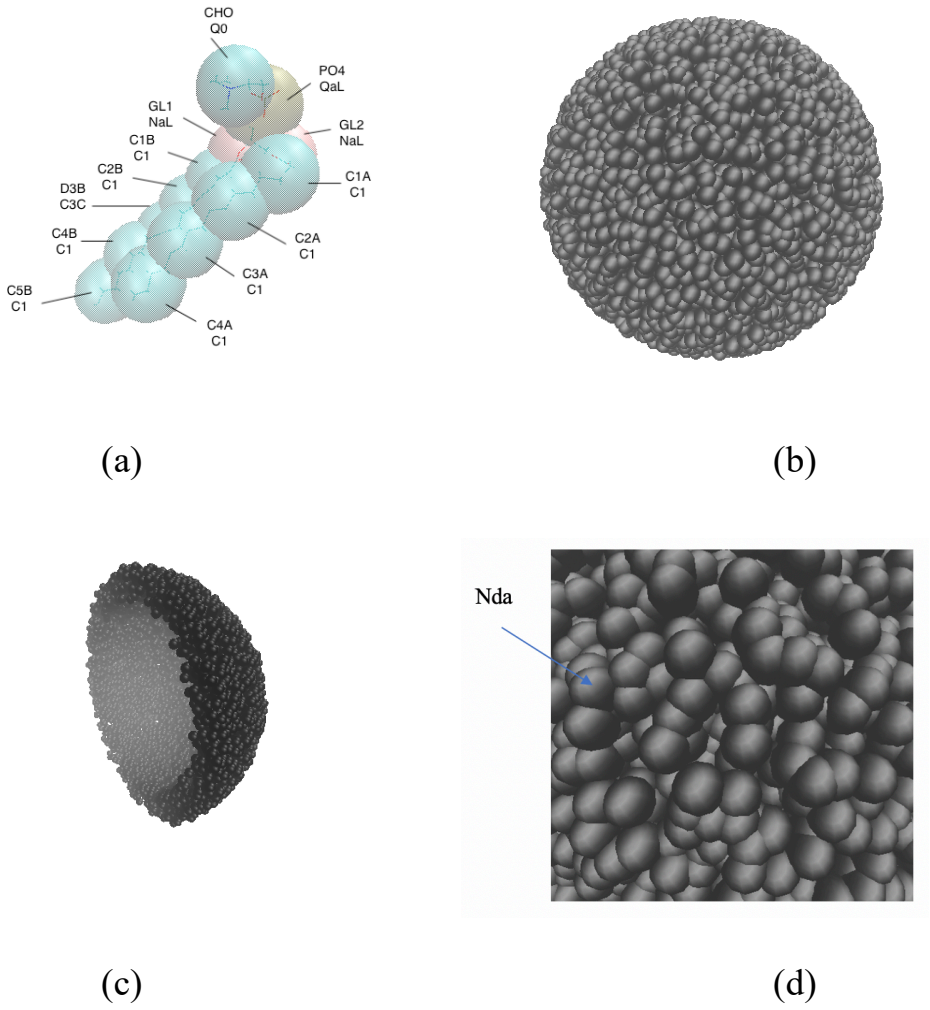


***Figure 3. 1: Model of POPC and NP***

*(a) Martini model of the POPC lipid molecule, where the lipid molecule is represented by 13 large spheres (beads). Each of the beads is so labelled that their names are identified on the upper row and their types are identified on the bottom row (for example, the name of the "golden" color bead is "$PO_4$" and its type is "QaL"). (b) Snapshot of the NP. (c) Snapshot of half of the NP. (d) Zoomed view of the NP surface.*

## *3.3. Results*

Figs. 3.2(a)-3.2(g) and Figs. 3.3(a)-3.3(g) show the MD simulation snapshots depicting the time evolution of the systems A and B, respectively. Both set of simulations confirm the self-assembly-driven formation of the NPSLBL. In all the subfigures, only $1/10^{th}$ of the total number of water molecules has been displayed to ensure a clearer view. In both the systems A and B, initially, the lipid molecules aggregate to form multiple small clusters [see Figs. 3.2(b, c) and Fig. 3.3(b, c)]. Subsequently, these clusters localize and merge near the surface of the NP and form a vesicle encapsulating the NP [see Fig. 3.2(d) and Fig. 3.3(d)]. Previous MD simulation studies on the self-assembly-driven formation of the planar lipid bilayers had reported the formation of such small clusters, which over time merge to form bigger cluster, eventually leading to the formation of the bilayers.[3] Here the critical difference is that this merging of the clusters occur in the vicinity of the NP. However, such nanostructure-supported vesicle formation (here the nanostructure is this NP) has been reported in previous simulation studies where the lipid molecule self-assemble around nanotubes to form lipid-nanotube vesicle.[18] Such aggregation of the lipid molecules around the nanostructure is possibly due to the corresponding lowering of the exposure of the lipid hydrophobic tails to the surrounding water. In the present study, NP-supported vesicle contains a large pore [see Fig. 3.2(e) and Fig. 3.3(e)]; furthermore, there are few small clusters that have not merged and are away from the vesicle [see Fig. 3.2(e) and Fig. 3.3(e)]. This entire structure (NP-supported vesicle with a large pore and some sparsely distributed clusters away from the vesicle) would take a long time to overcome the energy barrier for equilibration. To

accelerate the simulation, therefore, we increased the temperature from 310K to 340K in one step [starting from the MD simulation step represented in Fig. 3.2(f) and Fig. 3.3(f), i.e., MD simulation step corresponding to the 2 $\mu s$]. As a result, the pore gradually closed [see Figs. 3.2(f, g) and Figs. 3.3(f, g)] and the sparsely distributed clusters (located away from the vesicle) merged with the vesicle. Eventually, we obtained a perfect pore-free NP-supported vesicle, which is equivalent to the NPSLBL (henceforth, referred to as the NPSLBL) [see Fig. 3.2(h) and Fig. 3.3(h)]. Finally, we equilibrated these NPSLBL systems by running the simulations further for another 2 $\mu s$.

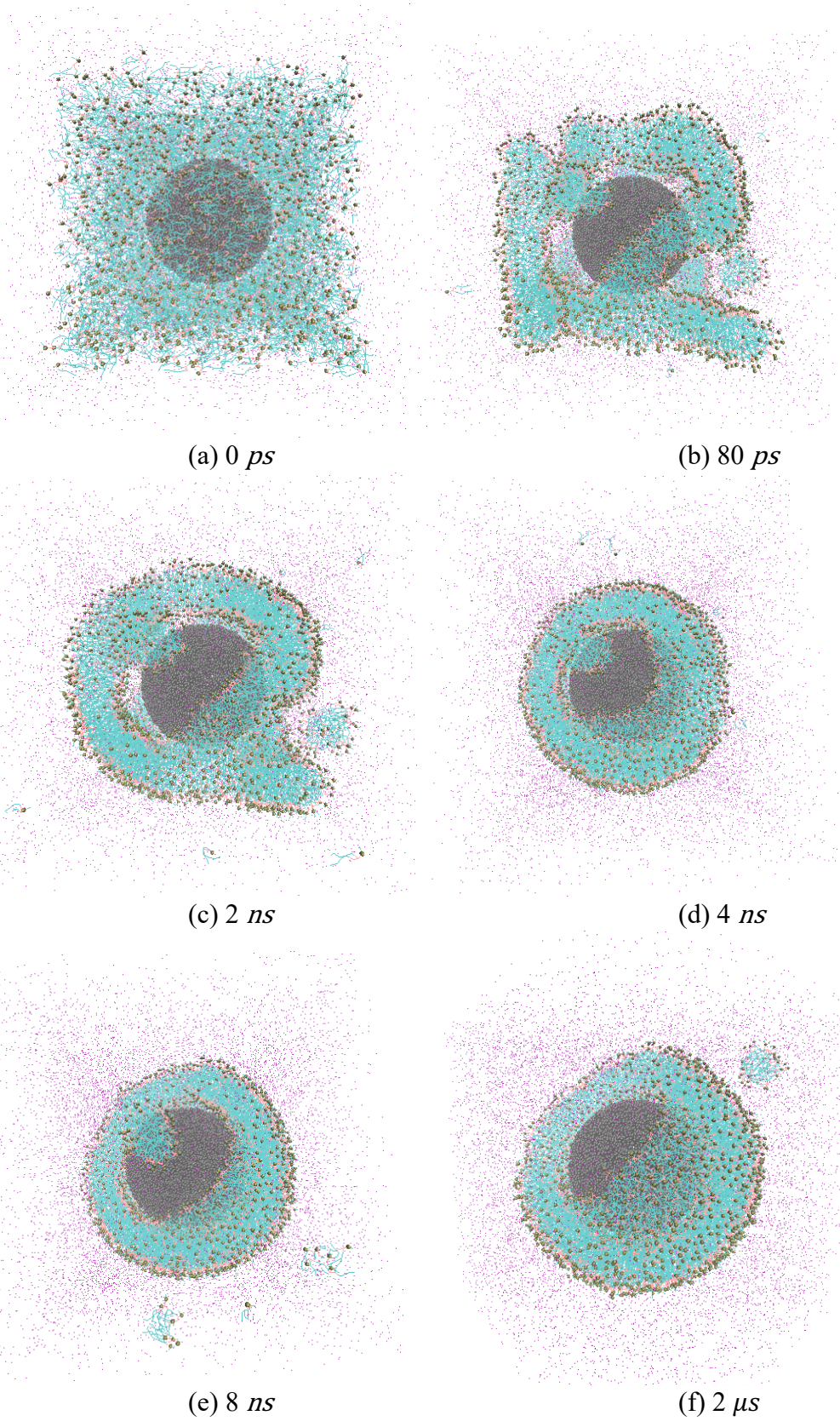

(a) 0 *ps*

(b) 80 *ps*

(c) 2 *ns*

(d) 4 *ns*

(e) 8 *ns*

(f) 2 *μs*

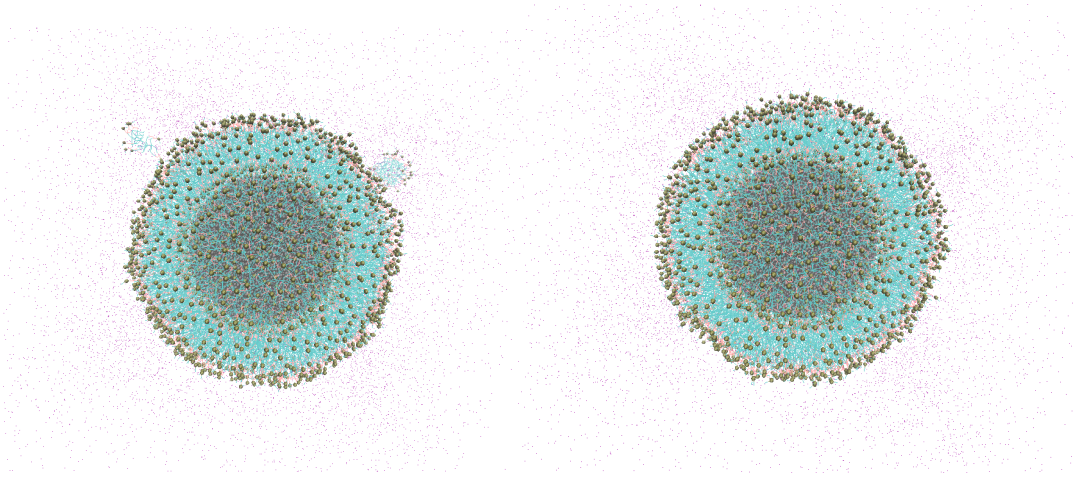

(g) $2.2\mu s$ (h) 2.3 $\mu s$

***Figure 3. 2:*** **Snapshot of the simulation of system A**

*(a): initial configuration; (b-h) snapshots quantifying the progress of the simulation. Also, the snapshots from (a-e) represent the simulations conducted at 310 K, while those from (f-h) represent the simulations conducted at 340 K. In (b) to (h), only 1/10$^{th}$ water are displayed for a clearer view. Below each snapshot, we provide the corresponding simulation step at which the snapshot has been taken. In the different subfigures, the following color codes have been used: Black: NP; light Green: hydrophobic tails of POPC molecules; bronze: hydrophilic heads of POPC molecules; purple: water.*

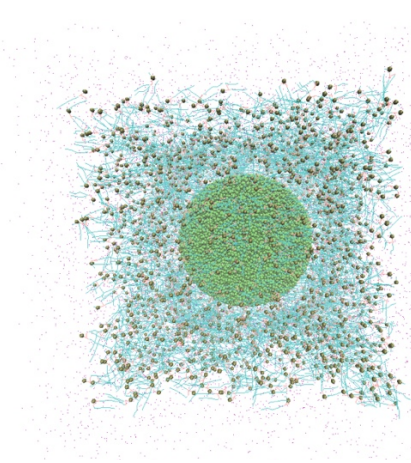

(a) 0 *ps*

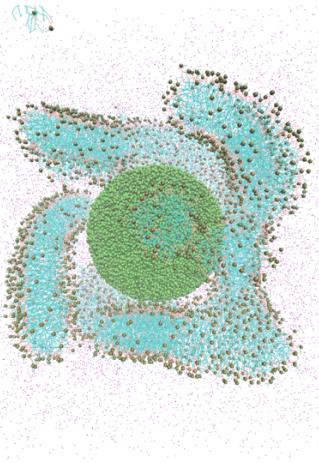

(b) 80 *ps*

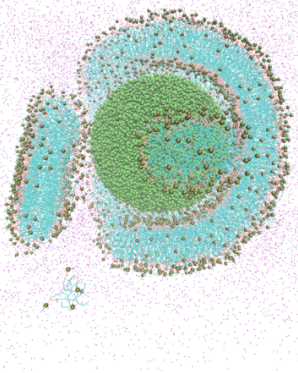

(c) 2 *ns*

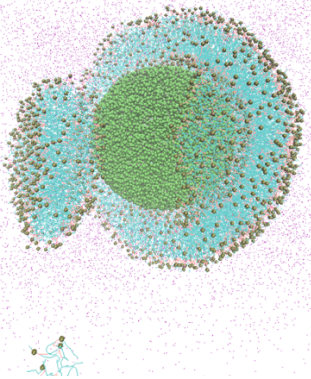

(d) 4 *ns*

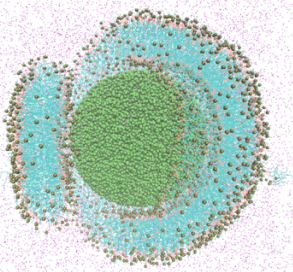

(e) 8 *ns*

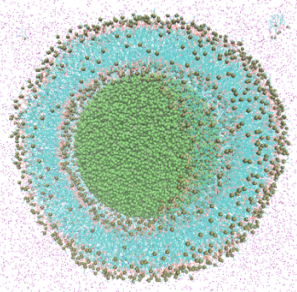

(f) 2 $\mu s$

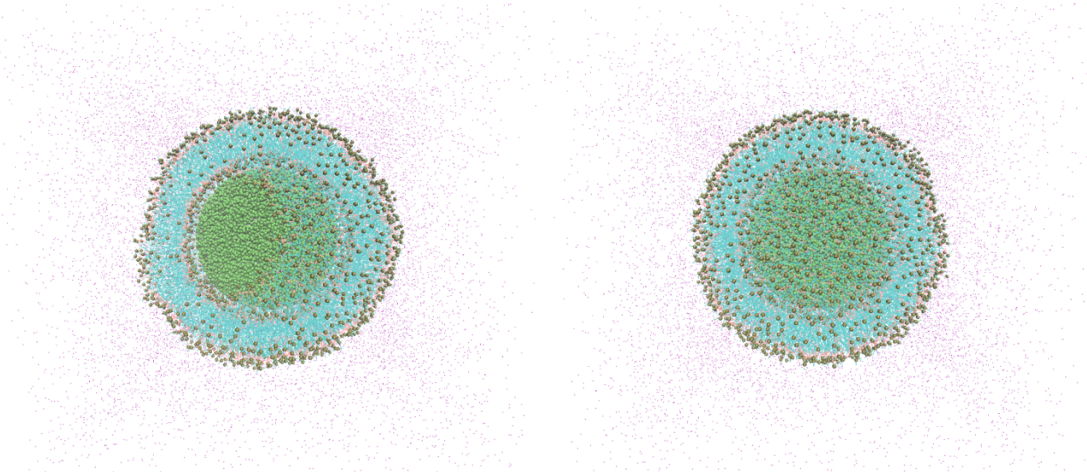

(g) $2.2\mu s$ (h) $2.3\ \mu s$

***Figure 3. 3:***: **Snapshot of the simulation of system B**

*(a): initial configuration; (b-h) snapshots quantifying the progress of the simulation. Also, the snapshots from (a-e) represent the simulations conducted at 310 K, while those from (f-h) represent the simulations conducted at 340 K. In (b) to (h), only $1/10^{th}$ water are displayed for a clearer view. Below each snapshot, we provide the corresponding simulation step at which the snapshot has been taken. In the different subfigures, the following color codes have been used: Green: NP; light Green: hydrophobic tails of POPC molecules; bronze: hydrophilic heads of POPC molecules; purple: water.*

After obtaining the equilibrium configuration, we measured the radial distribution of the hydrophilic head of the POPC molecules, represented by the PO4 beads. The result is shown in Figure 3.4 with the horizonal axis providing the distance between the beads and the center of the NP. The clustering of the lipid molecules occurs at two distinct ranges of the radial distances (namely 7nm $\leq r \leq$ 8.5nm and 10.5nm $\leq r \leq$ 12.5nm) confirming that there are two layers (or two leaflets) of lipids. We characterize the two leaflets by quantifying the number of lipid molecules present in each. We find that there are 1274 PO4 beads present at the location 7nm $\leq r \leq$ 8.5nm and 1994 PO4 beads present at the location 10.5nm $\leq r \leq$ 12.5nm for system A. In other words, there are 1274 POPC molecules located at the inner leaflet of the bilayer, and 1994 POPC molecules located at the outer leaflet of the bilayer for system A. If we define the radius of the inner (outer) leaflet as the average distance between the PO4 beads of inner (outer) leaflet and the NP center, then the inner radius is 7.86 nm and the outer radius is 11.79 nm. Therefore, the average LBL thickness is 3.93 nm. Also, from these quantifications we can infer that the surface coverage is 0.61 $nm^2$ per lipid for the inner leaflet and 0.88 $nm^2$ per lipid for the outer leaflet.

For system B, there are 1287 PO4 beads at the location 7nm $\leq r \leq$ 8.5nm and 1981 PO4 beads present at the location 10.5nm $\leq r \leq$ 12.5nm. As a result, there are 1287 POPC molecules located at the inner leaflet of the bilayer, and 1981 POPC beads located at the outer leaflet of the bilayer, with inner radius being 7.97 nm and the outer radius being 11.84 nm. Thus, the average LBL thickness is 3.87 nm. In addition,

the surface coverage is 0.62 $nm^2$ per lipid for the inner leaflet and 0.89 $nm^2$ per lipid for the outer leaflet.

Please note that for both the systems A and B, two mutually countering effects dictate the number of lipids in the inner and the outer leaflets. The outer leaflet has a larger surface area that allows it to accommodate a larger number of lipid molecules. On the other hand, the presence of the supporting NP implies that the lipids in the inner leaflet are more compact, which in turn allows the inner leaflet to accommodate more lipid per unit area (or equivalenetly, a smaller surface area coverage per lipid). The effect of the larger area of the outer leaflet becomes more dominating, leading to a net larger number of lipids in the outer leaflet as compared to the inner leaflet.

It is worthwhile to compare the above findings with those of our previous study,[48] where we considered a *preformed* NPSLBL. In that study,[48] the *preformed* NPSLBL consisted of 1639 POPC molecules in the inner leaflet and 1639 POPC molecules in outer leaflet at 310 K and the NP was composed of Nda beads. In comparison, for the present study, these numbers are 1274 POPC molecules in the inner leaflet and 1994 POPC molecules in the outer leaflet at 340 K. Therefore, the self-assembly MD simulations reveal a critical facet of the LBL structure of the NPSLBL that was missing in our previous study:[48] the number of lipid molecules in the inner and outer leaflet significantly vary from each other. The pre-assembled NPSLBL in our previous study showed very little change in the number of lipid molecules between inner and outer leaflet when the equilibration run was conducted with this pre-assembled state (with equal number of lipid molecules in the inner and outer leaflets). This stemmed from the fact that this pre-assembled state behaved as a

meta-equilibrated configuration trapped at the local minimum due to the high energy barrier of lipid flip-flop. It is also interesting to note that this large difference in the number of lipid molecules between the inner and outer leaflet as revealed by the present study is much similar to the free nanovesicle (NV) simulated in our previous work, where there are 1302 and 1967 POPC molecules in inner and outer leaflets respectively.[48] This configurational similarity between self-assembled NPSLBL and the free NV of the same size, in addition to the easy controllability of the size of the NPSLBL, potentially makes the NPSLBL a better choice for studying the membrane curvature sensing by curvature-sensitive moleucles.[32]

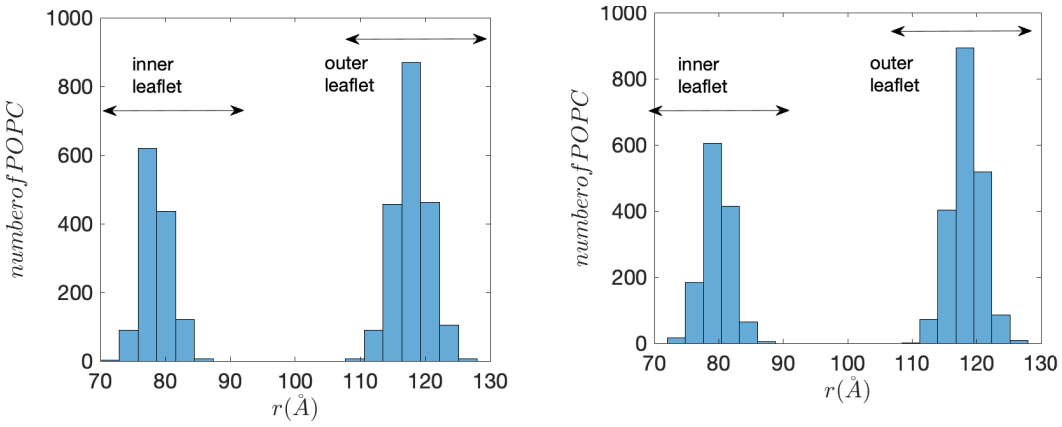


***Figure 3. 4: POPC Distribution***

*Radial distribution of the POPC molecules, with the radial distance being represented by the distance between the PO4 head group and the center of NP, for (a) System A and (b) System B.*

In Figure 3.5, we show the radial distribution of the coarse-grained (CG) water beads and anti-freeze (AF) water beads. The $y$ axis is the density of the CG water and AF water normalized over the standard density ($\rho_S$) of the corresponding water ($\rho_S = 33/4\times0.9$ and $\rho_S = 33/4\times0.1$ per $nm^2$ for the CG water and the AF water, respectively). The result shows that there is a thin layer of water entrapped between the NP and the inner lipid leaflet in the self-assembled NPSLBL structure for both the systems A and B. This entrapped water layer is a reflection of the large hydrophilicity of the Nda beads (for system A) and the P5 beads (system B) that ensures that the NP prefers to be in contact with a thin layer of water rather than in direct contact with the lipid molecules. It is useful to note that system B shows a larger value of the density of the entrapped water as compared to system A. This stems from the fact that P5 beads (constituting the NP in system B) are more hydrophilic than the Nda beads (constituting the NP in system A). For both the systems A and B, the average thickness of the confined water is found to be around 1.5nm. This thickness of the water layer trapped between the NP and the lipid inner leaflet is comparable to the experimental value of 1 to 2 nm (Ref. 55) and confirm the rational of our previous simulation design where we had introduced a two-layer thick coarse-grained water beads between the NP and the inner leaflet in our pre-assembled NPSLBL system.[48]

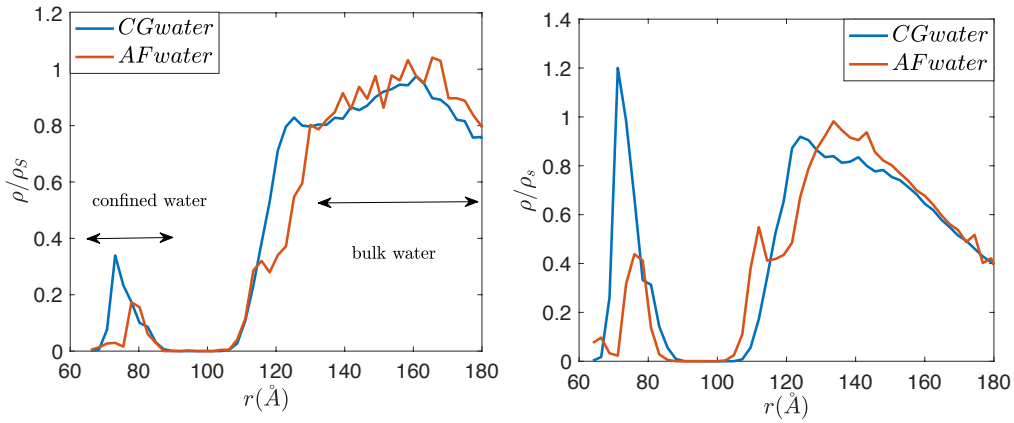


**(a)** **(b)**

***Figure 3. 5: Water Molecules Distribution***

*Radial distribution of the coarse-grained and anti-freeze water beads with the radial distance being represented by the distance between the PO4 head group and the center of NP, for (a) System A and (b) System B.*

In Figures 3.6(a) and 3.6(b), we plot the <MSD>-vs-t variation and thereby quantify the 3D diffusivity ($D_3$) of the lipid molecules occupying the inner and outer leaflets of the self-assembled NPSLBL by using Einstein relation, i.e.,

$$D_3 = \lim_{t\to\infty} \frac{1}{6}\frac{\langle MSD\rangle}{t}. \quad (3.1)$$

Here $\langle MSD\rangle$ is the mean square displacement and $t$ is the time. $D_3$ is calculated from the slope of the linear region of the $\langle MSD\rangle$-vs-$t$ curve. For system A, $D_3$ values for the lipid molecules occupying the inner and the outer leaflets are $2.45\times10^{-7}$ cm$^2$/s and $3.69\times10^{-7}$ cm$^2$/s, respectively. For system B, $D_3$ values for the lipid molecules occupying the inner and the outer leaflets are $2.67\times10^{-7}$ cm$^3$/s and $4.19\times10^{-7}$ cm$^3$/s, respectively. These findings confirm that for both the systems A and B, the diffusivity of the lipid molecules in the outer leaflet is significantly higher than that of the lipid molecules in the inner leaflet. Ref. 12, studying DPPC nanovesicles (i.e., spherical LBLs without any encapsulating NP) using MD simulations, has provided very similar values (as obtained for systems A and B from our simulations) of the diffusivities of the lipid molecules in the inner and outer leaflets clearly demonstrating larger diffusivity values for the lipid molecules in the outer leaflet. Ref. 56 provides an average experimental diffusivity value for the POPC lipid molecules of the POPC LBL system that is partly supported on a NP and partly on a planar substrate. Their diffusivity values are nearly one order less than that obtained from our MD simulation studies. We ascribe such a difference to the nature and size of the NP (both of which are different as compared to the system A of our study) as well as the presence of an additional planar support in Ref. 56. In addition, Ref. 57 and 58 measured the lateral diffusivity of the individual monolayer of silica

NPSLBLs directly and found that the diffusivity of lipids in outer leaflets is two times higher than inner leaflets.

Finally, in Fig. 3.6(c) and 3.6(d), we plot the <MSD>-vs-t variation for the confined water molecules entrapped between the NP and the inner leaflet and quantify the diffusivity ($D_3$) using eq. (2). For system A, $D_3$=1.98 $\times 10^{-6}$ $cm^3/s$ for the entrapped water molecules. This diffusivity value is very similar ($D_3$=1.95 $\times 10^{-6}$ $cm^3/s$) for the entrapped water molecules obtained from our previous MD simulation study with *preformed* NPSLBL.[35] On the other hand, for system B, we obtain $D_3$=0.94$\times 10^{-6}$ $cm^2/s$ for the entrapped water molecules; this diffusivity value is less than half of that of the system A stemming from the larger hydrophilicity of P5 beads as compared to the Nda beads.

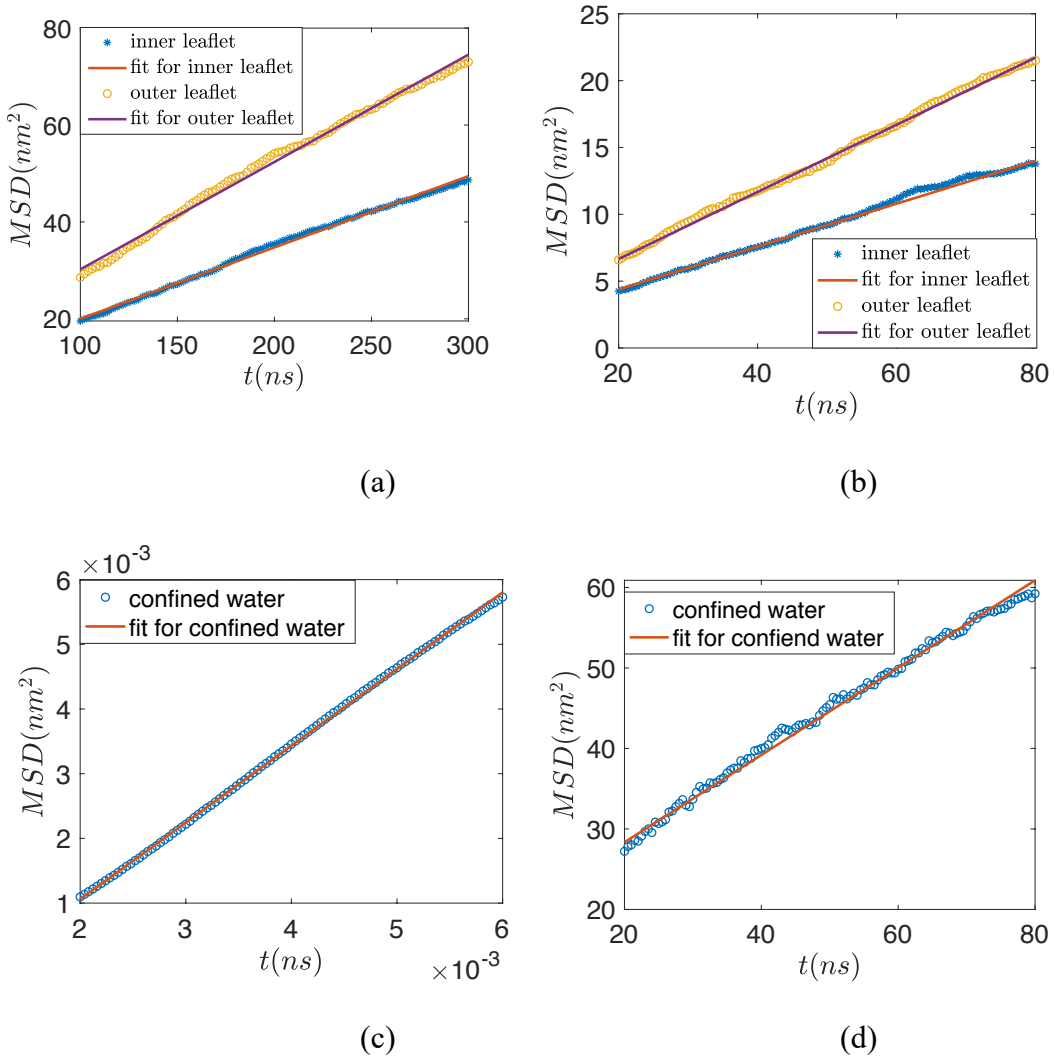


***Figure 3. 6: MSD for POPC and Water***

*(a) <MSD>-vs-time for the POPC lipid molecules occupying inner and outer leaflets for the NPSLBL for (a) System A and (b) System B. <MSD>-vs-time for the confined water entrapped between the NP and the inner leaflet of the lipid bilayer for (c) System A and (d) System B. We employ eq. (3.1) to obtain the corresponding $D_3$ values from the slope of each of the different <MSD>-vs-time plots.*

## *3.4. Conclusion*

Coarse-grained MD simulations have been employed to study for the first time the self-assembly-driven formation of NPSLBL. We discover critical mechanisms that drive the self-assembly process including the formation of small lipid clusters, merging of these clusters in the vicinity of the NP to form NP-embedded vesicle with a pore, and the disappearance of that pore overcoming a large energy barrier to eventually form the equilibrated NPSLBL. Our results also reveal critical information on the properties of the self-assembled NPSLBL, such as the area per lipids, the number of lipids, and the diffusivity of the lipids in the inner and outer leaflets as well as the thickness and diffusivity of the water molecular layer confined between the NP and the inner leaflet. These quantifications eventually enable us to revisit the predictions on the properties and configurations of the *preformed* NPSLBL system studied in our previous work[48] and establish the present study as the most complete computational predictive study on the properties and configurations of the NPSLBL till date that can be used for any future simulation-based analyses of NPSLBL system.

## *Bibliography*


1. Goetz, R.; Gompper, G.; Lipowsky, R. Mobility and Elasticity of Self-Assembled Membranes. *Phys. Rev. Lett.* **1999**, *82*, 221-224.
2. Brannigan, G.; Philips, P. F.; Brown, F. L. H. Flexible Lipid Bilayers in Implicit Solvent. *Phys. Rev. E* **2005**, *72*, 011915.
3. Schindler, T.; Kröner, D.; Steinhauser, M. O. On the Dynamics of Molecular Self-Assembly and the Structural Analysis of Bilayer Membranes using Coarse-grained Molecular Dynamics Simulations. *Biochim. Biophys. Acta* **2016**, *1868*, 1955-1963.
4. Skjevik, A, A.; Madej, B. D.; Dickson, C. J.; Teigen, K.; Walker, R. C.; Gould, I. R. All-atom Lipid Bilayer Self-assembly with the AMBER and CHARMM Lipid Force Fields. *Chem. Comm.* **2015**, *51*, 4402-4405.
5. Skjevik, A, A.; Madej, B. D.; Dickson, C. J.; Lin, C.; Teigen, K.; Walker, R. C.; Gould, I. R. Simulation of Lipid Bilayer Self-assembly using All-atom Lipid Force Fields. *Phys. Chem. Chem. Phys.* **2016**, *18*, 10573-10584.
6. Shelley, J. C.; Shelley, M. Y.; Reeder, R. C.; Bandyopadhyay, S.; Klein, M. L. A Coarse Grain Model for Phospholipid Simulations. *J. Phys. Chem. B* **2001**, *105*, 4464-4470.
7. Shelley, J. C.; Shelley, M. Y.; Reeder, R. C.; Bandyopadhyay, S.; Moore, P. B.; Klein, M. L. Simulations of Phospholipids Using a Coarse Grain Model. *J. Phys. Chem. B* **2001**, *105*, 9785-9792.

8. Wang, Z-J.; Deserno, M. Simulations of Phospholipids Using a Coarse Grain Model. *J. Phys. Chem. B* **2010**, *114*, 11207-11220.
9. Lyubartsev, A. P. Multiscale Modeling of Lipids and Lipid Bilayers. *Eur. Biophys. J.* **2005**, *35*, 53-61.
10. Orsi, M.; Michel, J.; Essex, J. W. Coarse-grain Modelling of DMPC and DOPC Lipid Bilayers. *J. Phys. Cond. Matt.* **2010**, *22*, 155106.
11. Wang, Y.; Sigurdsson, J. K.; Brandt, E. Dynamic Implicit-solvent Coarse-grained Models of Lipid Bilayer Membranes: Fluctuating Hydrodynamics Thermostat. *Phys. Rev. E* **2013**, *88*, 023301.
12. Marrink, S. J.; Mark, A. E. Molecular Dynamics Simulation of the Formation, Structure, and Dynamics of Small Phospholipid Vesicles. *J. Am. Chem. Soc.* **2003**, *125*, 15233-15242.
13. de Vries, A. H.; Mark, A. E.; Marrink, S. J. Molecular Dynamics Simulation of the Spontaneous Formation of a Small DPPC Vesicle in Water in Atomistic Detail. *J. Am. Chem. Soc.* **2004**, *126*, 4488-4489.
14. Scott, K. A.; Bond, P. J.; Ivetac, A.; Chetwynd, A. P.; Khalid, S.; Sansom, M. S. P. Coarse-Grained MD Simulations of Membrane Protein-Bilayer Self-Assembly. *Structure* **2008**, *16*, 621-630.
15. Bond, P. J.; Cuthbertson, J. M.; Deol, S. S.; Sansom, M. S. P. MD Simulations of Spontaneous Membrane Protein/Detergent Micelle Formation. *J. Am. Chem. Soc.* **2004**, *126*, 15948-15949.

16. Bond, P. J.; Sansom, M. S. P. Insertion and Assembly of Membrane Proteins via Simulation. Insertion and Assembly of Membrane Proteins via Simulation. *J. Am. Chem. Soc.* **2006**, *128*, 2697-2704.
17. Lee, H.; Pastor, R. W. Coarse-Grained Model for PEGylated Lipids: Effect of PEGylation on the Size and Shape of Self-Assembled Structures. *J. Phys. Chem. B* **2011**, *115*, 7830-7837.
18. Dutt, M.; Kuksenok, O.; Nayhouse, M. J.; Little, S. R.; Balazs, A. C. Modeling the Self-Assembly of Lipids and Nanotubes in Solution: Forming Vesicles and Bicelles with Transmembrane Nanotube Channels. *ACS Nano* **2011**, *5*, 4769-4782.
19. Khalid, S.; Bond, P. J.; Holyoake, J.; Hawtin, R. W.; Sansom, M. S. P. DNA and Lipid Bilayers: Self-assembly and Insertion. *J. R. Soc. Interface* **2008**, *5*, S241-S250.
20. Wallace, E. J.; Sansom, M. S. P. Carbon Nanotube Self-assembly with Lipids and Detergent: A Molecular Dynamics Study. *Nanotechnology* **2009**, *20*, 045101.
21. Orsi, M.; Essex, J. W. Physical Properties of Mixed Bilayers Containing Lamellar and Nonlamellar Lipids: Insights from Coarse-grain Molecular Dynamics Simulations. *Faraday Discuss.* **2013**, *161*, 249–272.
22. Marrink, S. J.; de Vries, A. H.; Mark, A. E. Coarse Grained Model for Semiquantitative Lipid Simulations. *J. Phys. Chem. B* **2004**, *108*, 750-760.

23. Shih, A. H.; Arkhipov, A.; Freddolino, P. L.; Schulten, K. Coarse Grained Protein-Lipid Model with Application to Lipoprotein Particles. *J. Phys. Chem. B* **2006**, *110*, 3674-3684.
24. Noguchi, H. Solvent-free Coarse-grained Lipid Model for Large-scale Simulations. *J. Chem. Phys.* **2011**, *134*, 055101.
25. Koldsø, H.; Shorthouse, D.; Helie, J.; Sansom, M. S. P. Lipid Clustering Correlates with Membrane Curvature as Revealed by Molecular Simulations of Complex Lipid Bilayers. *PLOS Comput. Biol.* **2014**, *10*, e1003911.
26. Olenick, L. L.; Troiano, J. M.; Vartanian, A.; Melby, E. S.; Mensch, A. C.; Zhang, L.; Hong, J.; Mesele, O.; Qiu, T.; Bozich, J.; et al. Lipid Corona Formation from Nanoparticle Interactions with Bilayers. *Chem* **2018**, *4*, 2709–2723.
27. Ashley, C. E.; Carnes, E. C.; Phillips, G. K.; Padilla, D.; Durfee, P. N.; Brown, P. A.; Hanna, T. N.; Liu, J.; Phillips, B.; Carter, M. B.; Carroll, N. J.; Jiang, X.; Dunphy, D. R.; Willman, C. L.; Petsev, D. N.; Evans, D. G.; Parikh, A. N.; Chackerian, B.; Wharton, W.; Peabody, D. S.; Brinker, C. J. The Targeted Delivery of Multicomponent Cargos to Cancer Cells by Nanoporous Particle-Supported Lipid Bilayers. *Nature Mater.* **2011**, *10*, 389-397.
28. Tarn, D.; Ashley, C. E.; Xue, M.; Carnes, E. C.; Zink, J. I.; Brinker, C. J. Mesoporous Silica Nanoparticle Nanocarriers: Biofunctionality and Biocompatibility. *Acc. Chem. Res.* **2013**, *46*, 792-801.
29. Liu, J.; Jiang, X.; Ashley, C.; Brinker, C. J. Electrostatically Mediated Liposome Fusion and Lipid Exchange with a Nanoparticle-Supported Bilayer

for Control of Surface Charge, Drug Containment, and Delivery. *J. Am. Chem. Soc.* **2009**, *131*, 7567-7569.

30. Lin, Y.-S.; Haynes, C. L. Impacts of Mesoporous Silica Nanoparticle Size, Pore Ordering, and Pore Integrity on Hemolytic Activity. *J. Am. Chem. Soc.* **2010**, *132*, 4834-4842.
31. Liu, J.; Stace-Naughton, A.; Jiang, X.; Brinker, C. J. Porous Nanoparticle Supported Lipid Bilayers (Protocells) as Delivery Vehicles. *J. Am. Chem. Soc.* **2009**, *131*, 1354-1355.
32. Fu, R; Gill, R. L.; Kim, E. Y.; Briley, N. E.; Tyndall, E. R.; Xu, J.; Li, C.; Ramamurthi, K. S.; Flanagan, J. M.; Tian, F. Spherical Nanoparticle Supported Lipid Bilayers for the Structural Study of Membrane Geometry-Sensitive Molecules. *J. Am. Chem. Soc.* **2015**, *137*, 14031-14034.
33. Gill Jr., R. L.; Castaing, J-P.; Hsin, J.; Tan, I. S.; Wang, X.; Huang, K. C.; Tian, F.; Ramamurthi, K. S. Structural Basis for the Geometry-driven Localization of a Small Protein. *Proc. Natl. Acad. Sci. USA* **2015**, *112*, E1908-E1915.
34. Kim, E. W.; Tyndall, E. R.; Huang, K. C.; Tian, F. Dash-and-Recruit Mechanism Drives Membrane Curvature Recognition by the Small Bacterial Protein SpoVM. *Cell Syst.* **2017**, *5*, 518-526.
35. Bayer TM; Bloom M. Physical Properties of Single Phospholipid Bilayers Adsorbed to Micro Glass Beads. A New Vesicular Model System Studied by 2h-Nuclear Magnetic Resonance. *Biophys. J.* **1990**, *58* (2), 357–362.

36. Wittenberg, N. J.; Johnson, T. W.; Oh, S-H. High-Density Arrays of Submicron Spherical Supported Lipid Bilayers. *Anal. Chem.* **2012**, *84*, 8207–8213.

37. De Cuyper, M.; De Meulenaer, B.; Van der Meeren, P.; Vanderdeelen, J. Catalytic Durability of Magnetoproteoliposomes Captured by High-Gradient Magnetic Forces in a Miniature Fixed-Bed Reactor. *Biotech. Bioeng.* **1996**, *49*, 654–658.

38. Troutier, A.-L.; L. Catherine. An Overview of Lipid Membrane Supported by Colloidal Particles. *Adv. Colloid Interface Sci.* **2007**, *133*, 1–21.

39. Gopalakrishnan G; Rouiller I; Colman DR; Lennox RB. Supported Bilayers Formed from Different Phospholipids on Spherical Silica Substrates. *Langmuir* **2009**, *25*, 5455–5458.

40. Wang F; Liu J. A Stable Lipid/$TiO_2$ Interface with Headgroup-Inversed Phosphocholine and a Comparison with $SiO_2$. *J. Am. Chem. Soc.* **2015**, *137*, 11736–11742.

41. Chung, P. J.; Hwang, H. L.; Dasbiswas, K.; Leong, A.; Lee, K. Y. C. Osmotic Shock-Triggered Assembly of Highly Charged, Nanoparticle-Supported Membranes. *Langmuir* **2018**, *34*, 13000−13005.

42. Liu, Y.; Wang, F.; Liu, J. Headgroup-Inversed Liposomes: Biointerfaces, Supported Bilayers and Applications. *Langmuir* **2018**, *34*, 9337−9348.

43. Liu, X.; Li, X.; Xu, W.; Zhang, X.; Huang, Z.; Wang, F.; Liu, J. Sub-Angstrom Gold Nanoparticle/Liposome Interfaces Controlled by Halides. *Langmuir* **2018**, *34*, 6628−6635.

44. Wang, X.; Li, X.; Wang, H.; Zhang, X.; Zhang, L.; Wang, F.; Liu, J. Charge and Coordination Directed Liposome Fusion onto $SiO_2$ and $TiO_2$ Nanoparticles. *Langmuir* **2019**, *35*, 1672−1681.

45. Liu, Y.; Liu, J. Leakage and Rupture of Lipid Membranes by Charged Polymers and Nanoparticles. *Langmuir* **2020**, *36*, 810−818.

46. Lopez, A.; Liu, J. DNA Oligonucleotide-Functionalized Liposomes: Bioconjugate Chemistry, Biointerfaces, and Applications. *Langmuir* **2018**, *34*, 15000−15013.

47. Liu, J. Interfacing Zwitterionic Liposomes with Inorganic Nanomaterials: Surface Forces, Membrane Integrity, and Applications. *Langmuir* **2016**, *32*, 4393−4404.

48. Jing, H.; Wang, Y.; Desai, P. R.; Ramamurthi, K. S.; Das, S. Nanovesicles Versus Nanoparticle- Supported Lipid Bilayers: Massive differencesin Bilayer Structures and in Diffusivities of Lipid Molecules and Nanoconfined Water. *Langmuir* **2019**, *35*, 2702-2708.

49. Chan, H.; Kral, P. Nanoparticles Self-Assembly within Lipid Bilayers. *ACS Omega* **2018**, *3*, 10631-10637.

50. Chong, G.; Foreman-Ortiz, I. U.; Wu, M.; Bautista, A.; Murphy, C. J.; Pedersen, J. A.; Hernandez, R. Defects in Self-Assembled Monolayers on Nanoparticles Prompt Phospholipid Extraction and Bilayer-Curvature-Dependent Deformations. *J. Phys. Chem. C* **2019**, *123*, 27951–27958.

51. Stelter D; Keyes T. Lipid Packing in Lipid-Wrapped Nanoparticles. *J. Phys. Chem. B* **2018**, *122*, 6755-6762.

52. Marrink, S. J.; Risselada, H. J.; Yefimov, S.; Tieleman, D. P.; de Vries, A. H. The MARTINI Force Field: Coarse Grained Model for Biomolecular Simulations. *J. Phys. Chem. B* **2007**, *111*, 7812-7824.
53. Martínez, L.; Andrade, R.; Birgin, E. G.; Martínez, J. M. PACKMOL: A Package for Building Initial Configurations for Molecular Dynamics Simulations. *J. Comput. Chem.* **2009**, *30*, 2157-2164.
54. Phillips, J. C.; Braun, R.; Wang, W.; Gumbart, J.; Tajkhorshid, E.; Villa, E.; Chipot, C.; Skeel, R. D.; Kale, L.; Schulten, K. Scalable Molecular Dynamics with NAMD. *J. Comput. Chem.* **2005**, *26*, 1781-1802.
55. Charitat, T.; Bellet-Amalric, E.; Fragneto, G.; Graner, F. Adsorbed and Free Lipid Bilayers at the Solid-Liquid Interface. *Eur. Phys. J. B* **1999**, *8*, 583-593.
56. Woodward, X.; Stimpson, E. E.; Kelly, C. V. Single-Lipid Tracking on Nanoscale Membrane Buds: The Effects of Curvature on Lipid Diffusion and Sorting. *BBA - Biomembranes* **2018**, 1860, 2064-2075.
57. Hetzer, M.; Heinz, S.; Grage, S.; Bayerl, T. M. Asymmetric Molecular Friction in Supported Phospholipid Bilayers Revealed by NMR Measurements of Lipid Diffusion. *Langmuir* **1998**, *14*, 982-984.
58. Schmitt, J.; Danner, B.; Bayer, T. M. Polymer Cushions in Supported Phospholipid Bilayers Reduce Significantly the Frictional Drag between Bilayer and Solid Surface. *Langmuir* **2001**, *17* (1), 244–246.

# Chapter 4: Lipid Flip-Flop and Desorption from Supported Lipid Bilayers is Independent of Curvature*

***Abstract:*** *Flip-flop of lipids of the lipid bilayer (LBL) constituting the plasma membrane (PM) plays a crucial role in a myriad of events ranging from cellular signaling and regulation of cell shapes to cell homeostasis, membrane asymmetry, phagocytosis, and cell apoptosis. While extensive research has been conducted to probe the lipid flipflop of planar lipid bilayers (LBLs), much less is known regarding lipid flip-flop for highly curved, nanoscopic LBL systems despite the vast importance of membrane curvature in defining the morphology of cells and organelles and in playing key roles in maintaining a variety of cellular functions, enabling trafficking, and recruiting and localizing shape-responsive proteins. In this chapter, we conduct molecular dynamics (MD) simulations to study the energetics, structure, and configuration of a lipid molecule undergoing flip-flop and desorption in a highly curved (with a large radius of curvature) LBL, represented as a nanoparticle-supported lipid bilayer (NPSLBL) system. We compare our findings against those of a planar substrate supported lipid bilayers (PSSLBL). Our MD simulation results reveal that despite the vast differences in the curvature and other curvature-induced properties (e.g., lipid packing fraction, difference in the number of lipids between inner and outer leaflets, etc.) between the NPSLBL and the PSSLBL, the energetics of lipid flip-flop and lipid desorption as well as the configuration of the lipid molecule*

*The contents of this Chapter have been submitted for publication as the following journal article: Jing, H.; Wang, Y.; Ramamurthi, K. S.; Das, S. "Lipid Flop-flop and Desorption from Supported Lipid Bilayers is Independent of Curvature." *Plos One* (Submitted for Publication).

*undergoing lipid flip-flop are very similar for the NPSLBL and the PSSLBL. In other words, our results establish that the curvature of the LBL plays an insignificant role in lipid flip-flop and desorption.*

## *4.1. Introduction*

The trans-bilayer migration of phospholipid molecules in cell membranes [1-3] is vital to the functioning of eukaryotic cells[4]; the migration event impacts, for example, cell signaling;[5] regulation of shape changes of cells, organelles, and vesicles;[6,7] cell homeostasis;[4] maintenance of membrane asymmetry;[8,9] phagocytosis;[10] and apoptosis.[11] When phospholipid migration occurs from the inner or cytoplasmic side of the bilayer to the outer or the exoplasmic side of the bilayer, it is denoted as a "flop", whereas it is denoted as "flip" when it occurs in the opposite direction.[1-3] Phospholipid translocations within the lipid bilayer (LBL) and the corresponding energy barriers associated with these processes provide vital clues to a myriad of events such as protrusion-mediated membrane-membrane and membrane-protein interactions,[12] clustering of ligands and proteins on the plasma membrane (PM),[13,14] pore formation in the PM,[15] localizing and activating enzymes on the PM,[16] and dictating the activity of lipid anchors[17]. Such energy barriers are inevitably encountered as hydrophilic entities like charged lipid headgroups translocate from one leaflet of the bilayer to the other through the hydrophobic membrane core.[1-3] Over the years, there have been extensive experimental efforts for quantifying these energetic barriers of trans-bilayer lipid migration, the corresponding kinetics of translocation, and the role of the factors like the lipid chain length and head group, membrane packing, and the presence of cholesterol and peptides within the

membrane in flip-flop kinetics.[18-34] Similarly, there have been a significant number of molecular dynamics (MD) simulation studies providing molecular level insights on the energetics of lipid flip flop (often quantified by the potential of mean force values obtained as a function of the lipid position within and outside the lipid bilayer or LBL), and detailed structural information on lipid molecules during their course of the flip flop.[35-38]

Interestingly, most of the simulation studies on lipid flip-flops have invariably considered a planar LBL and there has been no study for probing the energetics of lipid flip-flops on curved LBLs. This is specially surprising given the well-accepted roles of membrane curvature in defining the morphology of cells and organelles, playing important roles in maintaining certain cellular functions,[39] and enabling trafficking,[39] recruiting and localizing shape-responsive proteins.[40] Of course, there have been experiments and MD simulations investigating the role of membrane curvature on lipid diffusion and sorting;[41-44] In addition, experiments have shown that the energy barrier of lipid flip flop is independent from the membrane curvature for both unsupported and supported LBL.[45] However, due to the restriction of experimental resolution, the details of lipid flip flop are missing.

In the present study, we employ coarse-grained MD simulations for studying the energetics of flip-flop and desorption of lipid molecules in curved LBLs, represented by nanoparticle-supported lipid bilayers (NPSLBLs).} Such NPSLBLs have been extensively used for targeted delivery of drugs and genes[46-50] as well as for characterizing curvature-sensitive molecules.[51-53] The energetics of lipid flip-flop and desorption are quantified by studying the PMF (potential of mean force) of a single

lipid molecule as a function of its position within the LBL. In order to pinpoint the exact impact of the curvature on the flip-flop and desorption energetics, we compare our findings with those for a planar-substrate-supported lipid bilayer (PSSLBL). The curvature causes the NPSLBL and the PSSLBL to differ significantly from each other in terms of area per lipid, inner-to-outer leaflet lipid number ratios, etc. Despite that we find that for both the PSSLBL and the NPSLBL, the PMF profiles are very similar, establishing, most remarkably, very similar energetics of lipid flip-flop and desorption for the cases of PSSLBL and NPSLBL. Therefore, our results establish that the curvature has very little effect on the energetics and mechanisms associated with the lipid dynamics in supported LBL systems. This is the central result of this paper. A detailed analysis of the energetics, quantified through the corresponding variation of the PMF, reveal that for both the NPSLBL and the PSSLBL the equilibrium position of the lipid molecule is at either of the inner or the outer leaflet, while the energetically least favorable locations are the hydrophobic core between the two leaflets and the bulk water. In addition, for both the cases, the lipid molecule undergoes a rotation of nearly 180 degree as it traverses from the inner (outer) to the outer (inner) leaflet (where the lipid molecule is stretched) and occupies a near tangential configuration (in a compressed state) in the hydrophobic core.

## *4.2 Simulation Set Up*

### *4.2.1. Self-Assembly of PSSLBL and NPSLBL*

We used Martini model[54] for the simulation. There are two type of NPSLBL systems: *system A* consisted of POPC molecules for lipids and Nda beads for NP,

while *system B* is made of POPC molecules for lipids and P5 beads for NP. Fig. 4.1(a) shows the structure of the lipids while Fig. 4.2(b) shows the structure of the NP. In Fig. 4.1(c) we show the equilibrated *system A* and in Fig. 4.1(d) we show the equilibrated *system B.* The details about the self-assembly process of NPSLBL can be found in chapter 3 (Fig. 3.2 and Fig. 3.3). After equilibrated the NPSLBL at 340K, we decrease the temperature to 310K and equilibrated the system for another 2 $\mu s$.

For the PSSLBL, the support substrate comprised of Nda[54] beads which are randomly distributed in a rectangle space of 20nm*20nm*1.6nm. The density of the Nda beads is same as the support substrate used in NPSLBL. This initial structure was obtained by using packmol[55] and we name system as *system C*. The self-assembly of *system C* was shown in figure 4.2.

Similar to NPSLBL, we substitute the Nda beads in *system C* with P5 beads and name the new system as *system D.* To save simulation time, there are only 1250 POPC molecules randomly distributed above the substrate in the initial structure for *system D*. The self-assembly of *system D* was shown in figure 4.3.

The simulations are started from the initial structure shown in Fig. 4.2 (a) and Fig. 4.3 (a). The NAMD software package[56] was used to run the Simulations with the Martini force field.[54] Periodic boundary conditions were employed along with the NPT thermostat. The pressure was set to 1 bar, and simulation time step was set to 40fs. In addition, the temperature was set to 310K. The lipids quickly arranged and form an LBL above the substrate, becoming a PSSLBL within 8ns, and the PSSLBL is equilibrated for another 10ns. The equilibrated structure of system C and system D

were shown in Fig. 4.1(e) and Fig. 4.1(f) respectively. For all the four systems, the positions of the NPs are fixed during the simulation.

In table 1, we have summarized the key differences in the equilibrium parameters between the NPSLBL and the PSSLBL.

| | *System A* | *System B* | *System C* | *System D* |
|---|---|---|---|---|
| Area per lipid ($nm^2$), inner leaflet | 0.61 | 0.62 | 0.85 | 0.87 |
| Area per lipid ($nm^2$), outer leaflet | 0.88 | 0.89 | 0.82 | 0.86 |
| Inner-outer lipid number ratio | 0.64:1 | 0.65:1 | 0.95:1 | 0.98:1 |

***Table 4.1:*** *Difference in the equilibrium configurations properties between the NPSLBL and the PSSLBL*

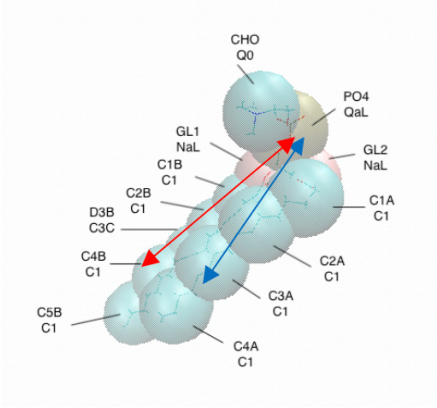
CHO
Q0
PO4
QaL
GL1
NaL
GL2
NaL
C1B
C1
C2B
C1
C1A
C1
D3B
C3C
C4B
C1
C2A
C1
C3A
C1
C5B
C1
C4A
C1

**(a)**

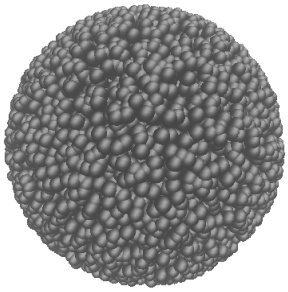

**(b)**

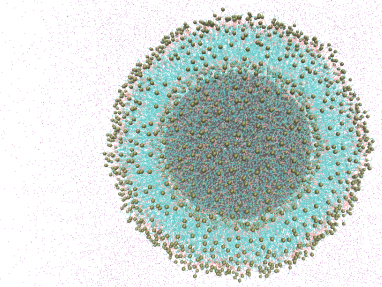

**(c)**

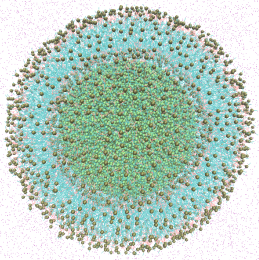

**(d)**

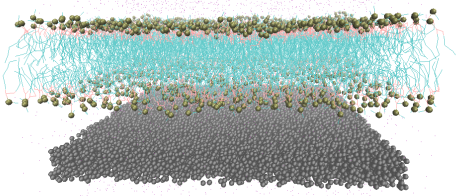

**(e)**

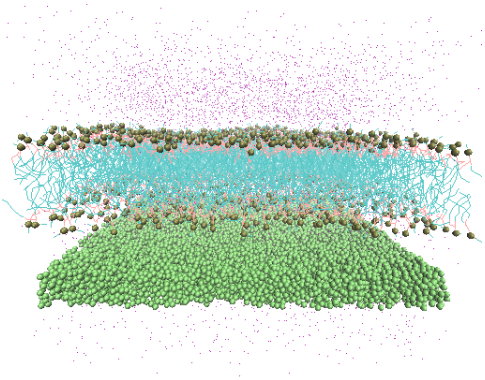

**(f)**

***Figure 1. (a)*** *Martini model of the POPC lipid molecule, where the lipid molecule is represented by 13 large spheres (beads). Each of the beads is so labelled that their names are identified on the upper row and their types are identified on the bottom row (for example, the name of the "golden" color bead is "$PO_4$" and its type is "QaL"). The red double arrow shows the definition of $l_B$, the distances between the PO4 beads and the center of C5B, C4B, and C3C beads while the blue double arrow shows the definition of $l_A$, the distances between the PO4 beads and the center of C2A, C3A, and C4A beads. The figure has been reproduced from our previous paper.[2] (b) Snapshot of the NP. (c) Snapshot of system A. (d) snapshot of system B. (e) Snapshot of system C. (f) Snapshot of system D.*

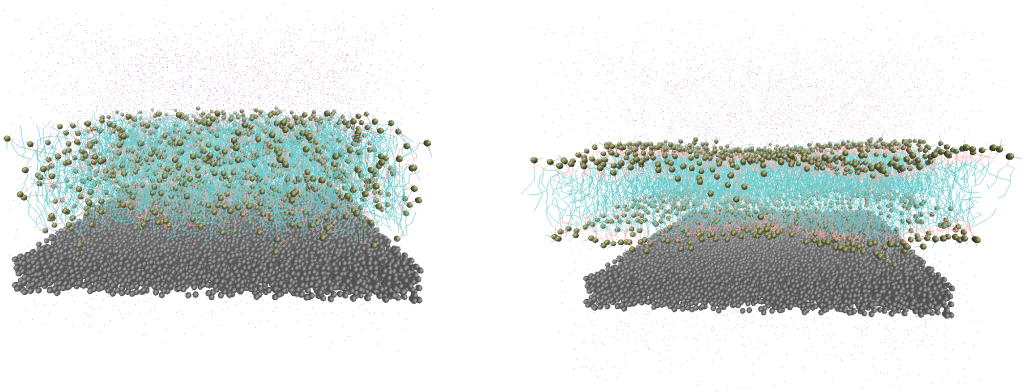

(a) 0 *ps* (b) 4 *ns*

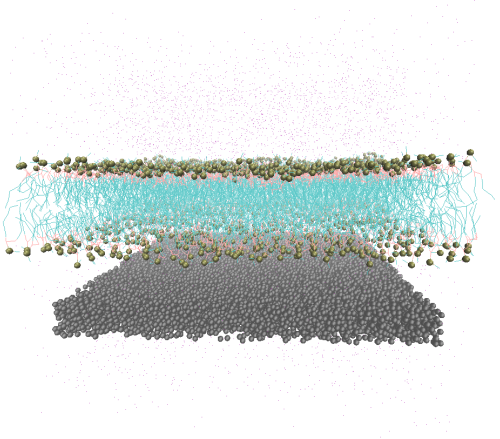

(c) *8ns*

***Figure 4.2:*** *MD simulation snapshots capturing the self-assembly driven equilibration of the system C. Below each snapshot, we provide the corresponding simulation step at which the snapshot has been taken. The following color codes have been used: black: support substrate; light green: hydrophobic tails of POPC molecules; bronze: hydrophilic heads of POPC molecules, purple: water.*

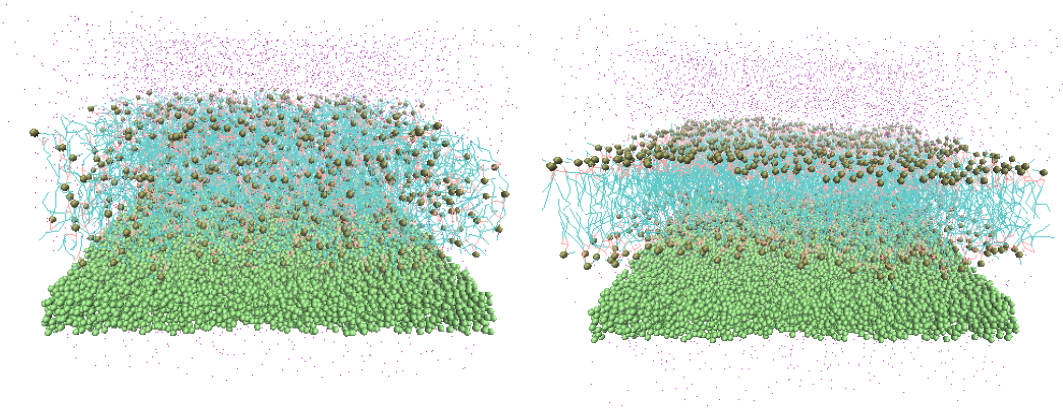

(a) 0 *ps* (b) 4 *ns*

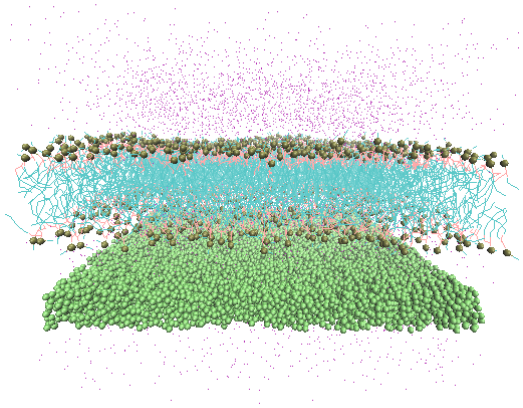

(c) *8ns*

***Figure 4.3:*** *MD simulation snapshots capturing the self-assembly driven equilibration of the system D. Below each snapshot, we provide the corresponding simulation step at which the snapshot has been taken. The following color codes have been used: green: support substrate; light green: hydrophobic tails of POPC molecules; bronze: hydrophilic heads of POPC molecules, purple: water.*

*4.2.2. Potential of Mean force Calculation*

In order to obtain the PMF (quantifying the energetics of lipid flip-flop and desorption) for both the NPSLBL and the PSSLBL, we first identify two lipids (denoted as *star lipids* with one located at the inner leaflet and the other located at the outer leaflet. Subsequently, we employ the umbrella potential to these two lipids. For the NPSLBL, the reaction coordinate was $a = R - r_0$. Here $R$ was the distance between the PO4 beads of the *star lipids* and the center of NPSLBL while $r_0$ was the radius of the inner leaflets [see Fig. 4.4(a)]. On the other hand, for the PSSLBL, the reaction coordinate, $a$, was set as the distance along the LBL normal direction between the PO4 beads of the *star lipids* and the inner leaflets of the LBL, as illustrated in Fig 4.4(a). For both cases, $a$ ranged from 0 to 70 Å. The *star lipids* were shifted by 2 Å per simulation window, and we considered 35 such simulation windows. The 35 initial structures corresponding to the 35 simulation windows were obtained by pulling the start lipids to their window location via the umbrella potential with a force constant 0f 2.5 kcal $mol^{-1}$ $Å^2$. Each simulation window was equilibrated for 200ns, followed by a 100ns production run. The PMFs were constructed from the simulations by using WHAM[57] program. Figs. 4.4(b) and 4.5(b) respectively provide the MD simulation based equilibrated structures of the PSSLBL and the NPSLBL. In Figs. 4.4(c-f) and 4.5(c-f), we provide the MD simulation snapshots for the different positions of the lipid molecules for quantifying the PMF of the lipid flip-flop and desorption for the PSSLBL and the NPSLBL, respectively.

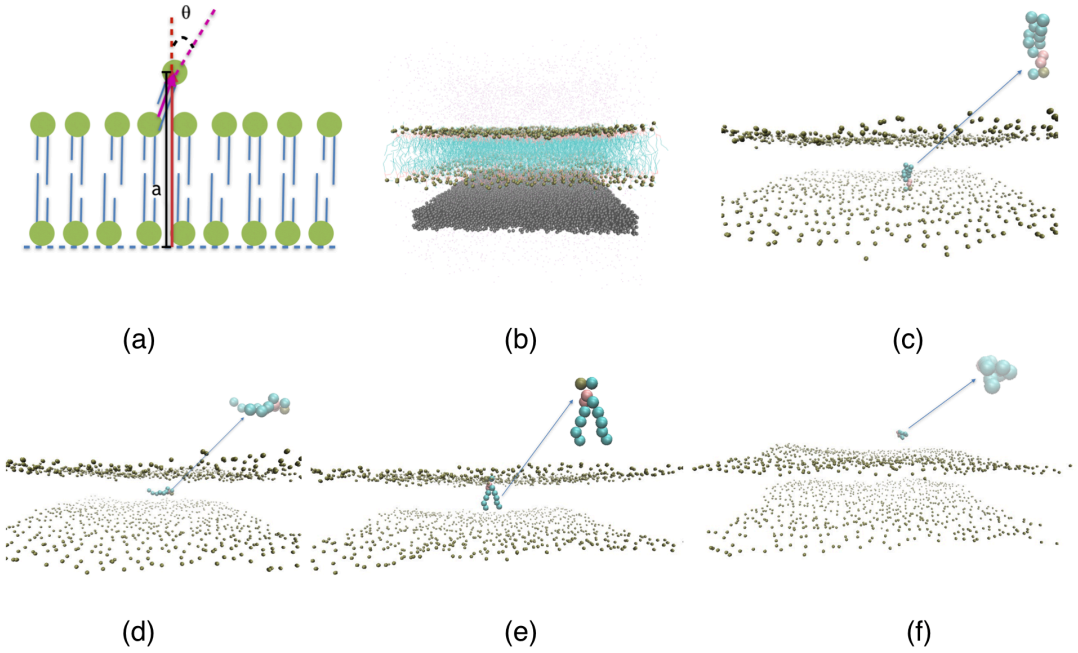


**Figure 4.4:** (a) The schematic depiction of the geometry of the PSSLBL. (b) MD simulation snapshot of the PSSLBL; only $1/10^{th}$ of the total number of water molecules are displayed for a clearer view. (c-f) Snapshots representing the positions (and configurations) of a single lipid molecule (zoomed in the inset showing the corresponding lipid configuration) corresponding to its different locations inside and outside the LBL of the PSSLBL. These different locations are (c) inner leaflet, $a = 0$ Å; (d) hydrophobic core, $a = 22$ Å; (e) outer leaflet, $a = 44$ Å; (f) bulk water, $a = 70$ Å. For all the cases we use the following color codes: purple for water; dark green for the planar support; light green for the hydrophobic tails of lipids; Bronze for the hydrophilic head of the lipids. For figures (c-f), only the hydrophilic heads of the lipid molecules of the LBL are displayed for a clearer view.

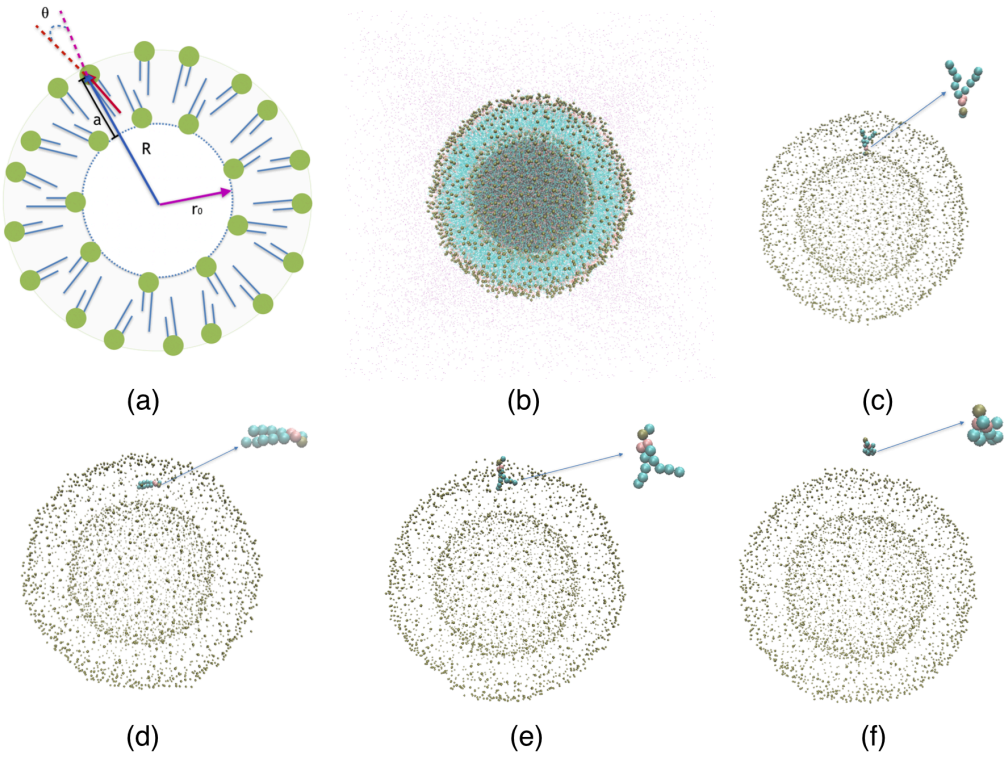


**Figure 4.5:** The schematic depiction of the geometry of the NPSLBL. (b) MD simulation snapshot of the NPSLBL; only $1/10^{th}$ of the total number of water molecules are displayed for a clearer view. (c-f) Snapshots representing the positions (and configurations) of a single lipid molecule (zoomed in the inset showing the corresponding lipid configuration) corresponding to its different locations inside and outside the LBL of the NPSLBL. These different locations are (c) inner leaflet, $a = 0$ Å; (d) hydrophobic core, $a = 22$ Å; (e) outer leaflet, $a = 44$ Å; (f) bulk water, $a = 70$ Å. For all the cases we use the following color codes: purple for water; dark green for the planar support; light green for the hydrophobic tails of lipids; Bronze for the hydrophilic head of the lipids. For figures (c-f), only the hydrophilic heads of the lipid molecules of the LBL are displayed for a clearer view.

## *4.3. Results*

Fig. 4.6 quantifies the energetics of lipid flip-flop and desorption for the NPSLBL and the PSSLBL by quantifying the corresponding *PMF-vs-a* variation. The reaction coordinate "*a*" has been defined in Fig. 4.4(a) and Fig. 4.5(a) (as well as in the text above) for the NPSLBL and the PSSLBL, respectively. The results clearly indicate that the PMFs are very similar for the two cases (cases of the NPSLBL and the PSSLBL) for the three different types of motions: (a) "flop" motion (when the lipid molecule moves from the inner to the outer leaflet), (b) "flip" motion (when the lipid molecule moves from the outer to the inner leaflet), and (c) desorption (when the lipid molecule moves from the outer leaflet to the bulk water). These results confirm the most important finding of this study: the energetics of lipid flip-flop and desorption is independent of the curvature in supported LBL systems. In addition to this overall finding on the energetics, we dissect the PMF curve to understand the position dependent behavior of the lipid molecule during their flip-flop and desorption. Invariably, for both the cases of the NPSLBL and the PSSLBL, the most stable configurations (or the equilibrium positions) of the lipid molecules are at the inner and the outer leaflets. On the other hand, the energetically most unfavorable location for the lipid molecule is bulk water. The hydrophobic core between the inner and outer leaflets is also energetically unfavorable. As the lipid molecule is pulled away from the inner (outer) lipid leaflet towards the inter-leaflet hydrophobic core during the flop (flip) motion, the lipid molecule experiences an energy unfavourability. This energy unfavourability is due to the hydrophilic head of the lipid molecule being forced in a hydrophobic core between the two leaflets. As the

lipids are closer to the hydrophobic core of the bilayer, the energy unfavourability attains a maximum at the boundary between the inner and leaflets and starts to decrease to another local minimum at the outer (inner) leaflet during the flop (flip) motion. Of course, when the lipids enter into the bulk water from the outer leaflet, the energy unfavourability rises significantly and reaches the peak when the lipid molecule is completely surrounded by water. It is important to emphasize here that the inner and the outer leaflets are entangled/overlapped with each other, i.e., the hydrophobic tails of one leaflet penetrates into the hydrophobic space formed by the tails of the other leaflet. Such an overlap/entanglement is evident from the fact that the thickness of the bilayer is smaller than twice of the length of a lipid molecule. Therefore, we define the boundary of the two leaflets as the place where the influence of a leaflet becomes dominant. In this work, the influence is evaluated as the stationary point in the PMF.

From Fig. 4.6(a) we can calculate the free energy barrier for flop, flip, and desorption are 17.9 $\pm$ 1.6 kcal/mol, 19.25 $\pm$ 1.6 kcal/mol, and 20.77 $\pm$ 1.6 kcal/mol respectively , while from Fig. 4(b), we obtain free energy barrier for flop, flip, and desorption are 17.59$\pm$1.4 kcal/mol, 18.84 $\pm$ 1.4 kcal/mol and 21.46$\pm$1.4 kcal/mol respectively. The error is estimated based on the standard derivation. Experiments have reported an energy barrier of 84-113 kJ/mol (20.1-27.7kcal/mol) for the lipid flip-flop motion for different PSSLBLs (DMPC, DPPC, and DSPC bilayers) at 20.9 °C.[2] These experimental results match excellently with our simulation findings. From the figures, it is noticed that the simulation data is more scattered at the outer leaflets than elsewhere. We attribute such scatter to the constraint of the 1D PMF calculation,

which means the shape of LBL is not strictly spherical nor planar, so that one reaction coordinate cannot fully capture the energetic signature.

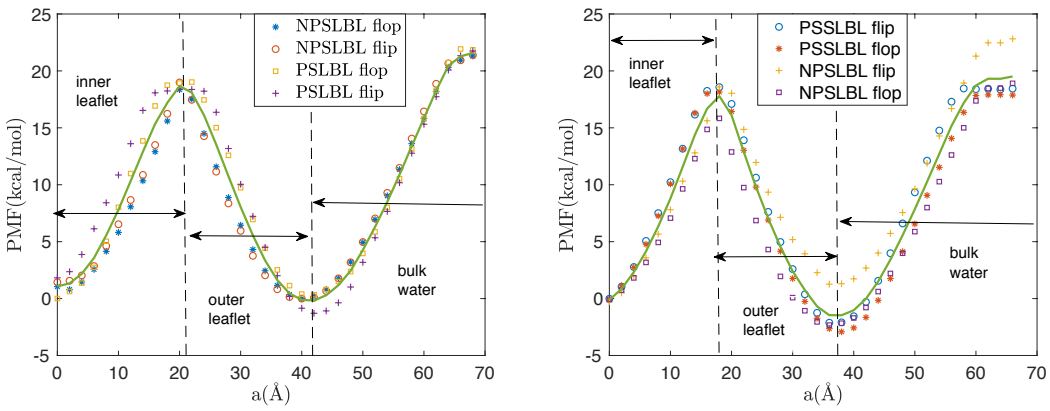


**(a)** **(b)**

**Figure 4.6:** Variation of the PMF (with respect to the reaction coordinate a) of a single lipid molecule traversing inside the LBL during the flip and the flop motions and outside the LBL during the desoprtion for the NPSLBL and PSSLBL. (a) *system A and system C,* (b) *system B and system D.* The solid lines are the averages of the simulation data. In the figure, we identify the locations of the lipid bilayer and the bulk water as well. Also $a = 0$ Å represents the location of the inner leaflet for both the NPSLBL and the PSSLBL.

Fig. 4.7 and Fig. 4.8 show the lengths $l_A$ and $l_B$ of the two hydrophobic tails A and B as the lipids move inside and outside the LBL for the cases of NPSLBL and the PSSLBL. $l_A$ and $l_B$, defined in Fig. 4.1, are the distances between the PO4 beads and the center of last three carbon beads of the tails A and B, respectively. Like the PMF variation, the variation for the tail length is very much similar for the cases of the NPSLBL and the PSSLBL. Both the tails for either of the two cases (NPSLBL or PSSLBL) get compressed as the lipid molecule moves from the inner (outer) leaflet to the hydrophobic core during the flop (flip) motion. This stems from the tendency of the hydrophilic heads to avoid the hydrophobic membrane core. On the other hand, both the tails for either of the two cases (NPSLBL or PSSLBL) get stretched as the lipid molecule moves from the outer leaflet surface into the bulk water stemming from the tendency of the hydrophobic tails of the lipid molecules to remain localized in the outer leaflet and not get in contact with water. Finally, when the lipid molecule is entirely in the bulk water (i.e., the lipid molecules has undergone desorption from the LBL), the molecule attains a coil-like shape to minimize the surface area: therefore, the lengths $l_A$ and $l_B$ significantly decreases in the bulk water for both the cases of NPSLBL and the PSSLBL.

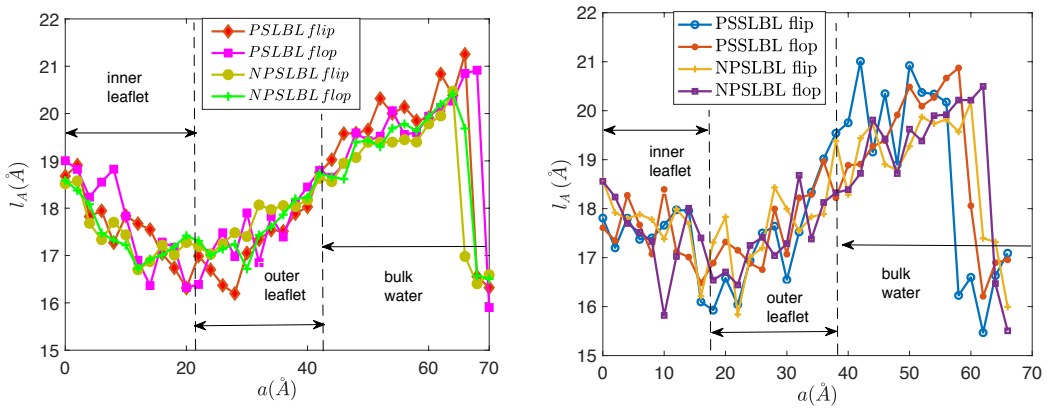


(a) (b)

***Figure 4.7:*** *Variation of the tail lengths $l_A$ for the star lipid molecules traversing inside and outside the LBL for the NPSLBL and the PSSLBL. $l_A$ have been defined in Fig. 1(a). (a) system A and C (b) system B and D. We identify the locations of the lipid bilayer as well as the bulk water. Also $a = 0$ Å represents the location of the inner leaflet for both the NPSLBL and the PSSLBL.*

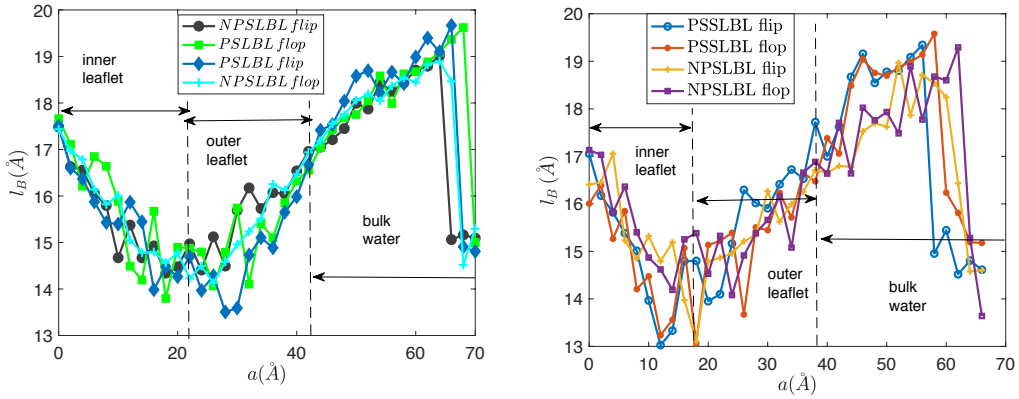


(a) (b)

***Figure 4.8:*** *Variation of the tail lengths $l_B$ for the star lipid molecules traversing inside and outside the LBL for the NPSLBL and the PSSLBL. $l_B$ have been defined in Fig. 1(a). (a) system A and C (b) system B and D. We identify the locations of the lipid bilayer as well as the bulk water. Also $a = 0$ Å represents the location of the inner leaflet for both the NPSLBL and the PSSLBL.*

Finally, Fig. 4.9 shows the orientation of the *star lipid* molecules (defined earlier) as a function of the reaction coordinate $\alpha$. Fig. 4.4(a) and Fig. 4.5(a) provide the definition of $\theta$ for the PSSLBL and the NPSLBL, respectively. For both the PSSLBL and the NPSLBL, the *star lipids* are anti-parallel to the membrane normal [also defined in Figs. 4.2(a) and 4.3(a)] at the inner leaflet (as a consequence, $\theta$ is nearly 180 degree), become perpendicular to the membrane normal when they approach the hydrophobic core (as a consequence, $\theta$ is close to 90 degree), and finally become parallel to the membrane normal at the outer leaflet (as a consequence, $\theta$ is close to 0 degree). The *star lipids* retain this orientation (at the outer leaflet) until become fully merged into the bulk water where they become coil like, and the definition of the orientation angle become meaningless.

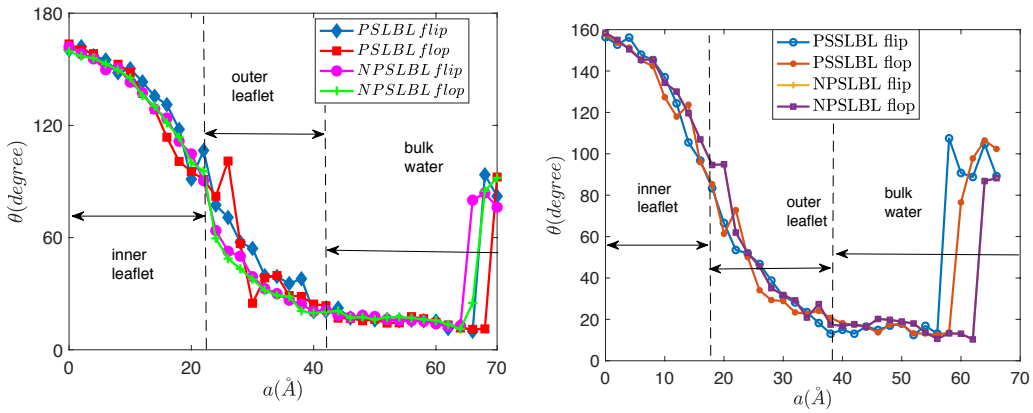


(a) (b)

***Figure 4.9:*** *Variation of θ (See Fig. 4.2 and Fig.4. 3 for definition) for the start lipid molecules as it traverses the LBL for both the PSSLBL and the NPSLBL. (a) system A and C (b) system B and D. We identify the locations of the lipid bilayer as well as the bulk water. Also* $a = 0$ Å *represents the location of the inner leaflet for both the NPSLBL and the PSSLBL.*

## *4.4. Conclusion*

To summarize, in this chapter we study an extremely important problem of the role of curvature on the energetics of lipid flip-flop and desorption on supported LBLs. Considering NPSLBL and PSSLBL as respective examples of supported curved and non-curved LBLs, our findings establish a highly intriguing finding: the energetics of lipid flip-flop and desorption are independent of curvature, which agrees with experimental findings[57]. This is most remarkable, given the significant variation in the number distribution as well as area per unit lipid (in the two leaflets) between the cases of NPSLBL and the PSSLBL. such a situation allows us to interpret the energetics of lipid motion within the bilayers of different sized vesicles by simply studying the lipid flip-flops in planar LBL systems that are experimentally tractable.[18-34]

## *Bibliography*


1. Higgins, C. F. Flip-Flop: The Transmembrane Translocation of Lipids. *Cell* **1994**, *79*, 393–395.
2. Allhusen, J. S.; Conboy, J. C. The Ins and Outs of Lipid Flip-Flop. *Acc. Chem. Res.* **2017**, *50*, 58–65.
3. Contreras, F-X.; Sánchez-Magraner, L.; Alonso, A.; Goñi, F. M. Transbilayer (flip-flop) Lipid Motion and Lipid Scrambling in Membranes. *FEBS Lett.* **2010**, *584*, 1779–1786.
4. van Meer, G.; Voelker, D. R.; Feigenson, G. W. Membrane Lipids: Where they are and How they Behave. *Nat. Rev. Mol. Cell Biol.* **2008**, *9*, 112−124.
5. Volinsky, R.; Kinnunen, P. K. Oxidized Phosphatidylcholines in Membrane-level Cellular Signaling: From Biophysics to Physiology and Molecular Pathology. *FEBS J.* **2013**, *280*, 2806−2816.
6. Papadopulos, A.; Vehring, S.; Lopez-Montero, I.; Kutschenko, L.; Stockl, M.; Devaux, P. F.; Kozlov, M.; Pomorski, T.; Herrmann, A. Flippase Activity Detected with Unlabeled Lipids by Shape Changes of Giant Unilamellar Vesicles. *J. Biol. Chem.* **2007**, *282*, 15559−155568.
7. Khalifat, N.; Rahimi, M.; Bitbol, A-F.; Seigneuret, M.; Fournier, J-B.; Puff, N.; Arroyo, M.; Angelova, M. I.; Interplay of Packing and Flip-flop in Local Bilayer Deformation. How Phosphatidylglycerol Could Rescue Mitochondrial Function in a Cardiolipin-deficient Yeast Mutant. *Biophys. J.* **2014**, *107*, 879−890.

8. Devaux, P. F.; Herrmann, A.; Ohlwein, N.; Kozlov, M. M. How Lipid Flippases can Modulate Membrane Structure. *Biophys. Biochim. Acta* **2008**, *1778*, 1591−1600.
9. Fadeel, B.; Xue, D. The Ins and Outs of Phospholipid Asymmetry in the Plasma Membrane: Roles in Health and Disease. *Crit. Rev. Biochem. Mol. Biol.* **2009**, *44*, 264−277.
10. Zwaal, R. F. A.; Schroit, A. J. Pathophysiologic Implications of Membrane Phospholipid Asymmetry in Blood Cells. *Blood* **1997**, *89*, 1121−1132.
11. Bratton, D. L.; Fadok, V. A.; Richter, D. A.; Kailey, J. M.; Frasch, S. C.; Nakamura, T.; Henson, P. M. Polyamine Regulation of Plasma Membrane Phospholipid Flip-Flop during Apoptosis. *J. Biol. Chem.* **1999**, *274*, 28113−28120.
12. Branningan, G.; Brown, F. L. H. A Consistent Model for Thermal Fluctuations and Protein-Induced Deformations in Lipid Bilayers. *Biophys. J.* **2006**, *90*, 1501−1520.
13. Johannes, L.; Pezeshkian, W.; Ipsen, J. H.; Shillcock, J. C. Clustering on Membranes: Fluctuations and More. *Trends Cell Biol.* **2018**, *28*, 405−415.
14. Garcia-Parajo, M. F.; Cambi, A.; Torreno-Pina, J. A.; Thompson, N.; Jacobson, K. Nanoclustering as a Dominant Feature of Plasma Membrane Organization. *J. Cell Sci.* **2014**, *127*, 4995−5005.
15. Gilbert, R. J. C.; Serra, M. D.; Froelich, C. J.; Wallace, M. I.; Anderluh, G. Membrane Pore Formation at Protein–Lipid Interfaces. *Trends Biochem. Sci.* **2014**, *39*, 510−516.

16. Salamone, M.; Pavia, F. C.; Ghersi, G. Proteolytic Enzymes Clustered in Specialized Plasma-Membrane Domains Drive Endothelial Cells' Migration. *Plos One* **2016**, DOI: 10.1371/journal.pone.0154709.
17. Ferguson, M. A. J. Lipid Anchors on Membrane Proteins. *Curr. Opin. Struct. Biol.* **1991**, *1*, 522−529.
18. McConnell, H. M.; Kornberg, R. D. Inside-Outside Transitions of Phospholipids in Vesicle Membranes. *Biochemistry* **1971**, *10*, 1111−1120.
19. Morrot, G.; Herve, P.; Zachowski, A.; Fellmann, P.; Devaux, P. F. Aminophospholipid Translocase of Human Erythrocytes: Phospholipid Substrate Specificity and Effect of Cholesterol. *Biochemistry* **1989**, *28*, 3456−3462.
20. Seigneuret, M.; Devaux, P. F. ATP-dependent Asymmetric Distribution of Spin-labeled Phospholipids in the Erythrocyte Membrane: Relation to Shape Changes. *Proc. Natl. Acad. Sci. U. S. A.* **1984**, *81*, 3751−3755.
21. Maekawa, M.; Fairn, G. D. Molecular Probes to Visualize the Location, Organization and Dynamics of Lipids. *J. Cell Sci.* **2014**, *127*, 4801−4812.
22. Devaux, P. F.; Fellmann, P.; Herve, P. Investigation on Lipid Asymmetry using Lipid Probes. Comparison between Spin-labeled Lipids and Fluorescent Lipids. *Chem. Phys. Lipids* **2002**, *116*, 115−134.
23. Nakano, M.; Fukuda, M.; Kudo, T.; Endo, H.; Handa, T. Determination of Interbilayer and Transbilayer Lipid Transfers by Time-Resolved Small-Angle Neutron Scattering. *Phys. Rev. Lett.* **2007**, *98*, 238101.

24. Nakano, M.; Fukuda, M.; Kudo, T.; Matsuzaki, N.; Azuma, T.; Sekine, K.; Endo, H.; Handa, T. Flip-Flop of Phospholipids in Vesicles: Kinetic Analysis with Time-Resolved Small-Angle Neutron Scattering. *J. Phys. Chem. B* **2009**, *113*, 6745−6748.
25. Homan, R.; Pownall, H. J. Transbilayer Diffusion of Phospholipids: Dependence on Headgroup Structure and Acyl chain length. *Biochim. Biophys. Acta, Biomembr.* **1988**, *938*, 155−166.
26. John, K.; Schreiber, S.; Kubelt, J.; Herrmann, A.; Muller, P. Transbilayer Movement of Phospholipids at the Main Phase Transition of Lipid Membranes: Implications for Rapid Flip-flop in Biological Membranes. *Biophys. J.* **2002**, *83*, 3315−3323.
27. Liu, J.; Conboy, J. C. Direct Measurement of the Transbilayer Movement of Phospholipids by Sum-Frequency Vibrational Spectroscopy. *J. Am. Chem. Soc.* **2004**, *126*, 8376−8377.
28. Liu, J.; Conboy, J. C. 1,2-Diacyl-phosphatidylcholine Flip-flop Measured Directly by Sum-frequency Vibrational Spectroscopy. *Biophys. J.* **2005**, *89*, 2522−2532.
29. Roseman, M.; Litman, B. J.; Thompson, T. E. Transbilayer Exchange of Phosphatidylethanolamine for Phosphatidylcholine and Nacetimidoylphosphatidylethanolamine in Single-walled Bilayer Vesicles. *Biochemistry* **1975**, 14, 4826−4830.
30. Roseman, M. A.; Thompson, T. E. Mechanism of the Spontaneous Transfer of Phospholipids between Bilayers. *Biochemistry* **1980**, *19*, 439−444.

31. Wimley, W. C.; Thompson, T. E. Transbilayer and Interbilayer Phospholipid Exchange in Dimyristoylphosphatidylcholine/dimyristoylphosphatidylethanolamine Large Unilamellar Vesicles. *Biochemistry* **1991**, *30*, 1702−1709.
32. Anglin, T. C.; Cooper, M. P.; Li, H.; Chandler, K.; Conboy, J. C. Free Energy and Entropy of Activation for Phospholipid Flip-Flop in Planar Supported Lipid Bilayers. J. Phys. Chem. B 2010, 114, 1903−1914.
33. Anglin, T. C.; Conboy, J. C. Kinetics and Thermodynamics of Flip-Flop in Binary Phospholipid Membranes Measured by Sum-Frequency Vibrational Spectroscopy. Biochemistry 2009, 48, 10220−10234.
34. McLean, L. R.; Phillips, M. C. Mechanism of Cholesterol and Phosphatidylcholine Exchange or Transfer between Unilamellar Vesicles. *Biochemistry* **1981**, *20*, 2893−2900.
35. Gurtovenko, A. A.; Vattulainen, I. Molecular Mechanism for Lipid Flip-Flops. *J. Phys. Chem. B* **2007**, *111*, 13554−13559.
36. Marti, J.; Csajka, F. S. Flip-flop Dynamics in a Model Lipid Bilayer Membrane. *Europhys. Lett.* **2003**, *61*, 409−414.
37. Marti, J.; Csajka, F. S. Transition Path Sampling Study of Flip-flop Transitions in Model Lipid Bilayer Membranes. *Phys. Rev. E* **2004**, *69*, 061918.
38. Tieleman, D. P.; Marrink, S.-J. Lipids Out of Equilibrium: Energetics of Desorption and Pore Mediated Flip-Flop. *J. Am. Chem. Soc.* **2006**, *128*, 12462−12467.

39. McMahon HT; Boucrot E. Membrane Curvature at a Glance. Journal of Cell Science 2015, 128 (6), 1065–1070 DOI: 10.1242/jcs.114454.
40. Ramamurthi KS. Protein Localization by Recognition of Membrane Curvature. Current Opinion in Microbiology 2010, 13 (6), 753–757 DOI: 10.1016/j.mib.2010.09.014
41. Domanov, Y. A.; Aimon, S.; Toombes, G. E. S.; Renner, M.; Quemeneur François; Triller, A.; Turner, M. S.; Bassereau, P. Mobility in Geometrically Confined Membranes. Proceedings of the National Academy of Sciences of the United States of America2011, 108 (31), 12605–12610.
42. Chao MH; Lin YT; Dhenadhayalan N; Lee HL; Lee HY; Lin KC. 3d Probed Lipid Dynamics in Small Unilamellar Vesicles. Small (weinheim an Der Bergstrasse, Germany) 2017, 13 (13) DOI: 10.1002/smll.201603408.
43. Abir Maarouf Kabbani; Xinxin Woodward; Christopher V. Kelly. Revealing the Effects of Nanoscale Membrane Curvature on Lipid Mobility. Membranes 2017, 7 (4) DOI: 10.3390/membranes7040060.
44. Risselada, H. J.; Marrink, S. J. Curvature Effects on Lipid Packing and Dynamics in Liposomes Revealed by Coarse Grained Molecular Dynamics Simulations. Physical Chemistry Chemical Physics 2009, 11 (12), 2056–2067.
45. Marquardt D; Heberle FA; Miti T; Eicher B; London E; Katsaras J; Pabst G. 1H NMR Shows Slow Phospholipid Flip-Flop in Gel and Fluid Bilayers. Langmuir : The Acs Journal of Surfaces and Colloids 2017, 33(15), 3731–3741 DOI: 10.1021/acs.langmuir.6b04485.

46. Ashley, C. E., Carnes, E. C.; Phillips, G. K.; Padilla, D., Durfee, P. N., Brown, P. A., Hanna, T. N., Liu, J.; Phillips, B., Carter, M. B., Carroll, N. J., Jiang, X., Dunphy, D. R., Willman, C. L., Petsev, D. N., Evans, D. G., Parikh, A. N., Chackerian, B., Wharton, W., Peabody, D. S., and Brinker, C. J., The Targeted Delivery of Multicomponent Cargos to Cancer Cells by Nanoporous Particle-Supported Lipid Bilayers. *Nat. Mater.* **2011**, 10, 389-397.

47. Tarn, D., Ashley, C. E., Xue, M., Carnes, E. C., Zink, J. I., and Brinker, C. J., Mesoporous Silica Nanoparticle Nanocarriers: Biofunctionality and Biocompatibility. *Acc. Chem. Res.* **2013**, 46, 792-801.

48. Liu, J., Jiang, X., Ashley, C., and Brinker, C. J., Electrostatically Mediated Liposome Fusion and Lipid Exchange with a Nanoparticle-Supported Bilayer for Control of Surface Charge, Drug Containment, and Delivery. *J. Am. Chem. Soc.* **2009**, 131, 7567-7569.

49. Lin, Y.-S., and Haynes, C. L., Impacts of Mesoporous Silica Nanoparticle Size, Pore Ordering, and Pore Integrity on Hemolytic Activity. *J. Am. Chem. Soc.* **2010**, 132, 4834-4842.

50. Liu, J., Stace-Naughton, A., Jiang, X., and Brinker, C. J., Porous Nanoparticle Supported Lipid Bilayers (Protocells) as Delivery Vehicles. *J. Am. Chem. Soc.* **2009**, 131, 1354-1355.

51. Fu, R., Gill, R. L., Kim, E. Y., Briley, N. E., Tyndall, E. R., Xu, J., Li, C., Ramamurthi, K. S., Flanagan, J. M., and Tian, F., Spherical Nanoparticle Supported Lipid Bilayers for the Structural Study of Membrane Geometry-Sensitive Molecules. *J. Am. Chem. Soc.* **2015**, 137, 14031-14034.

52. Gill Jr., R. L., Castaing, J-P., Hsin, J., Tan, I. S., Wang, X., Huang, K. C., Tian, F., and Ramamurthi, K. S., Structural Basis for the Geometry-driven Localization of a Small Protein. *Proc. Natl. Acad. Sci. USA* **2015**, *112*, E1908-E1915.

53. Kim, E. W., Tyndall, E. R., Huang, K. C., and Tian, F., Dash-and-Recruit Mechanism Drives Membrane Curvature Recognition by the Small Bacterial Protein SpoVM. *Cell Syst.* **2017**, *5*, 518-526.

54. Marrink, S. J.; Risselada, H. J.; Yefimov, S.; Tieleman, D. P.; de Vries, A. H. The MARTINI Force Field: Coarse Grained Model for Biomolecular Simulations. *J. Phys. Chem. B* **2007**, *111*, 7812-7824.

55. Martínez, L.; Andrade, R.; Birgin, E. G.; Martínez, J. M. PACKMOL: A Package for Building Initial Configurations for Molecular Dynamics Simulations. *J. Comput. Chem.* **2009**, *30*, 2157-2164.

56. Phillips, J. C.; Braun, R.; Wang, W.; Gumbart, J.; Tajkhorshid, E.; Villa, E.; Chipot, C.; Skeel, R. D.; Kale, L.; Schulten, K. Scalable Molecular Dynamics with NAMD. *J. Comput. Chem.* **2005**, *26*, 1781-1802.

57. Grossfield, Alan, "WHAM: the weighted histogram analysis method", version 2.0.10.2, http://membrane.urmc.rochester.edu/wordpress/?page_id=126

# Chapter 5: Physical Basis for Membrane Curvature Sensing Revealed by Molecular Dynamics Simulation*

***Abstract:*** *Certain amphipathic alpha helix-harboring proteins can bind preferentially to micron-scale positively curved (convex) membranes, which can drive subcellular localization of those proteins. Despite increased mechanistic understanding of how this occurs, the molecular differences between differently curved membranes at this scale that can allow membrane shape-sensing proteins to discriminate between them are unknown. Here we employ Molecular Dynamics (MD) simulations to probe the membrane interaction of SpoVM, a small amphipathic alpha helical bacterial protein that preferentially localizes to convex membranes. We investigate the energetics of SpoVM binding to two membrane systems of widely varying curvatures: a planar substrate supported lipid bilayer representing a non-curved membrane system and a nanoparticle-supported lipid bilayer representing a highly curved membrane system. We identify five different contributions that drive the energetics of protein adsorption to the differently curved membrane systems and identify that the dictating contribution comes from the energetics associated with migration of the protein from the membrane-bound to unbound state. We show that the interplay of electrostatic interactions between the lipid head groups and charged residues of the protein, combined with hydrophobic interactions between the lipid*

*The contents of this Chapter will be submitted for publication as the following journal article: Jing, H.; Wang, Y.; Ramamurthi, K. S.; Das, S. "Physical Basis for Membrane Curvature Sensing Revealed by Molecular Dynamics Simulation." *Cell Reports* (To be Submitted for Publication).

*tails and hydrophobic residues of the protein, is more favorable in highly curved membranes. Our model therefore proposes that differential interaction of SpoVM with phospholipid head groups and acyl chains of differently curved membranes mediates preferential desorption of the protein from membranes of unfavorable curvature.*

## *5.1. Introduction*

Over the last few decades, experiments have revealed that amphipathic alpha helix protein can sense membrane curvature, which plays an important role in protein localization.[1-4] However, the exact mechanism of such membrane sensing by proteins remains unclear stemming from the fact that amphipathic alpha helix binding to membrane are expected to be governed by the competition of several effects, including stereospecificity, hydrophobicity, and electrostatics.[5] There are three hypotheses to explain the mechanism of sensing membrane curvature by amphipathic alpha helix protein: (a) one can find more number of defects at the surface of membranes with higher curvatures, which in turn dictates the membrane curvature sensing by the proteins;[6-8] (b) the packing of the acyl chains of lipids, which is a function of membrane curvature, regulates the membrane sensing by the proteins;[9] (c) the folding of protein and protein absorption are coupled and larger curvatures facilitate protein folding thereby facilitating membrane sensing by the proteins (the Velcro model).[5] It is difficult to experimentally reveal the exact preferred mechanism of membrane sensing by proteins due to the requirement of atomistic-scale resolution.[5] In this study, we employ Molecular Dynamics (MD) simulations to reveal the mechanism of membrane curvature sensing by SpoVM (a small amphipathic

alpha helix protein). SpoVM is involved in the spore formation in the bacterium Bacillus subtilis.[9-11] SpoVM binds to the only available convex membrane surface in the bacterium cell, namely the outer surface of the *forespore* (which is an aspherical internal organelle that is elaborated by the rod shape bacterium and evolves into a dormant spore).[12] *In vitro* experiments showed that the SpoVM is a membrane curvature sensing protein as it prefers the convex membrane with higher curvature.[4]

Our calculations consider two representative examples of membranes with large differences in curvatures: they are planar substrate supported lipid bilayer (PSSLBL) representing a flat (non-curved) membrane system and a nanoparticle supported lipid bilayer (NPSLBL) representing a highly curved membrane system. The mechanism of *membrane curvature sensing* by the SpoVM, is quantified by scrutinizing the differences in the energetics of the SpoVM binding to the PSSLBL and the NPSLBL. Our calculations consider as many as five different contributions constituting the energetics of protein binding to the differently curved membrane systems. Among these contributions, we unravel that the contribution associated with the migration of the SpoVM from the membrane to the bulk, dictated by the combination of the protein-lipid-heads electrostatic (hydrophilic) and protein-lipid-tails hydrophobic interactions, dominates and is more favorable for the NPSLBL system. Accordingly, we infer that the SpoVM molecule would show a larger preference to bind to the NPSLBL system (i.e., the highly curved membrane system): this helps to identify membrane curvature sensing activity of the SpoVM.

## *5.2 Simulation Set Up*

### *5.2.1. SpoVM absorbed to the PSSLBL*

Fig. 5.1(a) shows the 3D structure of the SpoVM protein, which is obtained from the experiments and the all atom MD simulations conducted by Gill *et al.*[13]. The all atom model was coarse grained, as shown in Fig 5.1(c), by using the Martini Model[14] by via the CG Builder of NAMD[15].

The SpoVM was initially placed in the bulk water 1.5 nm away from the upper surface of the self-assembled PSSLBL discussed in Chapter 4, as shown in Fig. 5.2(a). After 0.1 $\mu s$ of simulations, the SpoVM absorbed to the PSSLBL spontaneously. The entire structure was then equilibrated for another 0.5 $\mu s$, resulting in the structure as elucidated in Fig. 5.2(b).

After obtaining these two initial configurations, the SpoVM was decoupled from the LBL of PSSLBL by the applied umbrella potential[16] and the corresponding restraints. Therefore, the binding free energy is the opposite of the decoupling free energy.

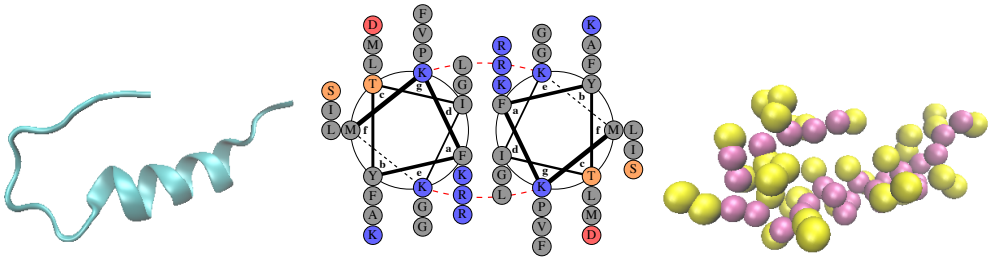

(a) (b) (c)

***Figure 5. 1: Model of SpoVM***

*(a) molecular Structure of SpoVM. (b) Helix wheel plot of SpoVM. (c) Coarse grained model of SpoVM*

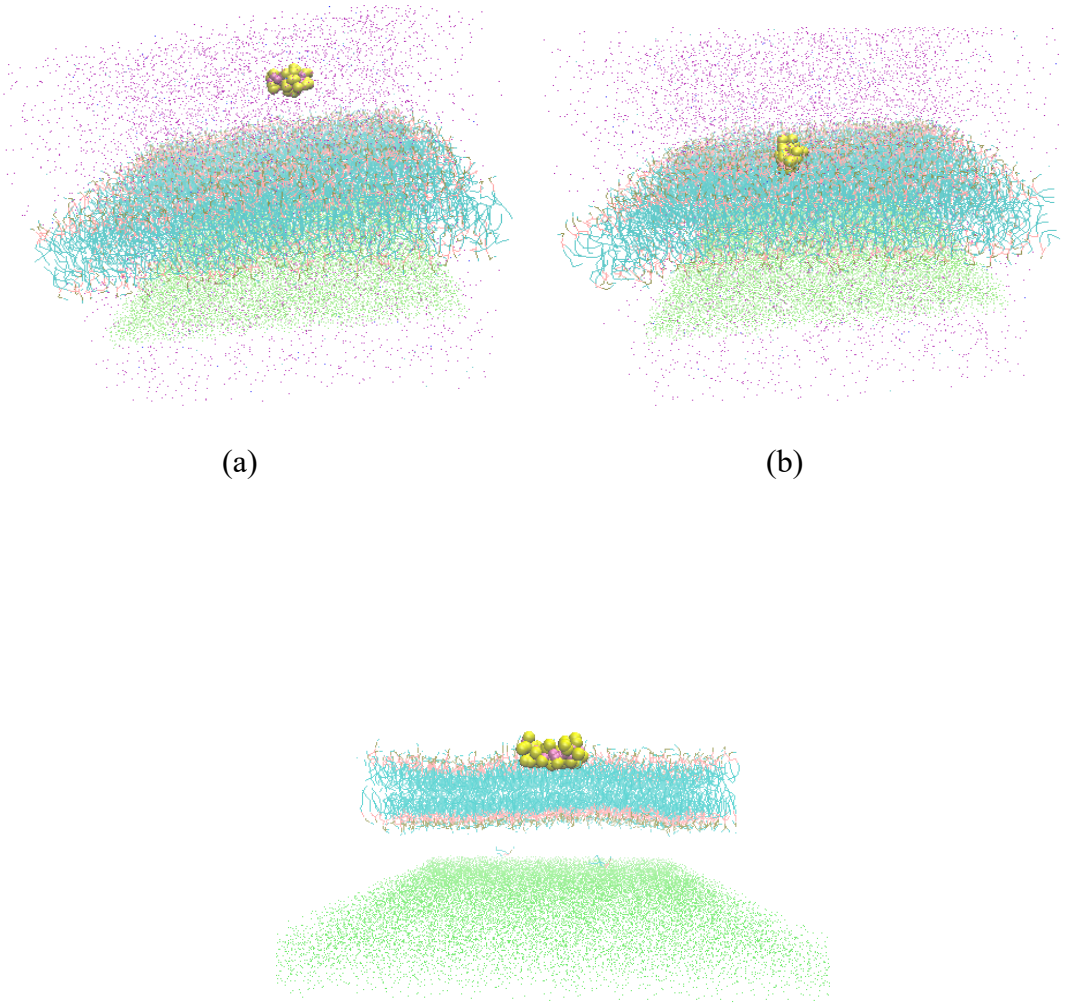

(a) (b)

(c)

***Figure 5. 2: SpoVM absorbed to PSSLBL***

*(a) MD simulation snapshot of the initial configuration of the SopVM protein approaching a self-assembled equilibrated PSSLBL. (b) MD simulation snapshot of the SpoVM absorbed to the PSSLBL. (c) snapshot shows the position of the protein in the LBL. The color code is arranged as: orange: hydrophilic heads of the lipids; green: hydrophobic tails of the lipids; purple: water; light green: support substrate.*

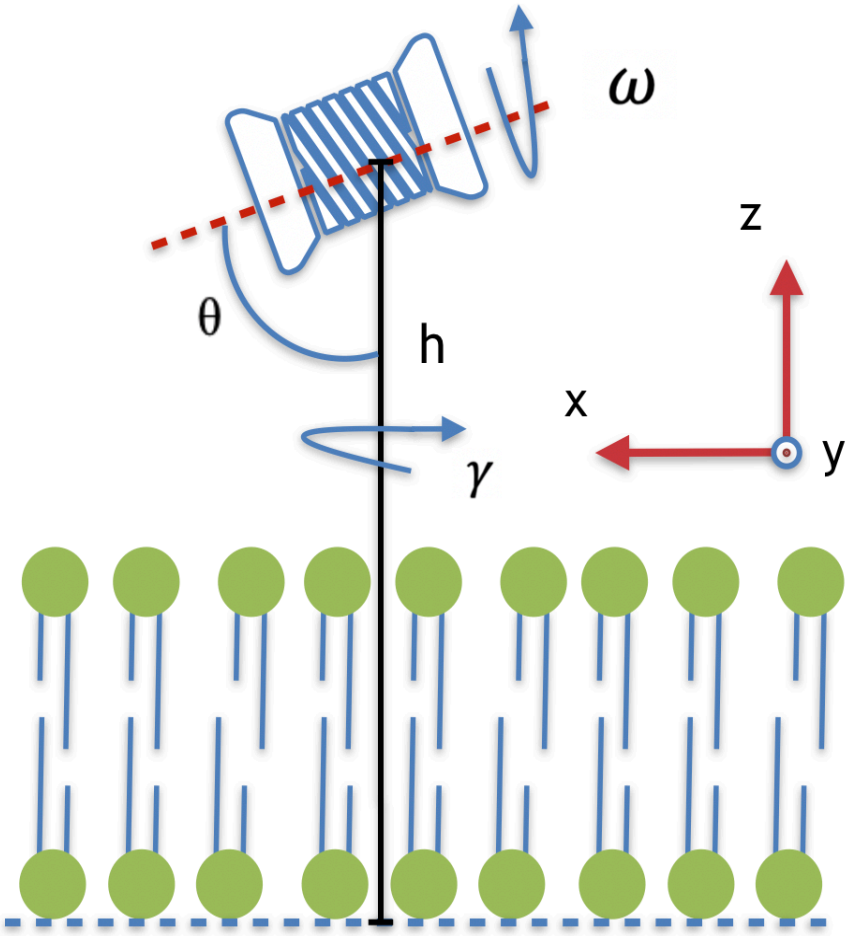


***Figure 5. 3: Schematic of the relative position between SpoVM and PSSLBL***

*Schematic showing the relative position between SpoVM and PSSLBL and defining the different reaction coordinates needed (such as θ, ω, h…) to compute the various PMFs needed to quantify the several free energy components.*

In Fig. 5.3, we show the definition of three Euler angle $\theta, \omega, \gamma$, and the distance $h$. Umbrella Sampling[16] was used to calculate the PMFs needed to obtain $\Delta G_X$ (where $X$= $C$, $\theta$, $\omega$, $B$, and $a$).

*5.2.2. SpoVM absorbed to the NPSLBL*

The SpoVM was initially placed in the bulk 1.5 nm away from the outer surface of the self-assembled NSSLBL discussed in Chapter 4, as shown in Fig. 5.4(a). After 0.1 $\mu s$ simulations, the SpoVM absorbed to the NSSLBL spontaneously. The entire structure was then equilibrated for 1 $\mu s$, resulting in the structure as shown in Fig. 5.4(b).

As indicated by Gill *et al*.,[13] the helical region of the protein is deeply buried inside the lipid bilayer. The same configuration is also observed in our simulations, as elucidated in Figs. 5.2(c) and 5.4(c).

After obtaining these two initial configurations, the SpoVM was decoupled from the LBL of NPSLBL by the applied umbrella potential and the corresponding restraints, Therefore, the binding free energy is the opposite of the decoupling free energy.

In Fig. 5.5, we show the definition of three Euler angle $\theta, \omega, \gamma$, and the distance $r$. The first polar angle $\varphi$ is the angle between $r$ vector and $z$ axis; The second polar angle $\phi$ is the projection of angle between $r$ vector and $x$ axis to the $xy$ plane. Umbrella Sampling was used to calculate the PMFs needed to obtain $\Delta G_X$ (where $X$= $C$, $\theta$, $\omega$, $B$, and $a$).

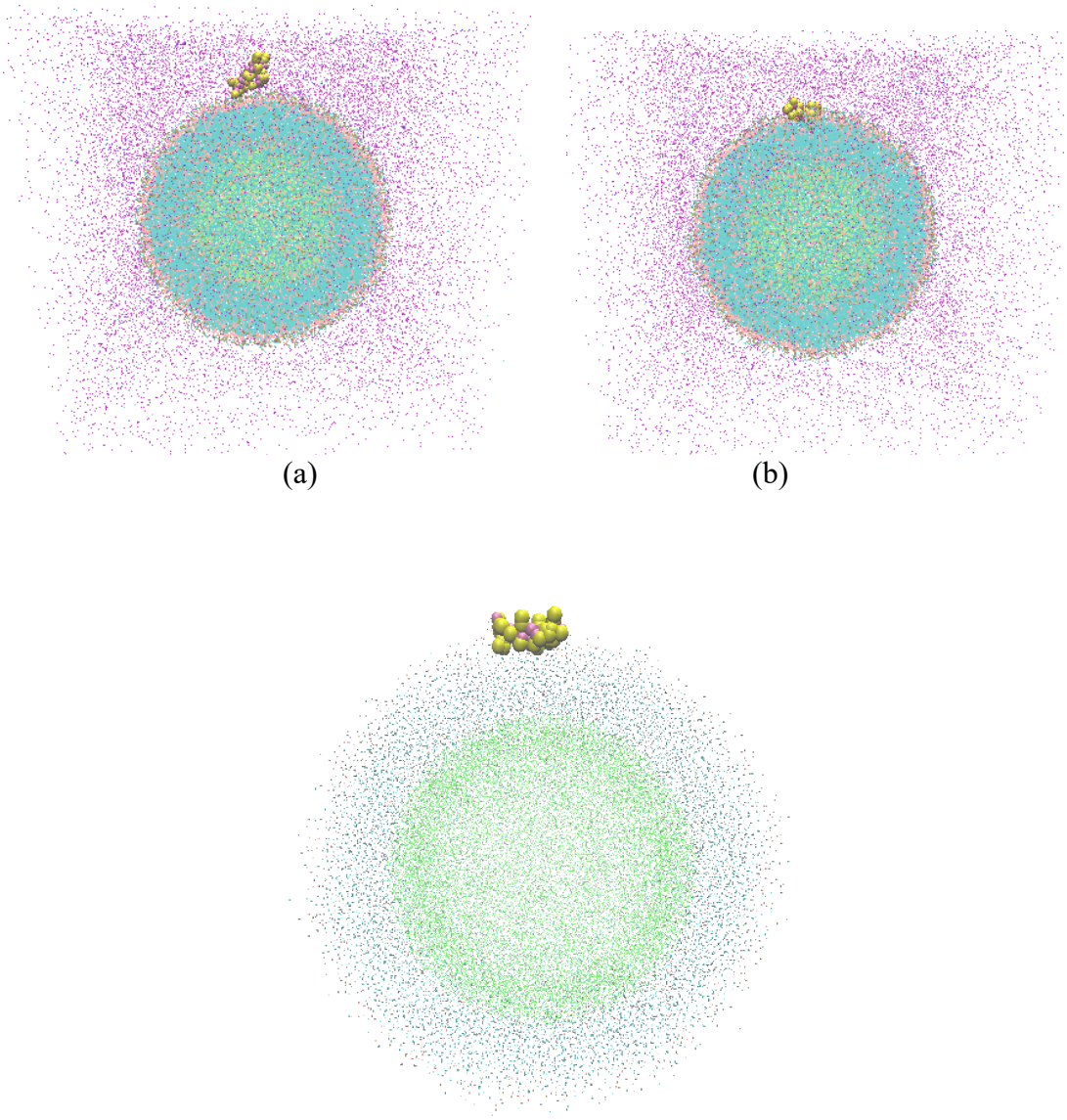

(a) (b)

(c)

***Figure 5. 4: SpoVM absorbed to NPSLBL***

*MD simulation snapshot of the initial configuration of the SopVM protein approaching a self-assembled equilibrated NPSLBL. (b) MD simulation snapshot of the SpoVM absorbed to the NPSLBL. (c) snapshot shows the position of the protein in the LBL. The color code is arranged as: orange: hydrophilic heads of the lipids; green: hydrophobic tails of the lipids; purple: water; light green: nanoparticle.*

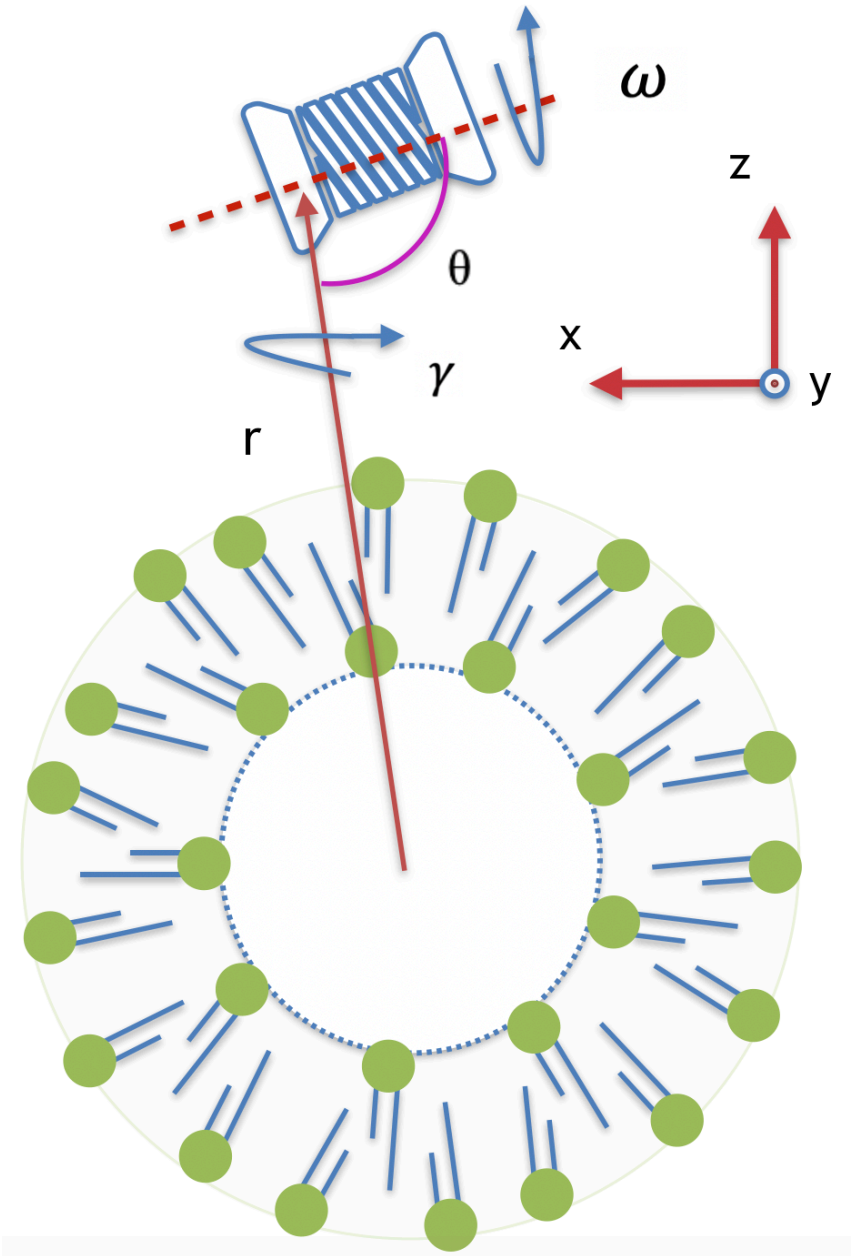


***Figure 5. 5: Schematic of the relative position between SpoVM and NPSLBL***

*Schematic showing the relative position between SpoVM and NPSLBL and defining the different reaction coordinates needed (such as θ, ω, h……) to compute the various PMFs needed to quantify the several free energy components.*

## *5.3 Free Energy Calculation*

The free energy change associated with the protein binding to the membrane (such *preferential* binding is the mechanism of membrane curvature sensing by the proteins) comprises of five different contributions, reduced from eight contributions, as identified by Ref. 17 and 18, due to the isotropy of the membrane surface. These contributions, which would be computed from the different PMFs obtained with specific reaction coordinates (and restraining other coordinates), are as follow: 1) the free energy change $\Delta G_C$ associated with deforming the protein in the bilayer (quantified by the root mean square deviation (RMSD) of the protein inside the membrane, $rmsd_m$; hence $rmsd_m$ will serve as the reaction coordinate for calculating the PMF needed to compute $\Delta G_C$) with respect to the conformation of the protein in the membrane, 2) the free energy change $\Delta G_\theta$ associated with reorienting the protein in the bilayer about the first Euler angle $\theta$ (hence $\theta$ will serve as the reaction coordinate for calculating the PMF needed to compute $\Delta G_\theta$) keeping the conformation of the protein restrained, 3) the free energy change $\Delta G_\omega$ associated with reorienting the protein in the bilayer about the second Euler angle $\omega$ (hence $\omega$ will serve as the reaction coordinate for calculating the PMF needed to compute $\Delta G_\omega$) keeping the protein conformation in the bilayer as well as the first Euler angle restrained, 4) the free energy change $\Delta G_a$ associated with changing the position of the center of the protein from the membrane to the bulk water with the protein conformation in the bilayer as well as both the Euler angles restrained [here $a$, which is defined differently for the PSSLBL and the NPSLBL (see Figs. 5.3, 5.5), serves as the reaction coordinate needed to calculate the PMF that provides $\Delta G_a$], and 5) the

free energy change $\Delta G_B$ associated with the deformation of the protein in the bulk water with respect to the conformation of the protein in the membrane and quantified by the root mean square deviation of the protein inside the bulk $rmsd_B$ (hence $rmsd_B$ will serve as the reaction coordinate for calculating the PMF needed to compute $\Delta G_B$; $\Delta G_B$ is expected to be the same for the PSSLBL and NPSLBL). The free energy changes with respect to the third Euler angle and the two polar angles can be neglected because the PSSLBL is isotropic in the x and y directions and the NPSLBL is isotropic in the latitudinal and longitudinal directions.

The force constant for $rmsd_m$, the reaction coordinate to calculate the PMF that leads to the calculation of $\Delta G_C$, is 10 kcal/$(mol \cdot Å^2)$, and $rmsd_m$ was shifted 1 $Å^2$ per simulation window, and there are 10 simulation windows. The force constant for $\theta$, the reaction coordinate to calculate the PMF that leads to the calculation of $\Delta G_\theta$, is 1 kcal/$(mol \cdot degree^2)$, and $\theta$ is shifted 4 degree per simulation window, and there are 10 simulation windows. The force constant for $\omega$, the reaction coordinate to calculate the PMF that leads to the calculation of $\Delta G_\omega$, is 1 kcal/$(mol \cdot degree^2)$, and $\omega$ is shifted 4 degree per simulation window, and there are 10 simulation windows. The force constant for $r$, which are used as a reaction coordinate to calculate the PMF that leads to the calculation of $\Delta G_a$, is 2.5 kcal/$(mol \cdot Å^2)$, and $r$ is shifted 2 Å per simulation window, and there are 15 simulation windows. The reaction coordinate $a = r - r_0$, where $r_0$ is the initial value of $r$ as protein binding to the membrane. The force constant for $rmsd_B$, the reaction coordinate to calculate the PMF that leads to the calculation of $\Delta G_B$, is 10 kcal/$(mol \cdot Å^2)$, and $rmsd_B$ was shifted 1 $Å^2$ per simulation window, and there are 10 simulation windows.

All PMF simulations are carried out by using NAMD[15] software, with martini force field[14] and NPT thermostats. The temperature is set to 310 K, and the pressure is set to 1 bar. All molecules are coarse grained by using Martini Model[14].

Under these circumstances, the total free energy change can accordingly be expressed as:[16]

$$-\Delta G^0 = \Delta G_C + \Delta G_\theta + \Delta G_\omega + \Delta G_a - \Delta G_B - \Delta G_O. \qquad (5.1)$$

In eq. (5.1), in addition to the contributions described above, we also account for $\Delta G_O$ (expressed later), which represents the free energy change associated with the loss of entropy due to the restraints on θ and ω (describe above) in bulk water. In eq. (5.1) the free energy changes $\Delta G_X$ (with $X$=$C$, $\theta$, $\omega$, or $B$), which represents the entropy lost due to the applied restraints, can be expressed as:

$$\Delta G_X = \frac{\int dX \exp\left(-\beta H_X\right)}{\int dX \exp\left[-\beta\left(H_X + u_X\right)\right]}. \qquad (5.2)$$

In eq.(5.2), $H_X$ is the PMF obtained from the simulations, $u_X = \frac{1}{2}k\left(X - X_0\right)^2$ ($X$ is the reaction coordinate, $X_0$ is the equilibrium position, and $k$ is the force constant) is the restraint potential imposed on the protein, and $\beta = \frac{1}{k_B T}$ ($k_B$ is the Boltzmann constant and $T$ is the temperature).

Secondly, we can express $\Delta G_a$ appearing in eq. (5.1) as:

$$\Delta G_a = \frac{1}{\beta}\ln\left[2\pi A^2 C \int ds \exp\left\{-\beta\left(H_a(s) - H_a(A)\right)\right\}\right]. \qquad (5.3)$$

In eq.(5.3), C = 1/1661Å$^3$ is the standard concentration,[18] $A$ is a reference point far from the membrane, and $H_a(s)$ is the PMF associated with changing the position of

the center of the protein from the membrane to the bulk water under the conditions where the protein conformation within the membrane and both the Euler angles are restrained. It is useful to note that $\Delta G_a$ is independent of the choice of $A$.[17]

Finally, $\Delta G_O$ appearing in eq. (5.1) can be expressed as:

$$\Delta G_O = -\frac{1}{\beta}\ln\left[\frac{1}{4\pi}\int_0^{\theta} d\theta \sin\theta \int_{-\pi}^{\pi} d\omega \exp\left[-\beta\left(u_\theta + u_\omega\right)\right]\right], \quad (5.4)$$

where $u_\theta$ and $u_\omega$ are provided through the generic expression of $u_X$ [please see below eq. (5.2)].

***Table 5. 1:*** **Free energy changes corresponding to different restraints and reaction coordinates**

| $\Delta G_X$ *(kcal/mol)* | PSSLBL | NPSLBL | $\Delta\Delta G_X$ |
|---|---|---|---|
| $\Delta G_C$ | 0.67±0.00 | 0.66±0.00 | 0.01 |
| $\Delta G_\theta$ | 0.57±0.00 | 0.73±0.00 | -0.16 |
| $\Delta G_\omega$ | 1.01±0.00 | 0.87 | 0.14 |
| $\Delta G_B$ | 0.79 | 0.79 | 0 |
| $\Delta G_a$ | 40.30±0.01 | 43.23±0.01 | -2.93±0.02 |
| $\Delta G_O$ | 4.20 | 4.20 | 0 |
| $\Delta G$ | -37.59±0.01 | -40.50±0.01 | 2.94±0.02 |

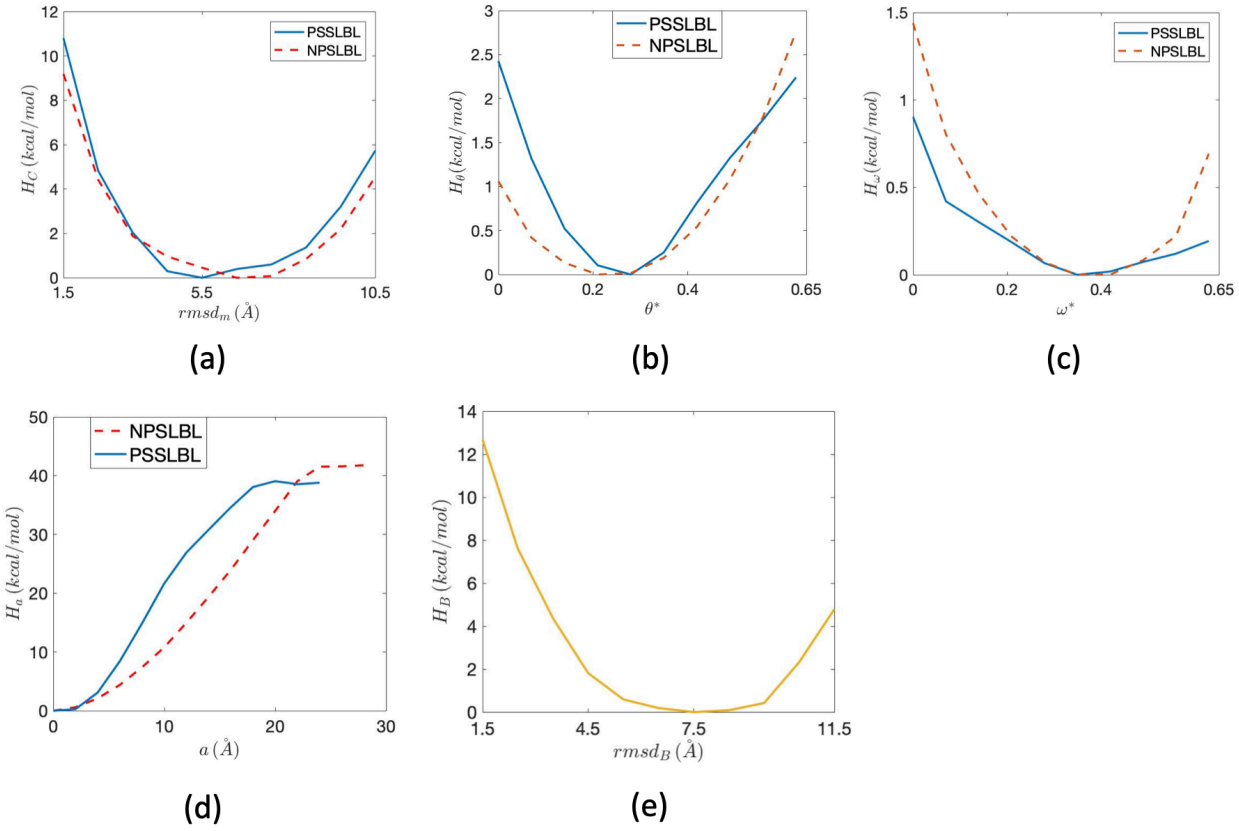


***Figure 5. 6: PMF corresponding to different reaction coordiantes***

*(a) PMF ($H_C$) as a function of $rmsd_m$ when protein is binding to the membrane for the NPSLBL and the PSSLBL. (b) PMF ($H_\theta$) as a function of $\theta^*$ for both the NPSLBL and the PSSLBL with $rmsd_m$ set to 0. In the figure, $\theta^* = \theta - \theta_1$, where $\theta_1$=1.95 for NPSLBL and $\theta_1$=1.06 for PSSLBL. c) PMF ($H_\omega$) as a function of $\omega^*$ for both the NPSLBL and the PSSLBL with $rmsd_m$ set to 0 for both the NPSLBL and the PSSLBL and $\theta$ set to 1.34 and 2.16 for the PSSLBL and the NPSLBL, respectively. In the figure, $\omega^* = \omega - \omega_1$, where $\omega_1$=2.27 for NPSLBL and $\omega_1$=-3.07 for PSSLBL (d) PMF ($H_a$) as a function of a for both the NPSLBL and the PSSLBL with $rmsd_m$ set to 0 for both the NPSLBL and the PSSLBL, $\theta$ set to 1.34 and 2.16 for the PSSLBL and the NPSLBL, respectively, and $\omega$ set to $-2.69$ and 2.65 for the PSSLBL and the NPSLBL, respectively. (e) PMF ($H_B$) as a function of $rmsd_B$ when the protein is in bulk water.*

## *5.4 Results*

Figs. 5.6(a-e) provide the PMFs needed to calculate $\Delta G_X$ (with $X$=$C$, $\theta$, $\omega$, or $B$) and $\Delta G_a$ for the SpoVM protein interacting with both the PSSLBL and NPSLBL. The corresponding free energy change obtained by integration [see eq. (5.2) and eq. 5.3)], have been listed in Table I. Fig. 5.6(a) provides the variation of the PMF ($H_C$) of the SpoVM molecule, needed to calculate the corresponding $\Delta G_C$, with the reaction coordinate $rmsd_m$ for both the PSSLBL and the NPSLBL. The results show a slightly larger $\Delta G_C$ (i.e., a more favorable overall $\Delta G$; $\Delta G$ and $\Delta G_C$ have opposite signs, see eq. 5.1) for the PSSLBL (see Table 5.1). As a result, the high curvature plays an insignificant role in facilitating the folding of SpoVM. Next, we study the variation of the PMFs ($H_\theta$ and $H_\omega$), used to compute the free energy changes $\Delta G_\theta$ and $\Delta G_\omega$, as functions of corresponding reaction coordinates $\theta$ and $\omega$ for both the PSSLBL and the NPSLBL. Changing the first Euler angle $\theta$ for the SpoVM is harder in the PSSLBL than that in NPSLBL, while it is easier to change the second Euler angle $\omega$ for the SpoVM in the PSSLBL than in the NPSLBL. Accordingly, the free energy change $\Delta G_\omega$ is lower for NPSLBL (i.e., leads to less favorable overall energy change $\Delta G$ for the NPSLBL; $\Delta G$ and $\Delta G_\omega$ have opposite signs, see eq. 5.1) and $\Delta G_\theta$ is lower for the PSSLBL (i.e., leads to less favorable overall energy change $\Delta G$ for the PSSLBL; $\Delta G$ and $\Delta G_\theta$ have opposite signs, see eq. 5.1). The protein deformation and rotation with respect to the second Euler angle occurs at the outer membrane surface (i.e., the outer leaflet of the LBL); accordingly, $\Delta G_\omega$ depends on the extent of defects present on the outer leaflet. The surface area per lipid at the outer leaflet is 0.85 $nm^2$ and 0.82 $nm^2$ for the NPSLBL and the PSSLBL, respectively; as a result,

there are more defects (here defects refer to the presence of the low-density region rather than a real hole) at the outer surface of NPSLBL and accordingly, $\Delta G_\omega$ is smaller (i.e., change in the Euler angle ω occurs with a lesser resistance due to the presence of more defects or less compactness of the outer leaflet) for the NPSLBL. However, the protein rotation with respect to the first Euler angle occurs at the hydrophobic core, which is denser in the NPSLBL as compared to PSSLBL, see Fig. 5.7. As a result, the free energy change, $\Delta G_\theta$, is lower for the PSSLBL. These two effects are well balanced as $\Delta\Delta G_m + \Delta\Delta G_\theta + \Delta\Delta G_\omega \approx 0$. In Fig. 5.6(d), we study the change in PMF ($H_a$) needed to compute the corresponding change in the free energy component $\Delta G_a$ by changing the position of the protein from the membrane to the bulk water for both the NPSLBL and the PSSLBL. Therefore, for both the cases, the reaction coordinate is *a*, which is defined differently for the PSSLBL and NPSLBL and provided a measure of the distance of the protein from the LBL of the PSSLBL and the NPSLBL. A smaller $\Delta G_a$ for the PSSLBL suggests a less favorable overall free energy change ΔG (having a sign opposite to that of $\Delta G_a$, please see eq. 5.1). Physically, such a variation of $\Delta G_a$ is an overall effect of the different packing of the hydrophilic head (this packing is larger for the PSSLBL and hence the resistance is larger for the SpoVM interacting with the PSSLBL) and hydrophobic tails of the lipid bilayer (this packing is larger for the NPSLBL and hence the resistance is larger for the SpoVM interacting with the NPSLBL) as electrostatics interactions rely on the packing of the hydrophilic head while hydrophobic interaction relies on the packing of the hydrophobic tails. Finally, in Fig. 5.6(e), we provide the variation of PMF ($H_B$), needed to compute the free energy change $\Delta G_B$, with the variation of the

corresponding reaction coordinate $rmsd_B$. Variation of $H_B$ and hence $\Delta G_B$ (see Table I) are identical for the cases of PSSLBL and the NPSLBL as is the value of $\Delta G_O$ (see Table I). From a comparison of the values associated with the different components of the free energies, we can clearly see that $\Delta G_a$ plays the most dominant role in determining the overall $\Delta G$ associated with the SpoVM binding to the membrane as a function of the membrane curvature. This overall $\Delta G$ is smaller for the case where the SpoVM binds to the NPSLBL as compared to the case where the SpoVM binds to the PSSLBL, confirming the preference of the SpoVM to favorably bind to the convexly curved LBL as compared to the planar LBL. This establishes for the first time a definite proof of the mechanism that is involved in a protein molecule sensing membrane curvature: our results establish that SpoVM preferentially senses the membrane curvature driven primarily by the free energy changes associated with the migration of the SpoVM molecule from the LBL to the bulk, and the structure basis for the SpoVM membrane sensing is that higher curvature cause more loosely packing of the hydrophilic heads of the LBL and more densely packing of the acyl chains of the LBL.

We adopted the following equations proposed by Zhu et al.[19] to evaluate the error of PMFs:

$$e_{kj} = (k\Delta x)^2 \left[\frac{var(\bar{x}_j)+var(\bar{x}_k)}{4} + \sum_{i=j+1}^{k-1} var(\bar{x}_i)\right]. \quad (5.4)$$

In the above equation, $e_{kj}$ is the error between the $k^{th}$ and $j^{th}$ simulation windows. k is the harmonic force constant used in the umbrella biasing potential, $\Delta x$ is the distance between two simulation windows, $var(\bar{x}_i)$ is the variances of the mean coordinates $\{\bar{x}_i\}$ of $i^{th}$ simulation window and can be calculated as

$$var(\bar{x}_i) = \frac{1}{n(n-1)} \sum_{b=0}^{n-1} \left[ \frac{1}{m} \sum_{x=bm+1}^{(b+1)m} x_{ip} - \bar{x}_i \right]^2 . \quad (5.5)$$

In Eq. 5.5, the time series $x_{ip}$ is obtained from the simulation of $i^{th}$ simulation window, which is distributed into *n* blocks of size *m.* In practice, *n* is usually between 5 and 10. After obtaining $e_{kj}$ corresponding to each reaction coordinate corresponding to *X*, the error of the $\Delta G_X$ is calculated by taking $e_{kj}$ into the corresponding equations (Eq. 5.2 and Eq. 5.3).

The values of the free energy change of SpoVM absorption to LBLs obtained in our simulations are higher than the experiments reported by Gill et al[9], in which the free energy change, converted from the experimental equilibrium constant, is -7.71 kcal/mol for 8um diameter NPSLBL and -8.4 kcal/mol for 2um diameter NPSLBL. We attribute the difference to the fact that (1) we cannot simulate the SpoVM folding in the MD and the folding of SpoVM can result in significant free energy change, 2) POPC is used in MD while different type of lipids is used in the experiment, and 3) the sizes of NPSLBL in the experiments are larger than that considered in the simulations.

## *5.5 Conclusion*

In this paper, we have carried out coarse-grained MD simulation to quantify the mechanism of membrane curvature sensing by the SpoVM by separately calculating the free energy changes associated with the binding of the SpoVM molecule to the PSSLBL (representing non-curved membrane system) and NPSLBL (representing highly curved membrane system). Our results confirm that SpoVM can

sense the membrane curvature and prefer to bind to the curved membrane rather than planar membrane as $\Delta G_{NPSLBL} < \Delta G_{PSSLBL}$. We pinpoint that the main contribution in dictating difference stems from the free energy changes associated with the migration of the SpoVM from the membrane to the bulk. In addition, we confirm that the defects at the membrane surface and the packing of the acyl chains of lipids are the key physical factors that ensure this preferential binding of the SpoVM to the NPSLBL. Experiments report the defects at the membrane surface are more dominant for highly curved membrane whose radius < 200 nm, while the packing of the acyl chains of lipids are more vital for slightly curved membrane whose radius > 2μm. Such exact size-based (or equivalently, extent of curvature-based) quantification of these different effects in determining the membrane curvature sensing by SpoVM and other types of proteins will be topics of future investigations.

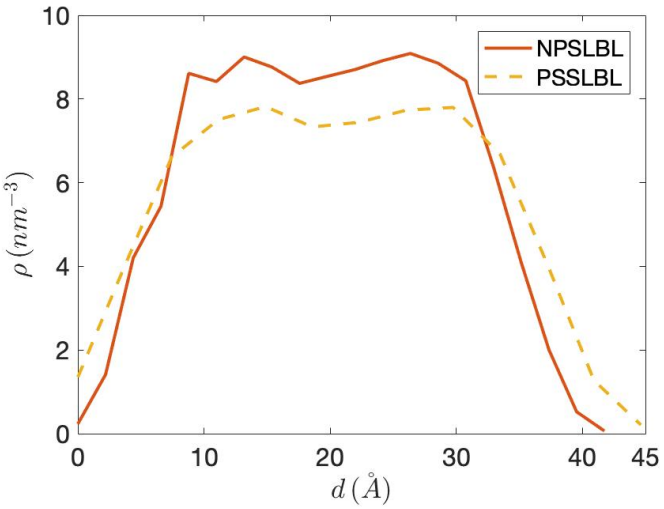


***Figure 5. 7: Density of hydrophobic beads***

*Density of the hydrophobic beads in the PSSLBL and NPSLBL. The x axis refers to the distance between the region of interest and the inner surface of the lipid bilayer.*

## *Bibliography*


1. K. Machida and S.-I. Ohnishi, Effect of Bilayer Membrane Curvature on Activity of Phosphatidylcholine Exchange Protein. *Biochim. Biophys. Acta* **596**, 201–209 (1980).
2. H. Huang, J. M. Ball, J. T. Billheimer, and F. Schroeder, Interaction of the n-terminus of Sterol Carrier Protein 2 with Membranes: Role of Membrane Curvature. *Biochem. J.* **344**, 593–603 (1999).
3. J. Bigay, P. Gounon, S. Robineau, and B. Antonny, Lipid Packing Sensed by Arfgap1 Couples Copi Coat Disassembly to Membrane Bilayer Curvature. *Nature* **426**, 563–566 (2003).
4. K. S. Ramamurthi, S. Lecuyer, H. A. Stone, and R. Losick, Geometric Cue for Protein Localization in a Bacterium. *Science* **323**, 1354–1357 (2009).
5. B. Antonny, Mechanisms of Membrane Curvature Sensing. *Annu. Rev. Biochem.* **80**, 101–123 (2011).
6. J. Bigay and B. Antonny, Curvature, Lipid Packing, and Electrostatics of Membrane Organelles: Defining Cellular Territories in Determining Specificity. *Developmental Cell* **23**, 886–895 (2012).
7. S.-T. Yang, J. Y. Lee, H.-J. Kim, Y.-J. Eu, S. Y. Shin, K.-S. Hahm, and J. I. Kim, Contribution of a Central Proline in Model Amphipathic α-helical Peptides to Self-Association, Interaction with Phospholipids, and Antimicrobial Mode of Action. *FEBS J.* **273**, 4040–4054 (2006).
8. N. S. Hatzakis, V. K. Bhatia, J. Larsen, K. L. Madsen, P.-Y. Bolinger, A. H. Kunding, J. Castillo, U. Gether, P. Hedegård, and D. Stamou, How Curved

Membranes Recruit Amphipathic Helices and Protein Anchoring Motifs. *Nature Chem. Biol.* **5**, 835 (2009).

9. R. L. Gill, J.-P. Castaing, J. Hsin, I. S. Tan, X. Wang, K. C. Huang, F. Tian, and K. S. Ramamurthi, Structural Basis for the Geometry-driven Localization of a Small Protein. *Proc. Natl. Acad. Sci.* **112**, E1908–E1915 (2015).
10. P. A. Levin, N. Fan, E. Ricca, A. Driks, R. Losick, and S. Cutting, An Unusually Small Gene Required for Sporulation by Bacillus Subtilis. *Molecular Microbiol.* **9**, 761–771 (1993).
11. C. van Ooij and R. Losick, "Subcellular Localization of a Small Sporulation Protein in Bacillus Subtilis. *J. Bacteriology* **185**, 1391–1398 (2003).
12. D. Higgins and J. Dworkin, Recent Progress in Bacillus Subtilis Sporulation. *FEMS Microbiol. Rev.* **36**, 131–148 (2012).
13. Gill, R. L.; Castaing, J.-P.; Hsin, J.; Tan, I. S.; Wang, X.; Huang, K. C.; Tian, F.; Ramamurthi, K. S. Structural Basis for the Geometry-driven Localization of a Small Protein. *Proc. Natl. Acad. Sci.* **112**, E1908–E1915 (2015).
14. Marrink, S. J.; Risselada, H. J.; Yefimov, S.; Tieleman, D. P.; de Vries, A. H. The MARTINI Force Field: Coarse Grained Model for Biomolecular Simulations. *J. Phys. Chem. B* **2007**, *111*, 7812-7824.
15. Phillips, J. C.; Braun, R.; Wang, W.; Gumbart, J.; Tajkhorshid, E.; Villa, E.; Chipot, C.; Skeel, R. D.; Kale, L.; Schulten, K. Scalable Molecular Dynamics with NAMD. *J. Comput. Chem.* **2005**, *26*, 1781-1802.

16. Torrie, G. M.; Valleau, J. P. Nonphysical Sampling Distributions in Monte Carlo Free-Energy Estimation: Umbrella Sampling. *J. Comput. Phys.* **23**, 187–199 (1977).
17. H.-J. Woo and B. Roux, Calculation of Absolute Protein–ligand Binding Free Energy from Computer Simulations. *Proc. Natl. Acad. Sci.* **102**, 6825–6830 (2005).
18. J. C. Gumbart, B. Roux, and C. Chipot, Standard Binding Free Energies from Computer Simulations: What is the best strategy? *J. Chem. Theory Comput.* **9**, 794–802 (2013).
19. Zhu, F.; Hummer, G. Convergence and Error Estimation in Free Energy Calculations Using the Weighted Histogram Analysis Method. *Journal of Computational Chemistry* **2012**, *33* (4), 453–465.

# Chapter 6: Future Development

In Chapters 2 and 3, we conducted MD simulation to study the self-assembly and properties of NPSLBL and how the hydrophilicity of the NP can influence the LBL.

In Chapter 4, the lipid flip-flop and desorption in NPSLBL and PSSLBL were simulated using MD, and our results indicated that membrane curvature played non-significant role in lipid flip-flop and desorption.

In Chapter 5, we used MD simulation to confirm that the free energy change of SpoVM binding to NPSLBL is lower than PSSLBL and we proposed the reason is the membrane curvature increase the hydrophobic density of the LBL

Based on the findings of this dissertation, we anticipate more work can be done to better advance this topic in the following areas:

1) Developing new or modify the current polarizable force fields to enable the correct simulation of SpoVM folding.

2) Carrying out Experiments to confirm the conclusion of Chapter 5. In the experiments, the hydrophobic density of the LBL can be modified by using different lipid species with the same hydrophilic head group but different hydrophobic tails.

3) In addition, it will be useful to explore how the free energy changes of the SpoVM binding to membrane vary as functions of 1/r, where r is the radius of the NPSLBL.

4) In chapters 2 and 3, we only investigate how the NPSLBL is influenced by the properties of the NP. It would be interesting to see how the lipid types (like charged head group, uncharged head group, mixture of different lipids) can affect the properties of the NPSLBL. In addition, it is more exciting if one can determine

whether other molecules, like surface protein or cholesterol, can affect the formation and properties of the NPSLBL.

5) The water molecules between the NP and the LBL in the NPSLBL is nanoconfined. Thus, it would be interesting to see how this nanoconfinement affects the property of the water molecules. We can also explore the possibility of the presence of ions (and the corresponding structure of the hydration shells of the ions) between the NP and LBL in presence of an added salt?

6) We can repeat the above study in presence of salts consisting of multivalent ions and LBLs consisting of charged lipids.